University of Cape Town

Department of Environmental & Geographical Science

Assessing the representation of teleconnective drivers of rainfall over Eastern Africa in global and regional climate models and projected future changes

Author:

Hussen Seid Endris

hussen.seid1@gmail.com

Supervisors:

Prof. Bruce Hewitson

hewitson@csag.uct.ac.za

Dr. Christopher Lennard

lennard@csag.uct.ac.za

Dissertation submitted for the degree of Doctor of Philosophy

January 26, 2017

Declaration I

I know the meaning of plagiarism, and declare that this thesis is my own work and has not been submitted for any academic degree or diploma from the university or other institutions. The use of all material from other sources has been properly cited and acknowledged.

Signed by candidate

Hussen Seid Endris

Declaration II

The work of this thesis is based on the work of the following publications.

1. **Endris, H. S.,** Omondi, P., Jain, S., Lennard, C., Hewitson, B., Chang'a, L., Awange, J.L., Dosio, A., Ketiem, P., Nikulin, G., Panitz, H.J., Buchner, M., Stordal, F. & Tazalika, L. (2013). Assessment of the Performance of CORDEX Regional Climate Models in Simulating East African Rainfall. *Journal of Climate*, 26(21), 8453-8475.

2. **Endris, H. S.,** Lennard, C., Hewitson, B., Dosio, A., Nikulin, N., & Panitz, H. (2015). Teleconnection responses in multi-GCM driven CORDEX RCMs over Eastern Africa. *Climate Dynamics*,46, 2821-2846. DOI: 10.1007/s00382-015-2734-7.

3. **Endris, H. S.,** Lennard, C., Hewitson, B., Dosio, A., & Nikulin, N. (2016). Future changes in rainfall associated with ENSO and IOD over Eastern Africa. *Climate Dynamics*. Under review.

Hereby I declare that the intellectual content of this thesis and the included papers is the product of my own work. My two supervisors directed and supervised the research that forms the basis for the thesis. The other co-authors listed in these publications provided the datasets (model outputs) and gave assistance with improving style and grammar.

I also confirm that a permission has been obtained from the university doctoral degree board for full inclusion of the publications in the thesis.

Abstract

Climate variability is an important characteristic of regional climate, and a subject to significant control from teleconnections. An extended diagnosis of the capacity of climate models to represent remote controls of regional climate (teleconnections) is vital for assessing model-based predictions of climate variability, understanding uncertainty in climate projections and model development. An important driver of climate variability for Africa is the sea surface temperature (SST) - rainfall teleconnection, such as the El Niño/Southern Oscillation (ENSO) and Indian Ocean Dipole (IOD). In this study, an assessment of the teleconnection between tropical SSTs and Eastern African rainfall in global and regional climate models is presented, with particular attention paid to the propagation of large-scale teleconnection signals (as represented by model reanalyses and Coupled Global Climate models (CGCMs)) into the domain of the Regional Climate Models (RCMs). The teleconnection-rainfall relationship with the Eastern Africa region is assessed in two rainfall seasons (June-July-August-September and October-November-December) under present and future periods. Evaluation runs (RCMs driven by reanalysis datasets) and historical simulations (RCMs driven by CGCMs) are assessed to quantify the ability of the models to capture the teleconnection relationship. The future analysis is performed for two Representative Concentration Pathway scenarios (RCP4.5 and RCP8.5) to assess future change in this relationship as a result of global warming.

Using ERA-interim reanalysis as perfect boundary conditions, the RCMs adequately simulate the spatial and temporal distribution of rainfall in comparison with observations, although the model performance varies locally and seasonally within the region. Furthermore, the RCMs correctly capture the magnitude and spatial extent regional-scale seasonal rainfall anomalies associated with large-scale oceanic modes (ENSO and IOD). When the lateral boundary conditions are provided by CGCMs, RCMs barely capture the regional teleconnection patterns associated with large-scale modes, and mostly depend on the selection of the driving CGCM. Comparison of the CGCM-driven RCM simulations with the reanalysis-driven RCM simulations revealed that most of the errors in teleconnection found in the RCM simulations are inherited from the host CGCMs. The ERA-Interim driven downscaled results show better agreement with observed spatial teleconnection patterns than the CGCM driven downscaled results.

Analysis of the CGCMs and corresponding downscaled results showed that in most cases both the CGCM and the corresponding downscaled simulations had similar teleconnection patterns, but in some cases the RCM results diverge to those of the driving CGCM results. It has been demonstrated that similarities in SST-rainfall teleconnection patterns between the RCM simulations and respective driving CGCM simulations are noted over the equatorial and southern part of the region during OND season, where the rainfall is primarily controlled by large-scale (synoptic-scale) features, with the RCMs maintaining the overall regional patterns from the forcing models. Differences in RCM simulations from corresponding driving simulations are noted mainly over northern part of the domain during JJAS, which is most likely related to mesoscale processes that are not resolved by CGCMs.

Looking at the model projections of the future, although the spatial pattern of teleconnections between ENSO/IOD and rainfall still persist, important changes in the strength of the teleconnection have been found. During JJAS, ENSO is an important driver of rainfall variability in the northern parts of the region where dry anomalies are associated with El Niño and wetter anomalies with La Niña. Both regional and global ensemble projections show higher rainfall during La Niña and lower rainfall during El Niño over the northern part of the region compared to the present period. During OND, the teleconnection between ENSO/IOD and rainfall is projected to strengthen (weaken) over Eastern horn of Africa (southern parts of the region) compared to the present period. This implies heavy seasonal rains associated with positive phases of ENSO

and IOD will increase in future across the Eastern horn of Africa. The change OND rainfall teleconnections are stronger and also more consistent between the models and scenarios as compared to the change in JJAS teleconnections. These findings have an important implication for the water and agricultural managers and policies in the region to tackle the anticipated droughts and floods associated anthropogenic climate change.

Finally, the analysis demonstrated that the largest source of uncertainty in the regional climate model simulations in the context of teleconnective forcing of rainfall over Eastern Africa is the choice of CGCM used to force the RCMs, reinforcing the understanding that the use of a single GCM to downscale climate predictions/projections and using the downscaled product for assessment of climate change projections is insufficient. Simulations from multiple RCMs nested in more than one GCM, as is undertaken in the Coordinated Regional Downscaling Experiment (CORDEX), are needed to characterize the uncertainty and provide estimates of likely ranges of future regional climate changes.

Acknowledgments

First of all I would like to thank my supervisors, Dr Christopher Lennard and Prof. Bruce Hewitson, for their valuable guidance and support throughout my research period. Their advice, contribution, patience and encouragement made the difference and I will forever be grateful. In particular, I would like to thank Dr Christopher Lennard for his continuous support. He was always accessible to advice and share his knowledge and experience throughout my study period.

My Phd study has been funded by the Norwegian government under the project of Socio-economic Consequences of Climate Change in Sub-equatorial Africa (SoCoCa). Therefore, I would like to express my deepest gratitude to the SoCoCa project team for the financial support to conduct my PhD study at University of Cape Town. In particular, I would like to thank Prof. Frode Stordal, the coordinator of the project at the University of Oslo, for processing and facilitating the funding in an efficient and timely manner. He played a huge role in the entire process. I appreciate his kindness and generous support.

Furthermore, I want to thank the staffs and students in the Climate System Analysis Group (CSAG). Particularly, my office mates (Izidine Pinto, Michael Kent, Brendan Argent and Steve Arowolo) for giving me all the help I needed during the whole period of this research.

Finally, and most importantly, I would like to thank my families for their moral support and consistent encouragement during the time I was doing this work. Without them, I would never have made it.

Contents

List of Figures

1

Introduction

1.1 Background

Eastern Africa is the easterly region of sub-Saharan Africa that consists of two distinct geographic regions: East Africa which includes Kenya, Tanzania and Uganda, and Horn of Africa which consists of Somalia, Ethiopia, Eritrea and Djibouti. Other nations such as Sudan, Burundi, Rwanda and South Sudan are also considered as a part of Eastern Africa. This is an interesting region for climate research as the climate of the region is very diverse and highly variable, with the Danakil desert known for its volcanoes and extreme heat at one side, and the cooler and wetter Ethiopian and East Africa highlands at the other. There are several processes that drive the climate of the region, with complex interrelations that are not yet fully understood (Nicholson, 1996; Lyon, 2014). The existence of large water bodies, mountains and valleys produce local circulations and modulate the region's climate by either amplifying or suppressing the general circulation of the atmosphere.

Rainfall is the most important climatic element over the region. This is primarily because of the local/regional economies are largely dependent by rain-fed agriculture, and secondly the largest source of electricity generation in the region is hydropower. The rainfall over the region shows high spatiotemporal variability. The spatial variability of rainfall has been attributed to the influence of local features (torography and water bodies) and large scales systems (Nicholson and Kim, 1997). The local factors such as the high mountains and large inland lakes modulates

regional climates through the generation of orographic precipitation and lake/land breeze circulation (Anyah and Semazzi, 2004; Song et al., 2004). The seasonality of rainfall over the region is primarily controlled by the bi-annual passage of the inter-tropical convergence zone (ITCZ) (Johnson, 1996; Anyah et al., 2006). The seasonal to inter-annual variability of rainfall over the region is strongly linked to large-scale patterns of sea surface temperature (SST) variability in the global Oceans, particularly associated with SST variability over the tropical Pacific and Indian Oceans (Ogallo et al., 1988; Nicholson and Kim, 1997; Indeje et al., 2000; Saji et al., 1999; Black et al., 2003; Nyakwada, 2009; Omondi et al., 2012). El Niño Southern Oscillation (ENSO) and Indian Ocean Dipole (IOD) are the two dominant modes of climate variability over the tropics that control Eastern Africa rainfall at inter-annual time scales and causing wetter or drier seasons. Although the association (teleconnection) between ENSO/IOD and seasonal rainfall variability in the region have been investigated, the underlying physical mechanisms responsible for rainfall variability and future changes in teleconnection patterns have yet to be fully elucidated.

Global Climate Models (GCMs) are the fundamental tools for simulating the past climate and projected future evolution of the climate system in response to anthropogenic forcings, such as the increase in greenhouse gas (GHG) and aerosol concentrations. However, since GCMs cover the entire globe, the simulations are typically run at relatively coarse horizontal resolution due to the computational costs. The most updated GCMs from the phase 5 Coupled Model Intercomparison Project (CMIP5) run on horizontal resolutions of the order of hundreds of kilometers (100-300km) (Stouffer et al., 2011; Taylor et al., 2012). GCMs at this resolution have the potential to capture the global climate characteristics and broad circulations patterns. (Shongwe et al., 2009). However, they are not capable of capturing sub-grid-scale processes/forcings such as mountains, lakes, land-use characteristics and atmospheric aerosols and others (Giorgi and Mearns, 1991, 1999; Denis et al., 2002; Wang et al., 2004; Giorgi et al., 2009; Rummukainen, 2009). These regional-scale forcings are responsible for modulating the large-scale circulation features that determine the regional climate. This is especially true for regions of complex topography, coastal locations and in regions of highly heterogeneous land-cover. Moreover, coarse resolution limits the applicability of global model outputs for impacts and adaptation studies, which are much finer than that provided by global models (tens of kilometers or less) (Evans, 2011).

In order to obtain regional climate information, different methods to downscale climate data from coarse-scale GCM output have been developed. These downscaling methodologies may be categorized into two broad classes: statistical and dynamical. Statistical downscaling is based on first developing a statistical model, which relates some large scale climate variables or predictors (e.g., sea level pressure, geopotential height, wind fields, relative humidity) and regional/local variables or predictands (such as rainfall or temperature) (Hewitson and Crane, 1996; Wilby et al., 2004). The large-scale variable from a GCM output is then fed into the statistical model to calculate the corresponding local/regional climate feature. Dynamical downscaling, on the other hand, is based on mathematical representations of the physical processes that create the

climate system, similar to GCMs, but applied over a limited area at a higher spatial resolution than the GCMs (Giorgi and Mearns, 1999). Dynamical downscaling is done with a Regional Climate Model (RCM). In case of dynamical downscaling, driving data from reanalysis or GCM is used to force the boundaries of an RCM over a limited area. The basic set of boundary conditions are temperature, moisture, and circulation (winds), as well as sea-surface temperature and sea ice. An accurate treatment of boundary conditions is a central issue in regional modeling (Rummukainen, 2009).

Both statistical and dynamical techniques have strengths and weaknesses. The main strength of statistical downscaling techniques is that they are computationally efficient, and thus can be easily applied to output from different GCM experiments, and as a result the range of uncertainty in the projections can be more easily explored. Moreover, statistical downscaling techniques have the capacity to downscale to specific point or gridded observations, so that the product is more readily compatible with the data typically used in impact models. The main weakness is they assume stationarity (i.e., the statistical relationships developed for the present day climate also hold under the different forcing conditions of possible future climate). The quality and coverage of observational data also often represent a notable constraint in statistical downscaling in data sparse regions since the technique is developed using existing observational datasets. The main strength of dynamical downscaling is their dynamical representation of higher resolution processes relevant to the local climate, and offer a range of climate variables. The main drawback in dynamical downscaling is the computational cost, which makes difficult to downscale many GCMs.

Both statistical and dynamical techniques also shared common issues. Both techniques use GCM output as input and thus are fully dependent on the accuracy of circulation patterns produced by GCMs. Dynamical models, however, through higher resolution or better representation of important physical processes, often can improve the physical realism of simulated regional circulation. Moreover, both techniques are dependent on adequate observational data (i.e for statistical downscaling data are needed to develop the downscaling relationships; for dynamical models data are used to develop the models parameterizations). Both techniques are also vulnerable to issues of stationarity. Statistical techniques are vulnerable in the statistical methods employed to capture the statistical relationships, whereas dynamical downscaling is vulnerable in terms of the parameterizations used in the model.

Recently, RCMs became the most widely used tools for climate process studies and to address regional climate information. RCMs consistently improve the spatial detail of simulated climate compared to GCMs (Giorgi et al., 2001). They have the ability to translate large scale climate patterns produced by a GCM to regional scales relevant to the analysis of local extremes of floods and droughts. They have also the potential to provide insights into regional scale responses to remote large scale climate dynamics such as El Niño Southern Oscillation (ENSO). During recent years, there has been a marked increase in the number of RCM simulations (IPCC, 2007, 2014). More importantly, coordinated modelling efforts for several regions of the world have started to

emerge to further improve the quality of the RCM results and also to explore the associated uncertainty of the regional climate model products. For example, over Europe (ENSEMBLES: Hewitt and Director (2005)), North America (NARCCAP: Paulsen et al. (2009)), and South America (Boulanger et al. (2010), CLARIS: Rusticucci and Barrucand (2004)) produced large ensembles of RCM simulations. Recently, the Coordinated Regional climate Downscaling Experiment (CORDEX: Giorgi et al. (2009)), which is an initiative of the World Climate Research Programme (WCRP), offers an opportunity to advance our understanding of regional climate processes and to provide valuable information for the impact community. The primary aim of CORDEX is to produce a new generation of large multi-model ensembles of regional climate change projections over domains covering all continental areas of the world for use in impact assessment and adaptation studies. This includes the construction of a many RCM driven by many GCM ensemble is vital for dealing with the uncertainty associated with future projections. Africa was selected as a priority region, thus providing an opportunity to improve climate-change projections over Africa.

Given the heterogeneity and complexity of Eastern Africa, and the capability of RCMs to resolve small scale features (topographical details and coastal regions) as well as the potential to provide insights into regional scale responses to remote large scale climate, the application of regional climate models over Eastern Africa offers significant potential to expand our understanding of regional change. This study uses an ensemble of regional climate simulations to explore the present and future climate variability and to investigate the physical mechanisms associated with variability over Eastern Africa. Even though some studies have employed regional climate models in the region, most results are based on a single model realization, either using one driving GCM or one RCM. Among these studies, many of them used the various versions of the International Centre for Theoretical Physics (ICTP) Regional Climate Model system (RegCM) model. For example, Sun et al. (1999a,b) employed the RegCM2 to simulate the interannual variability of rainfall over Eastern Africa for the short-rains season. Anyah and Semazzi (2004) and Anyah and Semazzi (2007) used RegCM2 and RegCM3 to study the response of Lake Victoria basin climate to changes in the lake surface temperatures, and the OctoberDecember (OND) rainfall variability, respectively. Similarly, Segele et al. (2009b) evaluated the ability of the RegCM3 model to reproduce the observed rainfall amounts and distribution over the Greater Horn of Africa, and Diro et al. (2012) examined the skill RegCM3 model to reproduce the spatial and temporal variability rainfall over Eastern Africa using boundary conditions from ERA-interim reanalysis and the European Centre for Medium-range Weather Forecast (ECMWF) atmosphere-Ocean coupled model seasonal forecasting system. Recently, Ogwang et al. (2015a) and Ogwang et al. (2015b) evaluated the capability of RegCM4 in simulating East African climate, focusing on October to December (OND) rainfall. It is, however, well known that each model has its own strengths and weaknesses. Yet, the application of ensemble of RCMs in climate studies over Eastern Africa has not been robustly evaluated. This study attempted to bridge the gap by using ensemble of RCM simulations to assess models' ability in

reproducing the rainfall telecoonection patterns over Eastern Africa and investigate the future projected changes under increase greenhouse gas concentrations.

1.2 Motivation

Eastern Africa is one of the most vulnerable regions to climate change and climate variability (IPCC, 2014). Climate extremes such as floods, droughts and heatwaves, which aggravated by climate change and its variability, are being experienced more frequently over the region. This negatively affects the food security and leads to widespread famine and humanitarian crises. For example, the heavy rainfall events in 1961, 1994 and 1997, which caused wide spread floods across East Africa and the Horn of Africa affected millions of people and led to significant economic disruption over the region (Odingo, 1962; Birkett et al., 1999). The 1982/83 severe drought combined with civil conflict triggered a famine that lead to an estimated one million fatalities in northern Ethiopia and Sudan (Devereux and Berge, 2000; Lyon, 2014). The two major recent droughts in the last two decades, 2008-2009 and 2010/2011, in wide regions of Kenya, Ethiopia, Djibouti and Somalia, affected food security and subjected millions of peoples to famine (UNOCHA, 2011). More recently, in 2015, the failure of March to May (MAM) rainfall and subsequently summer (JJAS) rainfall associated with El Niño event have caused a devastating impact over the region. According to the latest reports released by the government of Ethiopia and Humanitarian partners' document, in Ethiopia alone about 15 million people were food insecure and in need of emergency food aid. There is also a growing evidence that these impacts may be further amplified as global temperatures continue to rise in response to increase greenhouse gases. The latest Intergovernmental Panel on Climate Change Assessment Report (IPCC AR5) suggested that climate change will lead to an increase in the frequency and intensity of climate extremes over the region. Therefore, a better understanding of climate variability and change in the region is important to help minimize climate-related losses and further develop appropriate risk management and adaptation strategies.

It is widely established that inter-annual variability in Eastern Africa is mainly influenced by global-scale sea surface temperature (SST) anomalies through teleconnection responses (e.g., Ropelewski and Halpert, 1987; Nicholson and Kim, 1997; Omondi et al., 2012). In particular, SST anomalies over the tropical Pacific and Indian Ocean are suggested to be the dominant drivers of the rainfall variability over the region (Ogallo et al., 1988; Indeje et al., 2000; Saji et al., 1999; Black et al., 2003; Segele et al., 2009b; Diro et al., 2011). Adequate representation of such processes is important to obtain reliable model predictions of climate variability and also to provide a basis for changes in global Ocean temperatures to be credibly translated to regional rainfall changes in climate change simulations. To date there has been limited regional assessment of the ability of current climate models to represent these observed teleconnections and the underlying mechanisms over Eastern Africa. With this in mind, this study aims to examine the ability of climate models (global and regional) to simulate to remote influences

(teleconnections) on the regions rainfall variability. The study further investigates the future changes in teleconnection patterns under a warming scenario.

1.3 Aim and objectives of the study

Aims

- To examine the ability of climate models (regional and global) to reproduce the telconnection forcing of tropical SST on rainfall over Eastern Africa and
- To investigate whether or not the present teleconnection patterns persist in the future under increase greenhouse gas scenarios.

Objectives

- To evaluate the ability of the RCMs
  - ⋆ to simulate the observed spatial and temporal characteristics of regional rainfall
  - ⋆ reproduce the regional teleconnection responses to the propagated signal via the boundary forcing
- To assess how well models (global and regional) can simulate the regional atmospheric circulation patterns/anomalies associated with the teleconnections in the historical period
- To investigate whether the historical teleconnections persist in future under a global warming scenario

Emphasis is given in examining the propagation by RCMs of a large-scale teleconnection pattern, such as the ENSO and IOD (as represented by model reanalyses of historical climate and by CGCMs). The research focuses on seasonal time scale of rainy seasons: June - September (JJAS) and October- December (OND), when most of the region receives rainfall. It has been also established that the JJAS and OND rainfall seasons experience larger degree of interannual variability relative to climatology, and the variability is linked to tropical SST anomalies (Ogallo et al., 1988; Indeje et al., 2000; Saji et al., 1999; Diro et al., 2011). The long rainfall season that occurs in MAM (March - May) is not considered in the analysis since the rainfall has has a weak association with tropical SST anomalies at interannual timescale (e.g., Indeje et al., 2000; Nyakwada, 2009).

1.4 Significance of the study

This research study contributes to climate change knowledge in the following ways:

1. It advances scientific understanding of past and present climate variability in the region and the physical processes which control the seasonal climatic variability. Better scientific

understanding of the climate processes of the region is important to improve our ability to predict climate and help users incorporate its inherent uncertainty into decision-making.

2. It provides baseline information on model performance in reproducing the association between large-scale features (ENSO and IOD) and seasonal rainfall variability over Eastern Africa. In this regard, models that capture the teleconnection signals in the rainfall and circulation fields would be preferred for the study of the likely future rainfall changes, and for use in impact studies over the region.

3. It gives information to the modeling community about the strengths and weakness of the models, which help them to further improve their models in future.

4. It offers significant insights into the future rainfall changes associated with ENSO and IOD over the region. Given the potential impact of climate change on climate variability at regional scales, the future rainfall changes associated with ENSO and IOD provided in this study may be used to help inform major investment decisions and to enhance climate change related policy in the region relating to long-term water management.

1.5 Study region

The study focuses over Eastern Africa region or an area between 22^oE to 52^oE and 12^oS to 18^oN. The region comprises countries Kenya, Uganda, Tanzania, Ethiopia, Burundi, Rwanda, Sudan, South Sudan, Eritrea, Djibouti and Somalia. The region is characterized by complex topographical features. These main topographical features that affect the climate of the region include the Rwenzori Mountains, East African highlands, Ethiopian highlands, the Great Rift Valley Lakes (Turkana, Tanganyika and Victoria), Congo forest and the west Indian Ocean sector (Figure 1.1). The Rwenzori Mountains, East African and Ethiopian Highlands played localized role by generating upslope triggering convection, and these regions are generally characterized with high amounts of rainfall. The presence of large inland lakes in the region and their associated circulations also alter the local rainfall patterns. The section below discusses the climate of the region, and large-scale climate forcing mechanisms responsible for the climate variability of the region.

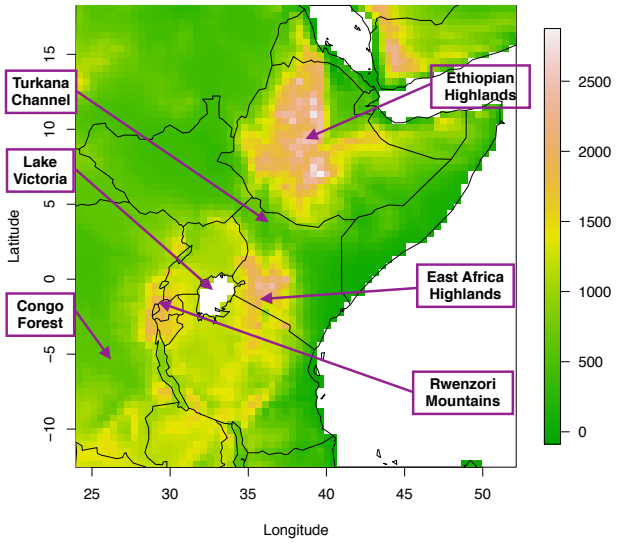

Figure 1.1: Map showing the study region (22^{o}E to 52^{o}E and 16^{o}S to 18^{o}N) and topographic elevation (m). The text in rectangular boxes highlight the important physical features affecting the climate of the region (Ethiopian Highlands, East Africa Highlands, Lake Victoria, Turkana Channel, Congo Forest and Rwenzori Mountains).

1.6 Climate of Eastern Africa and general atmospheric features affecting the region's climate

The East Africa region is one of the most complex climatic regions of the African continent. The climate of the region is controlled by different factors including sub-tropical high pressure areas over the Sahara, South Atlantic and Indian Oceans; the air flow equator-wards from these cells producing the Trade or Monsoon winds; and the Inter-Tropical Convergence Zone (ITCZ). Moreover, the local factors such the high mountains and large lakes have an important role in the climate of the region. For example, the large-scale mountain barriers leads to wetter conditions on the windward slopes of the mountains and drier conditions to the leeward side. Additionally, these features modulate the regional climate by either amplifying or suppressing the large-scale tropical controls. The large-scale tropical controls are superimposed upon regional factors associated with lakes, orography, and the Indian Ocean influence, resulting in complex climatic patterns which change rapidly over short distances (Nicholson, 1996). The ITCZ moves north and south following the sun determine the climatological annual cycle of the regional climate (rainfall). During the boreal summer (June to September) the ITCZ is situated in northern hemisphere while in austral summer (December to February) the ITCZ moves far South over the continental Southern Africa.

Figure 1.2 illustrates the general atmospheric circulation and rain belts over Africa during summer and winter. Most of Eastern Africa is under the influence of monsoons, the south-east monsoon during the northern summer and the north-east monsoon during the northern winter. The north-east monsoon is dry air coming from the desert areas of Arabia without any long sea track. Occasionally, during the north-east monsoon season relatively humid currents from

Atlantic Ocean penetrate the region (Nicholson, 1996). The south-east monsoon is comparatively moist but shallow near the coast. It approaches the coast of south Kenya and Tanzania as Trades from the east-south-east, but splits into two streams when it extends over land. One branch continues westwards across Tanzania as a weak current fanning out north and south over the interior; while the other branch flows northwards parallel to the Somali coast. This separation is caused by the plateau and highlands of Kenya and Ethiopia. One reason for the relative dryness of both monsoons is that they flow more or less parallel to the shore (Nicholson, 1996). In such a situation the frictional contrast between the shore and the water induces subsidence of the air (Bryson and Kuhn, 1961). Another suggested factor for the relative dryness of the both monsoons is that related to Coriolis force, easterly flow which moves equator-wards also tends to sink. As a result, in most of Eastern Africa, rainfall is highest during the transition seasons, when the strongly onshore flow is forced by orography and coastal friction to ascend.

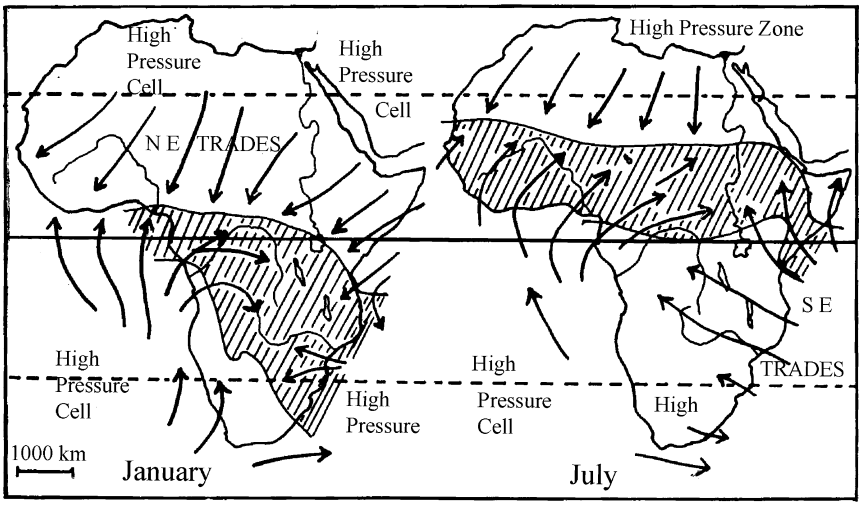

Figure 1.2: General atmospheric circulation and rain belts over Africa in January and July. Cross-hatched areas indicate regions receiving >50 mm of rainfall in January and July (from Boucher (1975)).

Annual cycles

The climatological annual cycle of the regional rainfall is strongly linked to the north-south movement of the inter-tropical convergence zone, where the trade winds converge. In general, Eastern Africa has two major climatological rainfall divisions, the bimodal area and the unimodal area. The northern part of Eastern Africa covering much of Ethiopian highlands and South Sudan is characterized by unimodal rainfall season spanning from June to September (JJAS). The equatorial part covering southern Uganda, Kenya and much of Northern Tanzania including area around Lake Victoria basin and most parts of Burundi and Rwanda has two rainy seasons (March - May and October - December) because of the double passage of the tropical rainbelt. These seasons are commonly known as long rains and short rains, respectively. The southern parts of Eastern Africa region have one rainfall maximum spanning from November to April

(November-April). The influence of ITCZ in modulating Eastern African rainfall is documented more detail in Ogallo et al. (1988) and Jury and Mpeta (2005).

Temporal variability

In the past, numerous studies have been done to understand the causes of seasonal rainfall variability over Eastern Africa. Some consider regional factors such as the position of convergence zones, whereas others consider large-scale factors such as sea surface temperature variability. At interannual time scales, the short rains (OND) has been found to have stronger interannual variability, stronger spatial coherence of rainfall anomalies across a large part of the region and the anomalies are strongly related to large-scale circulation anomalies in the tropical Oceans (Hastenrath et al., 1993; Mutai and Ward, 2000; Philippon et al., 2002). The long rains exhibits much more inconsistent variations from place to place, and are weakly correlated to large-scale climate anomalies (Nicholson, 1996; Camberlin and Philippon, 2002; Camberlin et al., 2009). In recent decades the long rains season has been showing a decline in rainfall totals. Recently, some studies have been done to understand the drivers of the recent downward trend. Lyon and DeWitt (2012) linked the drying with a shift to SSTs in tropical Pacific basin (i.e warmer SSTs over the western topical Pacific and cooler SSTs over the central and eastern tropical Pacific), whereas Williams and Funk (2011) suggest the Indian Ocean warming due to anthropogenic emissions greenhouse gases to be the dominant driver of the recent decline. Lyon (2014), Yang et al. (2014) and Vigaud et al. (2016) supported Lyon and DeWitt (2012)'s argument for a recent decline and recent droughts in MAM season, and emphasized the natural multi-decadal variability of SSTs in the tropical Pacific basin (Lyon, 2014; Yang et al., 2014) and the west/central tropical Pacific gradient (Vigaud et al., 2016). Hoell and Funk (2014) suggest the role of the Indowestern Pacific warm pool for the reduction in rainfall during the long rains. As the OND and MAM seasons, some studies have also attempted to identify the drivers JJAS rainfall variability in the northeastern Africa. It has been indicated that the primary driver of interannual variability of JJAS rainfall is the SST over tropical Oceans (e.g., Camberlin, 1997; Korecha and Barnston, 2007; Segele et al., 2009a; Diro et al., 2011).

Over all, a large percentage of the interannual rainfall variability of Eastern Africa is found to be linked with the global Oceans, particularly SSTs over the Pacific and Indian Ocean. Ropelewski and Halpert (1987), Ogallo et al. (1988) and Indeje et al. (2000) among others have studied the link between the SST over the Pacific and the interannual rainfall variability over Eastern Africa. Mutai et al. (1998), Nicholson and Kim (1997) and Clark et al. (2003) showed the influence of IOD on the variability of short rains over the region. The relationship between ENSO and summer (JJAS) rainfall variability has been investigated in studies by Gissila et al. (2004), Korecha and Barnston (2007), Segele et al. (2009a) and Diro et al. (2011). A brief discussion of the ENSO and IOD events and their influence in Eastern African rainfall is presented in the following subsections.

1.7 Coupled Ocean-atmosphere features and their relation with Eastern Africa rainfall

Tropical Oceans play major roles in the natural variability of the world climate. Anomalous coupled Ocean-atmosphere phenomena generated in the tropical Oceans produce global atmospheric and Oceanic circulation changes that influence regional climate conditions even in remote regions. ENSO and IOD are the two dominant modes of climate variability over the tropics controlling Eastern Africa rainfall at inter-annual time scales (Saji et al., 1999; Indeje et al., 2000; Ummenhofer et al., 2009).

Background to El Niño/Southern Oscillation (ENSO)

ENSO is a coupled Ocean-atmosphere phenomenon in the tropical Pacific which affects the weather and climate patterns around the globe. It occurs at intervals of 2 to 7 years. It is characterized by warming or cooling of surface waters in the tropical Eastern Pacific Ocean. The warming phase is known as El Niño and the cooling phase as La Niña. The Southern Oscillation, the index of the atmospheric component, is characterized by a see-saw in atmospheric pressure between the western and Eastern regions of the Pacific Ocean.

Under normal conditions, the air pressure over the cold waters off the coast of Peru/South America is high relative to the western Pacific Ocean where, over warm water, air pressure is very low. As a result, the trade winds over the Pacific Ocean move strongly from east to west. The easterly flow of the trade winds carries warm surface waters westward, bringing convective storms to Indonesia and Australia. During El Niño, however, air pressure drops over large areas of the central and along the coast of South America. The normal low pressure system is replaced by a weak high in the western Pacific (the southern oscillation). This change in pressure pattern causes easterly trade winds to collapse or even reverse. When the trade winds collapse, they release waves of warm water that move west to east across the Pacific Ocean, to accumulate warm Ocean water along the coastlines of Peru and Ecuador. This accumulation of warm water causes the thermocline to drop in the Eastern part of Pacific Ocean which cuts off the upwelling of cold deep Ocean water along the coast of Peru. The wet weather conditions normally present over the western Pacific moves to the east, and the arid conditions of the Peruvian coast appear in the west. As this happens, the changes in atmospheric circulation are not confined to the Tropics but extend globally and influence the jet streams and storm tracks in mid latitudes. La Niña, in general, is the intensification of normal conditions characterized by unusually cool Ocean temperatures in the central and Eastern tropical Pacific. The trade winds become extremely strong and an abnormal accumulation of cold water can occur in the central and Eastern Pacific.

ENSO is a coupled phenomenon that would not occur without interactions between the atmosphere and Ocean. Bjerknes (1969) recognized that El Niño is not just an Oceanic phenomenon and found a close connection between El Niño and the Southern Oscillation. He hypothesized that warm waters of El Niño and the pressure seasaw of Walkers Southern Oscillation are part

and parcel of the same phenomenon. Changes in the Ocean induce changes in the atmosphere and the latter feedback to the Ocean. In support of Bjerknes idea, Gill (1980) and Lindzen and Nigam (1987) indicated that an initial positive SST anomaly in the equatorial eastern Pacific reduces the east-west SST gradient and hence the strength of the Walker circulation, resulting in weaker trade winds around the equator. The weaker trade winds in turn drive the Ocean circulation changes that further reinforce the SST anomaly. This positive Ocean-atmosphere feedback leads the equatorial Pacific to a warm state known as El Niño.

Current theories on ENSO mechanisms generally grouped into two different frameworks, (1) a self-sustained, unstable, and naturally oscillatory mode of the coupled Ocean-atmosphere system with its timescale determined by the recharge and discharge of the equatorial upper-Ocean heat content (Zebiak and Cane, 1987; Jin, 1997; Meinen and McPhaden, 2000) (2) a stable (or damped) mode with each event triggered by with stochastic forcing or atmospheric noise, especially the westerly wind bursts in the tropical western Pacific (Moore and Kleeman, 1999; Lengaigne et al., 2004; Kessler, 2002). In both views, ENSO involves the positive Ocean-atmosphere feedback over the eastern tropical Pacific hypothesized by Bjerknes (1969).

Different methods are used to measure and monitor ENSO (i.e. to indicate whether it is an El Niño or La Ninã year or neither). The Southern Oscillation Index (SOI) is one of the earliest indicators of the the state of ENSO, and is obtained by calculating the difference in atmospheric surface pressure anomalies between Tahiti and Darwin. During El Niño, the pressure becomes below average in Tahiti and above average in Darwin, and the Southern Oscillation Index is negative. During La Niña, the pressure behaves oppositely, and the index becomes positive. The most widely used measure of the magnitude and state of ENSO is the sea surface temperature averaged over a specific region of the Pacific Ocean, such as the Ninõ3 (150^o W to 90^oW and 5^oS to 5^oN) and Niño3.4 region (170^oW to 120^oW and 5^oS to 5^oN). Outgoing longwave radiation (which indicates the extent of convection - thunderstorm activity) and wind indexes are also the other indicators for monitoring ENSO.

ENSO is known to be the largest source of inter-annual climatic variability in tropical regions and also outside the tropics (Ropelewski and Halpert, 1987; Yasunari, 1987; Van Oldenborgh et al., 2005). Both El Niño and La Niña events disrupt the normal patterns of tropical precipitation and atmospheric circulation, and have widespread impacts on climate in many parts of the world accompanied by the associated climate-related risks. Numerous studies have been done for investigating the effects of ENSO on climate (temperature, rainfall, climate extremes etc.) throughout the world. Once developed, El Niños are known to shift temperature and precipitation patterns in many different regions of the world. These shifts, although varying somewhat from one El Niño to the next, are fairly consistent in the some regions. The wide-ranging influence of ENSO has attracted the attention of the global change community, particularly due to the well-documented economic and cultural impacts (e.g., Adams et al., 1999), both today and throughout historical times, recorded locally and globally. Figure 1.3 show the global influence of ENSO in changing the precipitation and temperature patterns.

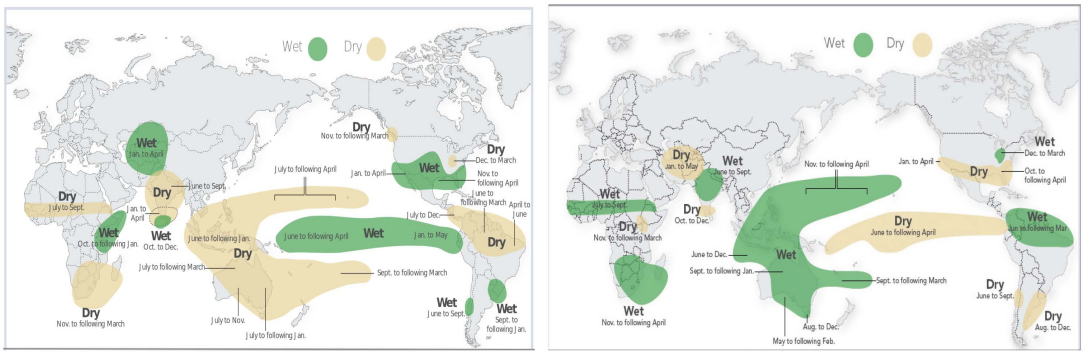

Figure 1.3: Schematic diagram showing global influence of El Niño and La Niña in changing the precipitation and temperature patterns. (Source: https://www2.ucar.edu/atmosnews).

The influence of ENSO on Eastern Africa rainfall

The ENSO phenomenon is known to have significant impacts over Eastern Africa, even though its influence shows distinct regional and inter-event variations. Several works have been carried out in an attempt to understand the link between ENSO and seasonal rainfall variability over Eastern Africa. Some of these studies concentrate on equatorial part of Eastern Africa in which rainfall has bi-modal peaks (MAM and OND). Others concentrate on northern part of Eastern Africa, where JJAS is the main rainfall season. As has been discussed above, the short rains (OND) have been found to have stronger interannual variability and strongly linked to large-scale circulation anomalies in the tropical Oceans, whereas the response of the long rains to SSTs is weaker. Studies by Ropelewski and Halpert (1987), Flohn (1987), Ogallo et al. (1988), Hastenrath et al. (1993), Indeje et al. (2000) and others have demonstrated a relationship between Eastern African short rainfall and the El Niño-Southern Oscillation (ENSO) phenomenon. These studies showed that warm events of ENSO (El Niños) are associated with above average rainfall and cold events of ENSO (La Niñas) are associated with below average rainfall during the short rains. The influence of ENSO over the northern part of the region during JJAS is opposite in sign. Observational and modeling studies by Folland et al. (1986), Diro et al. (2011), Gissila et al. (2004) and Segele et al. (2009a) have all showed that Ethiopian summer (JJAS) rainfall is dominantly controlled by the ENSO phenomenon. All these studies have indicated that Ethiopian summer rainfall is negatively associated with Eastern Pacific SST. This means that excess rainfall tends to occur when there is a La Niña, and deficit rainfall when there is an El Niño. Even though the influence of ENSO on Eastern African rainfall is clear, the potential physical mechanisms that could be responsible for the rainfall anomalies during warm and cold ENSO events are not yet well understood.

Background to Indian Ocean Dipole (IOD)

Like the Pacific Ocean, the Indian Ocean also shows the interannual climate variability. The coupled Oceanatmosphere phenomenon that occurs inter-annually in the tropical parts of the

Indian Ocean is called the Indian Ocean dipole (IOD). IOD was identified recently (in 1999) by scientists working in the Climate Variations Program of Frontier Research System for Global Change of the Japan Marine Science and Technology Centre (JAMSTEC). It is characterized by anomalous cooling of SST in the south Eastern equatorial Indian Ocean and anomalous warming of SST in the western equatorial Indian Ocean (Saji et al., 1999). A positive IOD period is characterized by cooler than normal water in the tropical Eastern Indian Ocean and warmer than normal water in the tropical western Indian Ocean. In the positive phase, the wind blows from east to west, and the warm water is moved to Africa. Associated with these changes the normal convection situated over the Eastern Indian Ocean warm pool shifts to the west and brings heavy rainfall over the east Africa and severe droughts over the Indonesian and southern Australia region. Conversely, a negative IOD period is characterized by warmer than normal water in the tropical Eastern Indian Ocean and cooler than normal water in the tropical western Indian Ocean. In the negative phase its winds move from west to east piling up the warm water along the coast and the moisture laden associated winds carry belts of cloud over southern Australia. Hence, a negative IOD SST pattern has been shown to be associated with an increase in rainfall over parts of southern Australia.

Different studies suggested that IOD is a coupled phenomenon and it is found independent of ENSO. Saji et al. (1999) indicated that the IOD is a coupled Ocean atmosphere phenomenon, it is independent of ENSO and about 12% of the SST variability in the Indian Ocean was associated with the dipole mode. They recognized anomalous conditions such as in 1961, 1994 and 1997 in the tropical Indian Ocean as a dipole mode characterized by low SST off Sumatra and high SST in the western equatorial Indian Ocean accompanied by wind and rainfall anomalies. Webster et al. (1999) suggested that a coupled Ocean atmosphere process in which Oceanic Rossby waves cause a deepening of the thermocline is a necessary feature that led to the sequence of events culminating in anomalies that contrast the in east-west direction. The propagation of baroclinic Kelvin and Rossby waves excited by anomalous winds, play an important role in the development of SST anomalies associated with the IOD (Vinayachandran et al., 2009). Recent study by Wang et al. (2016) demonstrated that cold (warm) sea surface temperature (SST) anomalies in the eastern Indian Ocean associated with IOD can be initiated by springtime Indonesian rainfall deficit (surplus) through local surface wind response. Overall, the Ocean-atmosphere coupling during an IOD involves different atmospheric and Oceanic processes such as atmospheric convection, winds, SST and upper Ocean dynamics.

The IOD is commonly measured by an index that is the difference between sea surface temperature (SST) in the western (50^oE to 70^oE and 10^oS to 10^oN) and Eastern (90^oE to 110^oE and 10^oS to 0^oS) equatorial Indian Ocean. The index is called the Dipole Mode Index (DMI).

The influence Indian Ocean Dipole (IOD) on Eastern Africa rainfall

Like ENSO, the IOD has been found to affect rainfall in many countries over the Indian Ocean region and beyond. The influence of the Indian Ocean to the variability of Eastern African

climate has received much attention in recent years. It is not only the warm water push more moisture onto the region, it also alter the position of the jet streams and other wind patterns. Several studies including Latif et al. (1999), Behera et al. (2003), Clark et al. (2003), Saji and Yamagata (2003), Black et al. (2003), Behera et al. (2005), Yamagata et al. (2004), and Marchant et al. (2007) have investigated the relationship between Eastern Africa rainfall and the SST over the Indian Ocean. Almost of all these studies focused on the influence IOD during short rainfall season (OND) as this is the season that experiences a larger degree of interannual variability relative to climatology, and found that there is a strong relationship between IOD and OND rainfall. The positive phase of IOD is associated with above normal rainfall, and the negative phase of IOD is associated with below normal rainfall. The December-January 1997/1998 rainfall anomalies that led to severe flooding in much of east Africa has been strongly linked to changes in the Indian Oceans SST (Latif et al., 1999).

Relationship between IOD and ENSO

It has been known that the Indian Ocean is characterized by several interacting processes, and one of the fundamental features is that its relationship with ENSO. Since the discovery of the IOD, there has been a strong debate concerning the relationship between the IOD and ENSO. Some authors (e.g., Black et al., 2003) argued that the IOD should not be viewed as being independent of ENSO, whereas others (e.g., Saji et al., 1999; Saji and Yamagata, 2003; Yamagata et al., 2004; Behera et al., 2005) recognize IOD independent of ENSO, as an inherent Ocean atmosphere coupled mode. It has been found that some of the IOD events occur in conjunction with ENSO but others develop as a consequence of intrinsic variations of the tropical Indian Ocean (e.g., Meyers et al., 2007). Pfeiffer and Dullo (2006), following the high resolution analysis of coral index, indicate that the El Niño index is strongly correlated with Indian Ocean SSTs over the past 150 years; supporting the notion that the ENSO strongly influences the Indian Ocean. On the other hand, Behera et al. (2006) using state of the art coupled GCM experiments, demonstrated that the IOD could evolve independently of ENSO. Annamalai et al. (2005) showed that ENSO variability is found to affect the strength, periodicity and formation processes of the IOD in the years of co-occurrence. However, Luo et al. (2008) indicated that the IOD could also influence the development of ENSO so the relation between ENSO and IOD is not fully understood, and one reason for this is the complexity of the system and the interplay between atmospheric and Oceanic circulation.

1.8 CORDEX-Africa domain and simulations

Figure 1.4 shows the CORDEX-Africa domain with the topography (m). The domain covers approximately the region from about 24.64^{o}W to 60.28^{o}E longitude and 45.76^{o}S to 42.24^{o}N latitude. This domain is common to all groups participating to the CORDEX-Africa initiative. Both the present day and future simulations are performed at 0.44-degree (50-km) resolution

over the same CORDEX Africa domain (Figure 1.4). For the evaluation period (1989 2008), the RCMs used boundary conditions from the ERA-Interim reanalysis (Dee et al., 2011). The simulations of the historical and future climate change downscale the results of CGCMs from the CMIP5 climate projections. The CMIP5 CGCM historical simulations are forced by observed natural and anthropogenic atmospheric composition, and cover the period from 1950 until 2005. The CMIP5 simulations of the future span the period from 2006 to 2100 and are forced by Representative Concentration Pathways, which are based on radiative forcings (globally radiative energy imbalance) by the year 2100 (Moss et al., 2010).

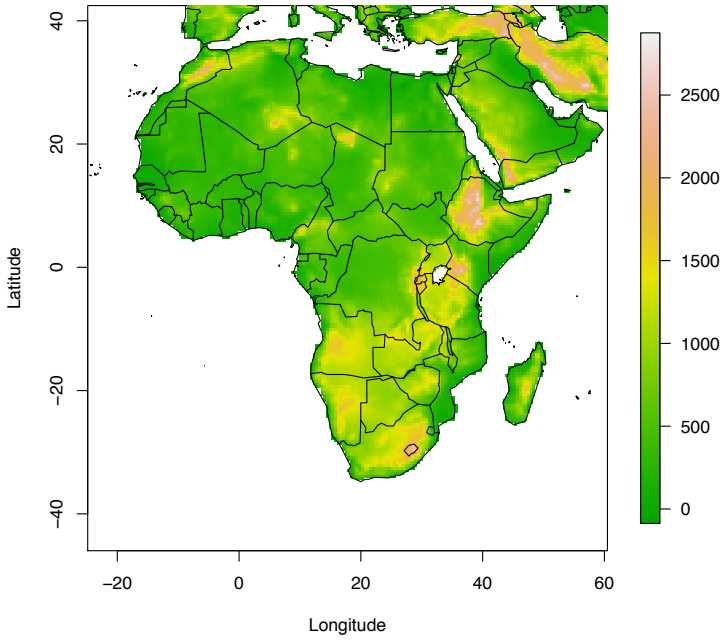

Figure 1.4: The cordex-Africa domain with the topography (m).

1.9 Thesis outline

This thesis builds on the work presented in three papers which together address the proposed research questions. The first paper evaluates the performance of 10 RCMs driven by reanalysis data in simulating the characteristics of rainfall patterns over Eastern Africa. In this work, results showed that most RCMs reasonably simulate the main features of the rainfall climatology over the region, and in most of the areas and time periods, the multimodel ensemble mean outperforms the results of individual models, even the forcing ERA-Interim. This work has been published in Journal of Climate as Endris et al. 2013. The second paper examines the performance of two RCMs, with lateral and surface boundary conditions derived from CGCMs, in simulating the teleconnection between tropical SSTs and rainfall over Eastern Africa. The study showed that RCMs are capable of reproducing the observed teleconnective SST-rainfall patterns. It also demonstrated that most errors in simulating the regional teleconnection patterns arise mainly from the driving GCMs. This work has been published in Climate Dynamics as Endris et al. 2015. The third paper assesses the future projections to investigate whether or not the current teleconnection patterns persists under a warming scenario. The results indicate that the teleconnections between ENSO/IOD and rainfall are stronger over Eastern horn of Africa compared to the present and the ENSO/IOD signal is weaker over the southern part of the region. This work has been submitted to Climate Dynamics and it is under review now. Between each paper is a synopsis and text to provide the cohesive storyline of the work. Finally a summary of the findings and conclusions are presented.

1.10 References

Adams, R. M., Chen, C.-C., McCarl, B. A., and Weiher, R. F. (1999). The economic consequences of enso events for agriculture. *Climate Research*, 13(3):165–172.

Annamalai, H., Xie, S., McCreary, J., and Murtugudde, R. (2005). Impact of indian ocean sea surface temperature on developing el niño*. *Journal of Climate*, 18(2):302–319.

Anyah, R. and Semazzi, F. (2004). Simulation of the sensitivity of lake victoria basin climate to lake surface temperatures. *Theoretical and applied climatology*, 79(1):55–69.

Anyah, R., Semazzi, F., and Xie, L. (2006). Simulated physical mechanisms associated with climate variability over lake victoria basin in east africa. *Monthly weather review*, 134(12):3588–3609.

Anyah, R. O. and Semazzi, F. H. (2007). Variability of east african rainfall based on multiyear regcm3 simulations. *International Journal of Climatology*, 27(3):357–371.

Behera, S., Luo, J., Masson, S., Delecluse, P., Gualdi, S., Navarra, A., and Yamagata, T. (2005). Paramount impact of the indian ocean dipole on the east african short rains: A cgcm study. *Journal of Climate*, 18(21):4514–4530.

Behera, S., Luo, J., Masson, S., Rao, S., Sakuma, H., and Yamagata, T. (2006). A cgcm study on the interaction between iod and enso. *Journal of climate*, 19(9):1688–1705.

Behera, S., Luo, J., Masson, S., Yamagata, T., Delecluse, P., Gualdi, S., and Navarra, A. (2003). Impact of the indian ocean dipole on the east african short rains: A cgcm study. *CLIVAR exchanges*, 27:43–45.

Birkett, C., Murtugudde, R., and Allan, T. (1999). Indian ocean climate event brings floods to east africa's lakes and the sudd marsh. *Geophysical Research Letters*, 26(8):1031–1034.

Bjerknes, J. (1969). Atmospheric teleconnections from the equatorial pacific 1. *Monthly Weather Review*, 97(3):163–172.

Black, E., Slingo, J., and Sperber, K. (2003). An observational study of the relationship between excessively strong short rains in coastal east africa and indian ocean sst. *Monthly Weather Review*, 131(1):74–94.

Boucher, K. (1975). *Global climate*. New York: Halsted Press.

Boulanger, J., Brasseur, G., Carril, A., et al. (2010). A europe-south america network for climate change assessment and impact studies. *Climate Change*, 98(3–4):307–329.

Bryson, R. A. and Kuhn, P. M. (1961). Stressdifferential induced divergence with application to littoral precipitation (durch beanspruchungsdifferenzial hervorgerufene divergenz in ihrer anwendung auf niederschläge an küsten). *Erdkunde*, pages 287–294.

Camberlin, P. (1997). Rainfall anomalies in the source region of the nile and their connection with the indian summer monsoon. *Journal of Climate*, 10(6):1380–1392.

Camberlin, P., Moron, V., Okoola, R., Philippon, N., and Gitau, W. (2009). Components of rainy seasons variability in equatorial east africa: onset, cessation, rainfall frequency and intensity. *Theoretical and applied climatology*, 98(3-4):237–249.

Camberlin, P. and Philippon, N. (2002). The east african march-may rainy season: Associated atmospheric dynamics and predictability over the 1968-97 period. *Journal of Climate*, 15(9):1002–1019.

Clark, C., Webster, P., and Cole, J. (2003). Interdecadal variability of the relationship between the indian ocean zonal mode and east african coastal rainfall anomalies. *Journal of Climate*, 16(3):548–554.

Dee, D., Uppala, S., Simmons, A., Berrisford, P., Poli, P., Kobayashi, S., Andrae, U., Balmaseda, M., Balsamo, G., Bauer, P., et al. (2011). The era-interim reanalysis: Configuration and performance of the data assimilation system. *Quarterly Journal of the Royal Meteorological Society*, 137(656):553–597.

Denis, B., Laprise, R., Caya, D., and Cote, J. (2002). Downscaling ability of one-way nested regional climate models: the big-brother experiment. *Climate Dynamics*, 18(8):627–646.

Devereux, S. and Berge, K. (2000). *Famine in the twentieth century*, volume 105. Institute of Development Studies Brighton.

Di Luca, A., de Elia, R., and Laprise, R. (2012). Potential for added value in precipitation simulated by high-resolution nested regional climate models and observations. *Climate dynamics*, 38(5-6):1229–1247.

Diro, G., Grimes, D., and Black, E. (2011). Teleconnections between ethiopian summer rainfall and sea surface temperature: part iobservation and modelling. *Climate dynamics*, 37(1):103–119.

Diro, G., Tompkins, A., and Bi, X. (2012). Dynamical downscaling of ecmwf ensemble seasonal forecasts over east africa with regcm3. *Journal of Geophysical Research: Atmospheres*, 117(D16).

Evans, J. (2011). Cordex–an international climate downscaling initiative. In *19th International Congress on Modelling and Simulation, Perth, Australia, 12–16 December 2011.*

Flohn, H. (1987). Rainfall teleconnections in northern and northeastern africa. *Theoretical and applied climatology*, 38(4):191–197.

Folland, C., Palmer, T., and Parker, D. (1986). Sahel rainfall and worldwide sea temperatures, 1901–85. *Nature*, 320(6063):602–607.

Gill, A. (1980). Some simple solutions for heat-induced tropical circulation. *Quarterly Journal of the Royal Meteorological Society*, 106(449):447–462.

Giorgi, F., Christensen, J., Hulme, M., Von Storch, H., Whetton, P., Jones, R., Mearns, L., Fu, C., Arritt, R., Bates, B., et al. (2001). Regional climate information-evaluation and projections. *Climate Change 2001: The Scientific Basis. Contribution of Working Group to the Third Assessment Report of the Intergouvernmental Panel on Climate Change [Houghton, JT et al.(eds)]. Cambridge University Press, Cambridge, United Kongdom and New York, US.*

Giorgi, F., Jones, C., Asrar, G., et al. (2009). Addressing climate information needs at the regional level: the cordex framework. *World Meteorological Organization (WMO) Bulletin*, 58(3):175.

Giorgi, F. and Mearns, L. (1991). Approaches to the simulation of regional climate change: a review. *Reviews of Geophysics*, 29(2):191–216.

Giorgi, F. and Mearns, L. (1999). Introduction to special section: Regional climate modeling revisited. *Journal of Geophysical Research*, 104(D6):6335–6352.

Gissila, T., Black, E., Grimes, D., and Slingo, J. (2004). Seasonal forecasting of the ethiopian summer rains. *International Journal of Climatology*, 24(11):1345–1358.

Hastenrath, S., Nicklis, A., and Greischar, L. (1993). Atmospheric-hydrospheric mechanisms of climate anomalies in the western equatorial indian ocean. *Journal of Geophysical Research*, 98(C11):20219–20.

Hewitson, B. and Crane, R. (1996). Climate downscaling techniques and application. *climate research*, 7:85–95.

Hewitt, C. and Director, E. (2005). The ensembles project. *EGU Newslett*, 13:22–25.

Hoell, A. and Funk, C. (2014). Indo-pacific sea surface temperature influences on failed consecutive rainy seasons over eastern africa. *Climate dynamics*, 43(5-6):1645–1660.

Indeje, M., Semazzi, F., Ogallo, L., et al. (2000). Enso signals in east african rainfall seasons. *International Journal of Climatology*, 20(1):19–46.

IPCC, I. (2007). Climate change 2007: the physical science basis. *Agenda*, 6:07.

IPCC, I. (2014). Climate change 2014: Synthesis report. contribution of working groups i, ii and iii to the fifth assessment report of the intergovernmental panel on climate change. *IPCC*.

Jin, F.-F. (1997). An equatorial ocean recharge paradigm for enso. part i: Conceptual model. *Journal of the Atmospheric Sciences*, 54(7):811–829.

Johnson, A. I. (1996). *Limnology, climatology and paleoclimatology of the East African lakes*. CRC Press.

Jury, M. and Mpeta, E. (2005). The annual cycle of african climate and its variability. *Water SA*, 31(1):1–8.

Kessler, W. S. (2002). Is enso a cycle or a series of events? *Geophysical Research Letters*, 29(23).

Korecha, D. and Barnston, A. G. (2007). predictability of june-september rainfall in ethiopia. *Monthly weather review*, 135(2):628–650.

Latif, M., Dommenget, D., Dima, M., and Grötzner, A. (1999). The role of indian ocean sea surface temperature in forcing east african rainfall anomalies during december-january 1997/98. *Journal of Climate*, 12(12):3497–3504.

Lengaigne, M., Guilyardi, E., Boulanger, J.-P., Menkes, C., Delecluse, P., Inness, P., Cole, J., and Slingo, J. (2004). Triggering of el nino by westerly wind events in a coupled general circulation model. *Climate Dynamics*, 23(6):601–620.

Lindzen, R. S. and Nigam, S. (1987). On the role of sea surface temperature gradients in forcing low-level winds and convergence in the tropics. *Journal of the Atmospheric Sciences*, 44(17):2418–2436.

Luo, J.-J., Behera, S., Masumoto, Y., Sakuma, H., and Yamagata, T. (2008). Successful prediction of the consecutive iod in 2006 and 2007. *Geophysical Research Letters*, 35(14).

Lyon, B. (2014). Seasonal drought in the greater horn of africa and its recent increase during the march–may long rains. *Journal of Climate*, 27(21):7953–7975.

Lyon, B. and DeWitt, D. G. (2012). A recent and abrupt decline in the east african long rains. *Geophysical Research Letters*, 39(2).

Marchant, R., Mumbi, C., Behera, S., and Yamagata, T. (2007). The indian ocean dipole–the unsung driver of climatic variability in east africa. *African Journal of Ecology*, 45(1):4–16.

Meinen, C. S. and McPhaden, M. J. (2000). Observations of warm water volume changes in the equatorial pacific and their relationship to el niño and la niña. *Journal of Climate*, 13(20):3551–3559.

Meyers, G., McIntosh, P., Pigot, L., and Pook, M. (2007). The years of el niño, la niña, and interactions with the tropical indian ocean. *Journal of Climate*, 20(13):2872–2880.

Moore, A. M. and Kleeman, R. (1999). Stochastic forcing of enso by the intraseasonal oscillation. *Journal of Climate*, 12(5):1199–1220.

Moss, R. H., Edmonds, J. A., Hibbard, K. A., Manning, M. R., Rose, S. K., Van Vuuren, D. P., Carter, T. R., Emori, S., Kainuma, M., Kram, T., et al. (2010). The next generation of scenarios for climate change research and assessment. *Nature*, 463(7282):747–756.

Mutai, C., Ward, M., and Colman, A. (1998). Towards the prediction of the east africa short rains based on sea-surface temperature–atmosphere coupling. *International Journal of Climatology*, 18(9):975–997.

Mutai, C. C. and Ward, M. N. (2000). East african rainfall and the tropical circulation/convection on intraseasonal to interannual timescales. *Journal of Climate*, 13(22):3915–3939.

Nicholson, S. (1996). A review of climate dynamics and climate variability in eastern africa. *The limnology, climatology and paleoclimatology of the East African lakes*, pages 25–56.

Nicholson, S. and Kim, J. (1997). The relationship of the el nino-southern oscillation to african rainfall. *International Journal of Climatology*, 17(2):117–135.

Nikulin, G., Jones, C., Giorgi, F., Asrar, G., Buchner, M., Cerezo-Mota, R., Christensen, O. B., Deque, M., Fernandez, J., Hansler, A., et al. (2012). Precipitation climatology in an ensemble of cordex-africa regional climate simulations. *Journal of Climate*, 25(18):6057–6078.

Nyakwada, W. (2009). Predictability of east african seasonal rainfall with sea surface temperature gradient modes. *Ph.D. Dissertation, Dept. of Met: University of Nairobi*.

Odingo, R. S. (1962). Abnormal and unseasonal rains in east africa. *Geographical Review*, 52(3):440–442.

Ogallo, L., Janowiak, J., and Halpert, M. (1988). Teleconnection between seasonal rainfall over east africa and global sea surface temperature anomalies. *Journal of the Meteorological Society of Japan JMSJAU*, 66(6).

Ogwang, B. A., Chen, H., Li, X., and Gao, C. (2015a). Evaluation of the capability of regcm4. 0 in simulating east african climate. *Theoretical and Applied Climatology*, pages 1–11.

Ogwang, B. A., Chen, H., Tan, G., Ongoma, V., and Ntwali, D. (2015b). Diagnosis of east african climate and the circulation mechanisms associated with extreme wet and dry events: a study based on regcm4. *Arabian Journal of Geosciences*, 8(12):10255–10265.

Omondi, P., Ogallo, L., Anyah, R., Muthama, J., and Ininda, J. (2012). Linkages between global sea surface temperatures and decadal rainfall variability over eastern africa region. *International Journal of Climatology*.

Paulsen, S. et al. (2009). A regional climate change assessment program for north america. *Eos*, 90(36).

Pfeiffer, M. and Dullo, W. (2006). Monsoon-induced cooling of the western equatorial indian ocean as recorded in coral oxygen isotope records from the seychelles covering the period of 1840–1994ad. *Quaternary Science Reviews*, 25(9):993–1009.

Philippon, N., Camberlin, P., and Fauchereau, N. (2002). Empirical predictability study of october–december east african rainfall. *Quarterly Journal of the Royal Meteorological Society*, 128(585):2239–2256.

Ropelewski, C. and Halpert, M. (1987). Global and regional scale precipitation patterns associated with the el niño/southern oscillation. *Monthly Weather Review*, 115(8):1606–1626.

Rowell, D. P., Booth, B. B., Nicholson, S. E., and Good, P. (2015). Reconciling past and future rainfall trends over east africa. *Journal of Climate*, 28(24):9768–9788.

Rummukainen, M. (2009). State-of-the-art with regional climate models. *Wiley Interdisciplinary Reviews: Climate Change*, 1(1):82–96.

Rusticucci, M. and Barrucand, M. (2004). Observed trends and changes in temperature extremes over argentina. *Journal of Climate*, 17(20):4099–4107.

Saji, N., Goswami, B., Vinayachandran, P., and Yamagata, T. (1999). A dipole mode in the tropical indian ocean. *Nature*, 401:360–363.

Saji, N. and Yamagata, T. (2003). Structure of sst and surface wind variability during indian ocean dipole mode events: Coads observations*. *Journal of climate*, 16(16):2735–2751.

Segele, Z. T., Lamb, P. J., and Leslie, L. M. (2009a). Large-scale atmospheric circulation and global sea surface temperature associations with horn of africa june–september rainfall. *International Journal of Climatology*, 29(8):1075–1100.

Segele, Z. T., Leslie, L. M., and Lamb, P. J. (2009b). Evaluation and adaptation of a regional climate model for the horn of africa: rainfall climatology and interannual variability. *International Journal of Climatology*, 29(1):47–65.

Shongwe, M., Van Oldenborgh, G., Van Den Hurk, B., De Boer, B., Coelho, C., and Van Aalst, M. (2009). Projected changes in mean and extreme precipitation in africa under global warming. part i: Southern africa. *Journal of climate*, 22(13):3819–3837.

Song, Y., Semazzi, F., Xie, L., and Ogallo, L. (2004). A coupled regional climate model for the lake victoria basin of east africa. *International journal of climatology*, 24(1):57–75.

Stouffer, R., K.E.Taylor, and Meehl, G. (2011). Cmip5 long-term experimental design. *CLIVAR Exchanges*, 56:5–7.

Sun, L., Semazzi, F. H., Giorgi, F., and Ogallo, L. (1999a). Application of the ncar regional climate model to eastern africa: 1. simulation of the short rains of 1988. *Journal of Geophysical Research: Atmospheres*, 104(D6):6529–6548.

Sun, L., Semazzi, F. H., Giorgi, F., and Ogallo, L. (1999b). Application of the ncar regional climate model to eastern africa: 2. simulation of interannual variability of short rains. *Journal of Geophysical Research: Atmospheres*, 104(D6):6549–6562.

Taylor, K. E., Stouffer, R. J., and Meehl, G. A. (2012). An overview of cmip5 and the experiment design. *Bulletin of the American Meteorological Society*, 93(4):485–498.

Ummenhofer, C. C., Sen Gupta, A., England, M. H., and Reason, C. J. (2009). Contributions of indian ocean sea surface temperatures to enhanced east african rainfall. *Journal of Climate*, 22(4):993–1013.

UNOCHA (2011). Eastern africa drought. humanitarian rep. 4, united nations organization for the coordination of human- itarian affairs, 10 pp.

Van Oldenborgh, G. J., Philip, S., and Collins, M. (2005). El nino in a changing climate: a multi-model study. *Ocean Science*, 1(2):81–95.

Vigaud, N., Lyon, B., and Giannini, A. (2016). Sub-seasonal teleconnections between convection over the indian ocean, the east african long rains and tropical pacific surface temperatures. *International Journal of Climatology*.

Vinayachandran, P., Francis, P., and Rao, S. (2009). Indian ocean dipole: processes and impacts. *Current trends in science*, pages 569–589.

Wang, H., Murtugudde, R., and Kumar, A. (2016). Evolution of indian ocean dipole and its forcing mechanisms in the absence of enso. *Climate Dynamics*, 47(7-8):2481–2500.

Wang, Y., Leung, L., Mcgregor, J., Lee, D., Wang, W., Ding, Y., and Kimura, F. (2004). Regional climate modeling: Progress, challenges, and prospects. *J Meteor Soc Japan*, 82(6):1599–1628.

Webster, P. J., Moore, A. M., Loschnigg, J. P., and Leben, R. R. (1999). Coupled ocean–atmosphere dynamics in the indian ocean during 1997–98. *Nature*, 401(6751):356–360.

Wilby, R., Charles, S., Zorita, E., Timbal, B., Whetton, P., and Mearns, L. (2004). Guidelines for use of climate scenarios developed from statistical downscaling methods. *TGICA IPCC August*.

Williams, A. P. and Funk, C. (2011). A westward extension of the warm pool leads to a westward extension of the walker circulation, drying eastern africa. *Climate Dynamics*, 37(11-12):2417–2435.

Yamagata, T., Behera, S., Luo, J., Masson, S., Jury, M., Rao, S., et al. (2004). Coupled ocean-atmosphere variability in the tropical indian ocean. *Earth Climate: The Ocean–Atmosphere Interaction, Geophys. Monogr*, 147:189–211.

Yang, W., Seager, R., Cane, M. A., and Lyon, B. (2014). The east african long rains in observations and models. *Journal of Climate*, 27(19):7185–7202.

Yasunari, T. (1987). Global structure of the el nino/southern oscillation. part i. el nino composites. *J. Meteor. Soc. Japan*, 65:67–79.

Zebiak, S. E. and Cane, M. A. (1987). A model el niñ–southern oscillation. *Monthly Weather Review*, 115(10):2262–2278.

2

Evaluation of reanalysis-driven simulations

This paper evaluates the ability of RCMs to simulate the important climate features over Eastern Africa when driven by reanalysis data, so-called "perfect boundary conditions'. This is an important first step to know the fidelity of RCMs in reproducing current climate of the region before analyzing climate change projections. The ability of the models to simulate the present climate is a necessary condition to use models to project climate changes. Model projections cannot be credible if models are not able to reproduce the current climate adequately. An assessment of the performance of 10 RCM simulations forced by the same lateral boundary conditions from the ERA-Interim reanalyses for the period 1990 - 2008 is presented in this analysis. The ability of models to reproduce the seasonal climatology rainfall, the annual cycle of rainfall, the inter-annual variability of rainfall as well as the representation of the large-scale climate forcing signals over Eastern Africa is compared with different gridded observational datasets as well as the driving ERA-Interim reanalysis. The results from this paper provide the basis from which to assess the impact of forcing on the regional climate simulations with "imperfect" boundary conditions from coupled global climate models (CGCMs) over Eastern Africa, which is the focus of Chapter 3.

Assessment of the Performance of CORDEX Regional Climate Models in Simulating East African Rainfall

HUSSEN SEID ENDRIS,[a] PHILIP OMONDI,[b] SUMAN JAIN,[c] CHRISTOPHER LENNARD,[a] BRUCE HEWITSON,[a] LADISLAUS CHANG'A,[d] J. L. AWANGE,[e] ALESSANDRO DOSIO,[f] PATRICK KETIEM,[g] GRIGORY NIKULIN,[h] HANS-JÜRGEN PANITZ,[i] MATTHIAS BÜCHNER,[j] FRODE STORDAL,[k] AND LUKIYA TAZALIKA[l]

[a] *University of Cape Town, Cape Town, South Africa*
[b] *IGAD Climate Prediction and Applications Centre, Nairobi, Kenya*
[c] *University of Zambia, Lusaka, Zambia*
[d] *Tanzania Meteorological Agency, Dar es Salaam, Tanzania*
[e] *Western Australian Centre for Geodesy and the Institute for Geoscience Research, Curtin University, Perth, Australia*
[f] *European Commission Joint Research Centre, Institute for Environment and Sustainability, Ispra, Italy*
[g] *Kenya Agricultural Research Institute, Nairobi, Kenya*
[h] *Rossby Centre, Swedish Meteorological and Hydrological Institute, Norrköping, Sweden*
[i] *Institut für Meteorologie und Klimaforschung, and Karlsruher Institut für Technologie, Karlsruhe, Germany*
[j] *Potsdam Institute for Climate Impact Research, Potsdam, Germany*
[k] *University of Oslo, Oslo, Norway*
[l] *Uganda Meteorological Department, Kampala, Uganda*

(Manuscript received 2 October 2012, in final form 7 May 2013)

ABSTRACT

This study evaluates the ability of 10 regional climate models (RCMs) from the Coordinated Regional Climate Downscaling Experiment (CORDEX) in simulating the characteristics of rainfall patterns over eastern Africa. The seasonal climatology, annual rainfall cycles, and interannual variability of RCM output have been assessed over three homogeneous subregions against a number of observational datasets. The ability of the RCMs in simulating large-scale global climate forcing signals is further assessed by compositing the El Niño–Southern Oscillation (ENSO) and Indian Ocean dipole (IOD) events. It is found that most RCMs reasonably simulate the main features of the rainfall climatology over the three subregions and also reproduce the majority of the documented regional responses to ENSO and IOD forcings. At the same time the analysis shows significant biases in individual models depending on subregion and season; however, the ensemble mean has better agreement with observation than individual models. In general, the analysis herein demonstrates that the multimodel ensemble mean simulates eastern Africa rainfall adequately and can therefore be used for the assessment of future climate projections for the region.

1. Introduction

The rainfall pattern over eastern Africa is highly variable both in space and time. The region is already witnessing dire consequences of erratic climatic conditions that are likely to be associated with regional climate change (FEWS NET 2011; Anyah and Qiu 2012). The region experiences serious food insecurity and resource-based conflicts in addition to recurring droughts and floods that have dramatic socioeconomic impacts (UNEP 2011; World Bank 2012). The 2007 Intergovernmental Panel on Climate Change (IPCC) report provided clear evidence of climate change in the region with increased risks of climate extremes. The economies and livelihoods of people in the majority of countries in the region still rely on rain-dependent systems and so are vulnerable to current rainfall variability and potential changes in rainfall due to climate change. Recent economic assessments (World Bank 2012) show that no

Corresponding author address: Hussen Seid Endris, Climate System Analysis Group, University of Cape Town, Cape Town, South Africa.
E-mail: hussen.seid1@gmail.com

DOI: 10.1175/JCLI-D-12-00708.1

TABLE 1. List of RCMs used and their details (Source: Nikulin et al. 2012).

	CNRM Action de Recherche Petite Échelle Grande Échelle (ARPEGE) 5.1	DMI HIRHAM5	ICTP regional climate model version 3 (RegCM3)	CLMcom COSMO-CLM (CCLM) version 4.8
Institute	Centre National de Recherches Météorologiques (CNRM), France	Danmarks Meteorologiske Institut (DMI), Danmark	Abdus Salam International Centre for Theoretical Physics (ICTP), Italy	Climate Limited-Area Modelling (CLM) Community (www.clm-community.eu)
Short name	ARPEGE	HIRHAM	RegCM3	CCLM
Projection resolution	Polar, stretching factor 2 (tl179)	Rotated pole 0.44°	Mercator 50 km	Rotated pole 0.44°
Vertical coordinate/levels	Hybrid/31	Hybrid/31	Sigma/18	Terrain following/35
Advection	Semi-Lagrangian	Semi-Lagrangian	Eulerian	Fifth-order upwind; Baldauf (2008)
Time step (s)	1200	600	100	240
Convective scheme	Bougeault (1985)	Tiedtke (1989)	Grell (1993); Fritsch and Chappell (1980)	Tiedtke (1989)
Radiation scheme	Morcrette (1990)	Fouquart and Bonnel (1980); Mlawer et al. (1997)	Kiehl et al. (1996)	Ritter and Geleyn (1992)
Turbulence vertical diffusion	Mellor and Yamada (1982)	Louis (1979)	Holtslag et al. (1990)	Herzog et al. (2002); Buzzi et al. (2011)
Cloud microphysics scheme	Ricard and Royer (1993)	Tiedtke (1989); Tompkins (2002)	Subgrid explicit moisture scheme (SUBEX); Pal et al. (2000)	Doms et al. (2007); Baldauf and Schulz (2004)
Land surface scheme	ISBA; Douville et al. (2000)	Schulz et al. (1998); Hagemann (2002)	BATS1E; Dickinson et al. (1993)	TERRA-ML; Doms et al. (2007)
Latest reference and comments	Déqué (2010)	Christensen et al. (2006)	Pal et al. (2007)	Rockel et al. (2008); Baldauf et al. (2011)

sustainable development can be attained in the region without effective regional systems for climate risk reduction including climate change adaptation.

Global climate models (GCMs) are suitable tools for the assessment of climate variability and change. Current GCMs have spatial resolution on the order of 100–250 km and have the potential to simulate the main characteristics of general circulation at the range of this scale (Shongwe et al. 2009). Although GCMs can satisfactorily simulate the atmospheric general circulation at the continental scale, they are not necessarily capable of capturing the detailed processes associated with regional–local climate variability and changes that are required for regional and national climate change assessments (Giorgi and Mearns 1999; Denis et al. 2002; Wang et al. 2004; Giorgi et al. 2009; Rummukainen 2010). This is particularly true for heterogeneous regions such as eastern Africa, where sub-GCM gridscale variations in topography, vegetation, soils, and coastlines have a significant effect on the climate. In addition, at coarse grid resolutions, the magnitude and intensity of subgrid-scale extreme events such as heavy rainfall (leading to floods) are often not captured, nor realistically reproduced. Generally, GCM data have been used to describe the climate processes of many African regions and to produce the climate information for applications in different socioeconomic sectors including agriculture, water, and health (Alley et al. 2007). However, in order to formulate adaptation policies in response to climate change impacts, reliable climate change information is usually required at finer spatial scales than that of a typical GCM.

Regional climate models (RCMs) dynamically downscale GCM output to scales more suited to end users (Sun et al. 2006) and are useful for understanding local climate

TABLE 1. (*Extended*)

KNMI Regional Atmospheric Climate Model, version 2.2 (RACMO2.2b)	MPI regional model (REMO)	SMHI Rossby Center Regional Atmospheric Model (RCA35)	UCT Providing Regional Climates for Impacts Studies (PRECIS)	UC Weather Research and Forecasting Model version 3.1.1. (WRF3.1.1)	UQAM fifth-generation Canadian Regional Climate Model (CRCM5)
Koninklijk Nederlands Meteorologisch Instituut (KNMI), Netherlands	Max Planck Institute (MPI), Germany	Sveriges Meteorologiska och Hydrologiska Institut (SMHI), Sweden	University of Cape Town (UCT), South Africa	Universidad de Cantabria, Spain	Université du Québec à Montréal (UQAM), Canada
RACMO	REMO	RCA	PRECIS	WRF	CRCM
Rotated pole 0.44°	Rotated pole 0.44°	Rotated pole 0.44°	Rotated pole 0.44°	Mercator 50 km	Rotated pole 0.44°
Hybrid/40	Hybrid/27	Hybrid/40	Hybrid/19	Terrain following ETA/28	Hybrid/56
Semi-Lagrangian 720	Semi-Lagrangian 240	Semi-Lagrangian 1200	Eulerian 300	Eulerian 240	Semi-Lagrangian 1200
Tiedtke (1989)	Tiedtke (1989)	Kain and Fritsch (1990, 1993)	Gregory and Rowntree (1990); Gregory and Allen (1991)	Kain (2004)	Kain and Fritsch (1990); Kuo (1965)
Fouquart and Bonnel (1980)	Morcrette et al. (1986); Giorgetta and Wild (1995)	Savijärvi (1990); Sass et al. (1994)	Edwards and Slingo (1996)	Dudhia (1989); Mlawer et al. (1997)	Li and Barker (2005)
Eddy-diffusivity (first-order K) mass flux approach	Louis (1979)	Cuxart et al. (2000)	Wilson (1992)	Hong et al. (2006)	Benoit et al. (1989); Delage (1997)
Tiedtke (1993)	Lohmann and Roeckner (1996)	Rasch and Kristjánsson (1998)	Smith (1990)	WRF single-moment 5-class microphysics scheme (WSM5); Hong et al. (2004)	Sundqvist et al. (1989)
TESSEL; ECMWF (2006)	Hagemann (2002) Rechid et al. (2009)	Samuelsson et al. (2006)	MOSES2; Essery et al. (2003)	Smirnova et al. (2000)	CLASS 3.5; Verseghy (2000)
van Meijgaard et al. (2008); based on ECMWF cycle 31r1; ECMWF (2006)	Jacob (2001) Jacob et al. (2007)	Samuelsson et al. (2011)	Jones et al. (2004)	Skamarock et al. (2008)	Zadra et al. (2008)

in regions that have complex topography such as eastern Africa. Globally, there has been a marked increase in the number of RCM simulations (Alley et al. 2007); however, very few RCM studies have been performed over the East African region (Sun et al. 1999a; Indeje et al. 2000; Anyah, 2005; Anyah et al. 2006; Anyah and Semazzi 2006; Anyah and Semazzi, 2007; Segele et al. 2009a; Diro et al. 2012), and these studies are largely based on the results from a single RCM. However, each model has its strengths and weaknesses. Thus, the application of a set of RCMs is needed, but this has not been done before because of the lack of a large ensemble of RCM output.

Currently, the Coordinated Regional Climate Downscaling Experiment (CORDEX) program, initiated by the World Climate Research Program, provides an opportunity for generating high-resolution regional climate projections, which can be used for assessment of the future impacts of climate change at regional scales (Giorgi et al. 2009). However, the ability of the RCMs has to be assessed before they are used for generating downscaled projections of the future climate.

This study aims to assess the performance of the CORDEX RCMs (Table 1) in simulating the current rainfall characteristics over the East African region defined as the area lying within 16°S–18°N, 22°–52°E (Fig. 1). We also investigate the ability of the RCMs to capture the influence of the large-scale climate circulation patterns (teleconnections) on regional rainfall. The research focuses on the selected East African CORDEX subregions (Fig. 1) that have been classified on the basis of their rainfall distribution as delineated by Favre et al. (2011). The seasons chosen for study are June–September (JJAS) for the northern sector and October–December (OND) for the equatorial and southern sectors. Previous

studies (Indeje et al. 2000; Mutemi 2003; Nyakwada 2009) show that the long rainfall season over the equatorial sector that occurs in March–May (MAM) is dominated by local factors rather than large-scale factors in the modulation of rainfall patterns. Relative to the long rains, the short rains tend to have stronger interannual variability, stronger spatial coherence of rainfall anomalies across a large part of the region, and a substantial association with ENSO and the Indian Ocean dipole (IOD) (e.g., Ropelewski and Halpert 1987, 1989; Ogallo 1988; Hastenrath et al. 1993; Nicholson and Kim 1997; Saji et al. 1999; Indeje et al. 2000; Mutemi 2003; Nyakwada 2009). Also, OND is the common rainfall season for both equatorial and southern parts of the eastern Africa. Consequently, our study focuses on JJAS for the northern sector and OND for the equatorial and southern sectors only.

The study is organized as follows: in section 2, we present a brief description of the study area, datasets, and methodology used. In section 3, we present the results and discussion beginning with the climatology, mean annual cycle, interannual variability, and the response of ENSO and IOD to regional rainfall anomalies. Finally in section 4, we summarize the key results and present our conclusions.

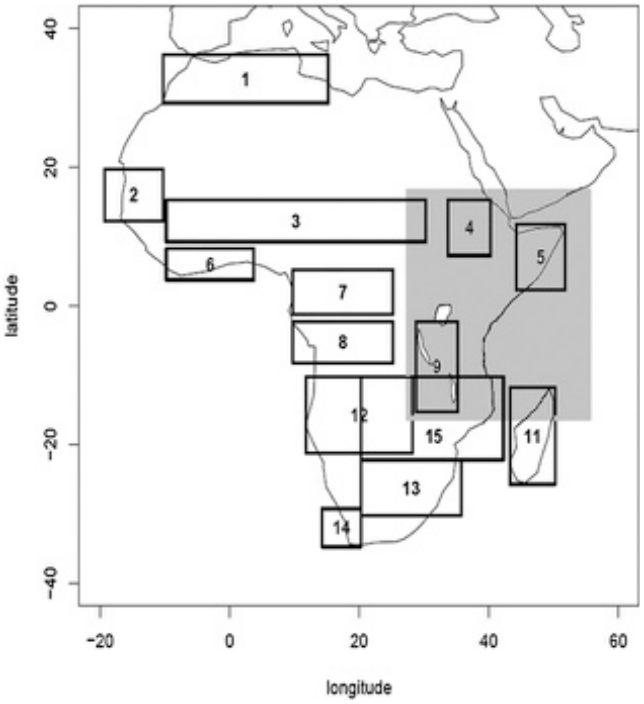

FIG. 1. Map of the study area (greater Horn of Africa), with three subregions represented by boxes 4 (NEA), 5 (EEA), and 9 (SEA) that are utilized for analysis (Favre et al. 2011).

2. Data and methodology

a. Study region

Our study focuses on the CORDEX eastern African region, which refers to the countries of the Greater Horn of Africa (GHA), namely, Burundi, Djibouti, Eritrea, Ethiopia, Kenya, Rwanda, Somalia, Sudan, South Sudan, Tanzania, and Uganda (Fig. 1). The region has a complex topography and is characterized by different rainfall regimes. Local factors such as complex terrain and land surface heterogeneity and their consequent interactions with large-scale climate forcing mechanisms contribute to the diverse spatial rainfall patterns over the region. The climatological annual rainfall cycle in much of eastern Africa is strongly linked to the north–south movement of the intertropical convergence zone (ITCZ). The assessment is performed over three subregions of the domain (Fig. 1), which are hereafter referred to as NEA (northern East Africa; 7.25°–15.25°N, 33.75°–40.25°E), EEA (eastern East Africa; 2.25°–11.75°N, 44.25°–51.75°E), and SEA (southern East Africa; 2.25°–15.25°S, 28.75°–35.25°E). These subregions have been chosen based on previous studies that classified CORDEX-Africa into 15 homogeneous subregions based on observed Global Precipitation Climatology Centre (GPCC) rainfall data (Favre et al. 2011), and also they are representative of different rainfall patterns over East Africa associated with different mechanisms.

NEA (region 4) covers the Ethiopian highlands, which exhibit a unimodal rainfall pattern between June and September. EEA (region 5) covers the eastern equatorial parts of East Africa and is characterized by a bimodal rainfall distribution with the major rainfall season in March–May and a shorter rainfall season in October–December. SEA (region 9) covers the southern part of eastern Africa and is mainly characterized by unimodal rainfall distribution spanning from November to April.

b. Data

1) RCM DATA

In this study, we used simulated monthly rainfall data from 10 CORDEX RCMs. The RCMs were forced by lateral and surface boundary conditions from the European Centre for Medium-Range Weather Forecasts (ECMWF) Interim Re-Analysis (ERA-Interim), and downscaled data are available for the period 1989–2008. All simulations were performed at ~50 km (0.44°) resolution over the CORDEX-Africa domain. Table 1 presents a full list of the RCMs used (with full expansions) and the details of their dynamics and their physical parameterizations. More information on model output can be obtained from Nikulin et al. (2012). This paper uses the short names for the CORDEX RCMs.

TABLE 2. Classification of ENSO and IOD zonal node (IODZM) events from 1989 to 2008 during the two seasons of study (source: http://www.marine.csiro.au/~mcintosh/Research_ENSO_IOD_years.htm).

Pure negative IODZM	Pure La Niña	Pure positive IODZM	Pure El Niño	Co-occurrence of El Niño and positive IODZM	Co-occurrence of La Niña and negative IODZM
1989	1998	1994		1991	
1992	1999	2004		1997	
	2007				

2) OBSERVED DATA

Generally, Africa lacks high-quality observation datasets at suitable temporal and spatial resolution necessary for evaluating RCM simulations. Sylla et al. (2012) presented an intercomparison of different observed daily precipitation datasets and a validation exercise of a regional climate model simulation (with the RegCM3 model). They found that substantial discrepancies exist among the different observational datasets, and this makes it difficult to assess the model performance. Similarly, Nikulin et al. (2012) show large differences between satellite and gauge-based products.

For this study, model results are compared against three observational datasets. Two gauge-based gridded observational datasets are used that are available at 0.5° spatial and monthly temporal resolution: the Global Precipitation Climatology Centre (version 5, 1901–2006; Rudolf et al. 2010) and Climatic Research Unit (CRU) (version 3.0, 1901–2006; Mitchell and Jones 2005). Furthermore, satellite-gauge combined dataset from the Global Precipitation Climatology Project (GPCP; version 2.2; http://www.esrl.noaa.gov/psd/data/gridded/data.gpcp.html) is used even though the resolution is coarse (2.5°).

GPCC data are chosen as a reference field to evaluate the performance of CORDEX RCMs in the context of rainfall over the region. The choice of GPCC data is based on its sufficiently long time series that cover the period (1989–2008) of simulated data. Other advantages are that the GPCC dataset has same resolution as the RCMs' simulated data, and as stated earlier the regions used in the analysis were classified based on GPCC data. ERA-Interim reanalysis data were not used as a comparison field since CORDEX RCMs are forced by ERA-Interim reanalysis and therefore there may be autocorrelation between the ERA-Interim precipitation field and the simulated precipitation fields. However, because of the lack of high-resolution wind data over the continent to compare the circulation pattern, ERA-Interim wind field data are used as comparison fields.

3) DATA LIMITATIONS

The data used in this analysis were produced by many different downscaling groups (see Table 1). These data were generally received in the native model format, projection, and grid and thus had to be postprocessed into a common data format with the same horizontal and vertical dimensions. This enormous task was performed at the Sveriges Meteorologiska och Hydrologiska Institut (SMHI), Sweden, and the institute also served as the repository for the postprocessed data. An initial set of diagnostic variables were processed by the SMHI at the start of the CORDEX-Africa analysis initiative, which started in 2011; however, as the analysis progressed additional prognostic variables were desired to understand the downscaled results (e.g., winds at particular levels to examine the presence of jets). Unfortunately these variables (except 850-hPa level wind) could not be made available at a later stage by all centers (for reasons such as space and deletion) so subsequently some variables were not available for inclusion in the analysis. It was therefore not possible to assess the dynamical drivers at different level of observed biases in the RCMs despite the desire to do so.

c. *Methodology*

We adopted two general criteria to assess the ability of CORDEX RCMs to simulate East African rainfall. The first criterion assesses the ability of the RCMs to reproduce the rainfall climatology. The second criterion assesses the ability of the RCMs to capture the interannual rainfall variability and teleconnection signals. Brief descriptions of each assessment are given below.

In the first assessment of rainfall climatology, a number of tests are performed. Comparison of observed and simulated seasonal mean rainfall climatology over the entire East African region is done to examine the ability of RCMs to capture the spatial distribution of rainfall. A paired difference Student's t test for hypothesis of zero difference between the mean of simulated and observed seasonal rainfall at 5% level of significance is applied for each subregion to detect significant differences in the two means. To assess the consistency of the models in representing the spatial distribution of rainfall with time, spatial correlation between observed and simulated rainfall is computed for each year. The annual cycle of rainfall, area averaged for each region, is computed for both observed and simulated data to determine how well the RCMs capture rainfall seasonality in the respective regions.

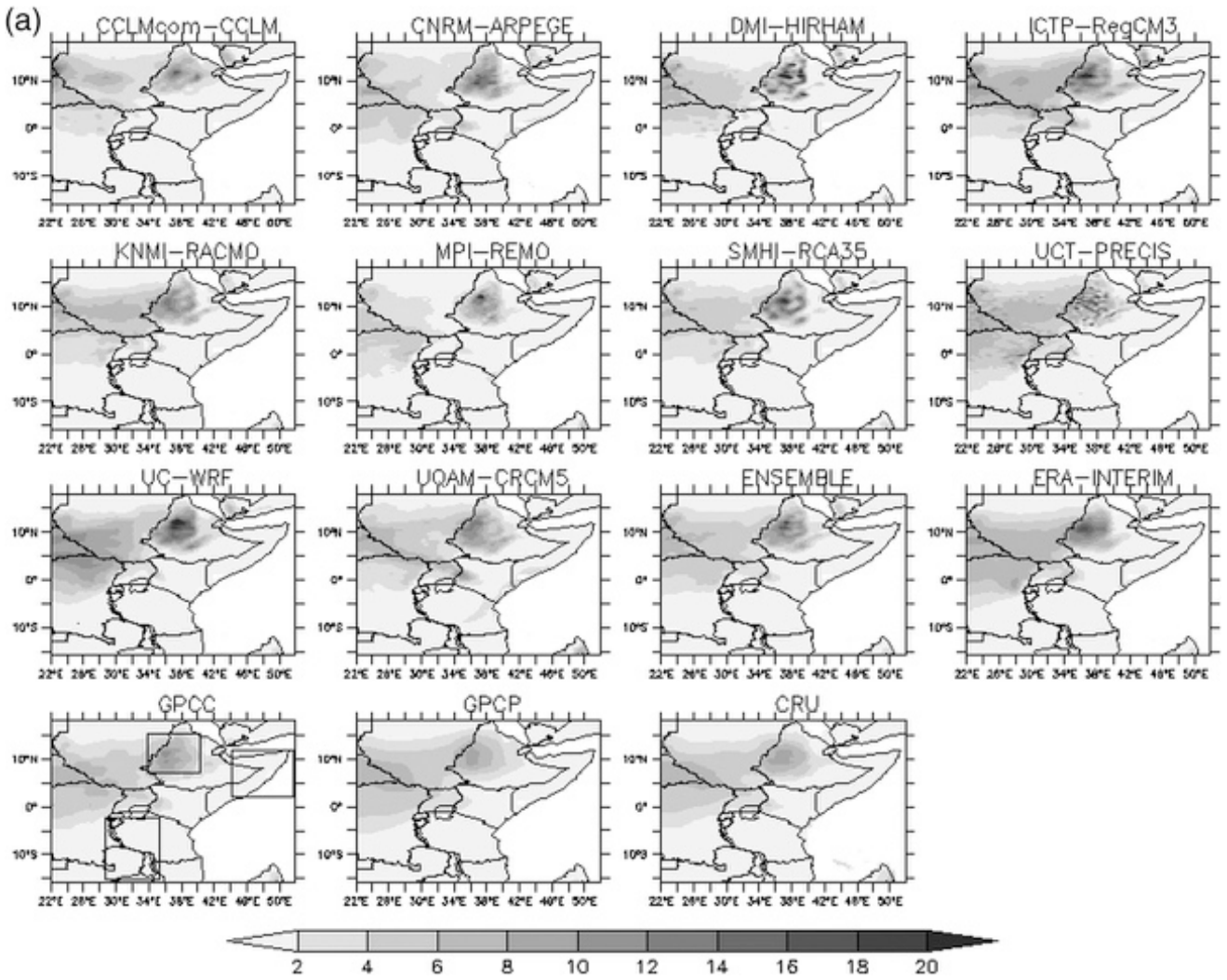

FIG. 2. (a) Climatology of rainfall in eastern Africa during JJAS as simulated by (top two and a half rows) the 10 CORDEX RCMs, (third row, last two panels) ensemble and ERA-Interim, and (bottom) observation (GPCC, GPCP, and CRU). All in mm day^{-1}. (b) As in (a), but for OND.

A Taylor diagram (Taylor 2001) is used to evaluate the spatiotemporal pattern errors (i.e., ''centered'' errors) in the model results. The diagram characterizes the statistical relationship between two fields, a ''test'' field (often representing a field simulated by a model) and a ''reference'' field (usually representing ''truth,'' based on observations). In the diagram, the distance from the origin is equal to the standard deviation, while the distance from the reference point (GPCC in this case) is the equal root-mean-square (RMS) difference between the reference and test fields, and the cosine of the polar angle is equal to the correlation. A ''perfect'' model under this definition would have no error as computed by the root-mean-square. It would perfectly correlate with the observed data, and would have the same standard deviation. Thus, ''skill'' measures correspondence among patterns, trends, and variability in the model and observations. Note that the means of the fields are subtracted out before computing their second-order statistics, so the diagram does not provide information about overall biases, but solely characterizes the *centered* pattern error. These statistics are related by the following equation:

$$E'^2 = \sigma_f^2 + \sigma_r^2 - 2\sigma_f\sigma_r R, \tag{1}$$

where R is the correlation coefficient between the model (f)and observed (r) given by Eq. (2);

$$R = \frac{\frac{1}{N}\sum_{n=1}^{N}(f_n - \bar{f})(r_n - \bar{r})}{\sigma_f\sigma_r}, \tag{2}$$

where N is the number of data points in the model and observed fields, whereas σ_f^2 and σ_r^2 are the variances of the model and reference fields given respectively by Eqs. (4a) and (4b).

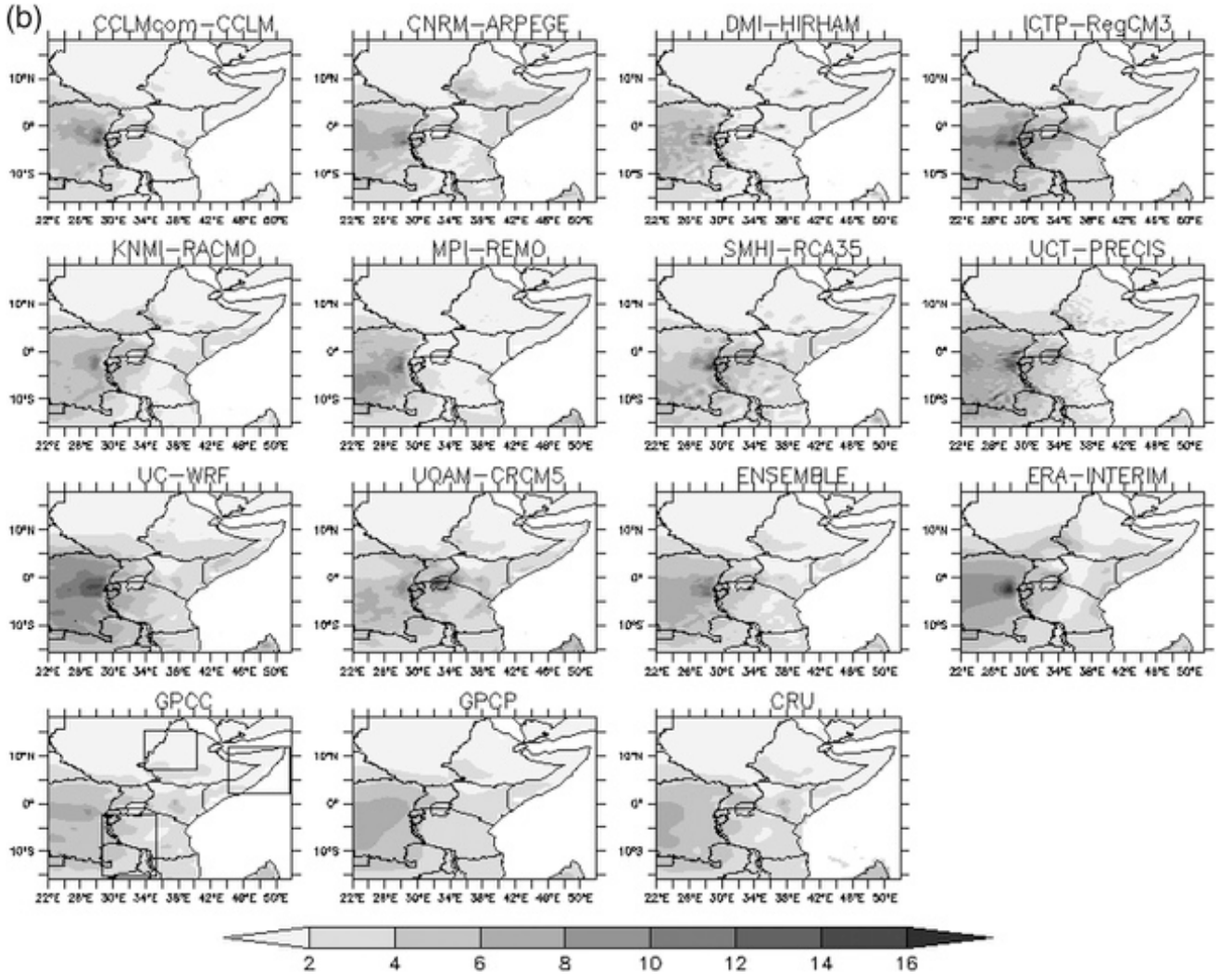

FIG. 2. (*Continued*)

The centered RMS difference between the fields E' is given by Eq. (3):

$$E' = \sqrt{\frac{1}{N}\sum_{n=1}^{N}[(f_n - \overline{f}) - (r_n - \overline{r})]^2}, \tag{3}$$

$$\sigma_f^2 = \frac{1}{N}\sum_{n=1}^{N}(f_n - \overline{f})^2, \tag{4a}$$

$$\sigma_r^2 = \frac{1}{N}\sum_{n=1}^{N}(r_n - \overline{r})^2. \tag{4b}$$

The *second* assessment of the ability of the RCMs is to capture the interannual rainfall variability and teleconnection signals. To assess the ability of the models in simulating the year-to-year variability of rainfall, time series of spatially averaged seasonal rainfall anomaly for JJAS over NEA and OND over EEA and SEA are analyzed.

Composite analysis is used to assess the RCMs' ability to reproduce rainfall anomalies associated with large-scale features such as ENSO and IOD. We use the Ummenhofer et al. (2009) classification and develop composites of strong ENSO, IOD, and co-occurring events. These events are classified on the basis of their sea surface temperature (SST) indices. The condition for defining an El Niño or La Niña year is when the SST anomaly over Niño-3 region (5°S–5°N, 90°–150°W) is more than 1°C or less than −1°C for two or more consecutive months between and including June and February of the following year, respectively. A year is counted as being positive or negative IOD when the SST anomaly over the western Indian Ocean region (10°S–10°N, 50°–70°E) is larger than 1°C or less than −1°C for two or more consecutive months between and including June and December, respectively. Details of the method for classifying years can be found in Meyers et al. (2007) and Ummenhofer et al. (2009). Using Table 2, we composite

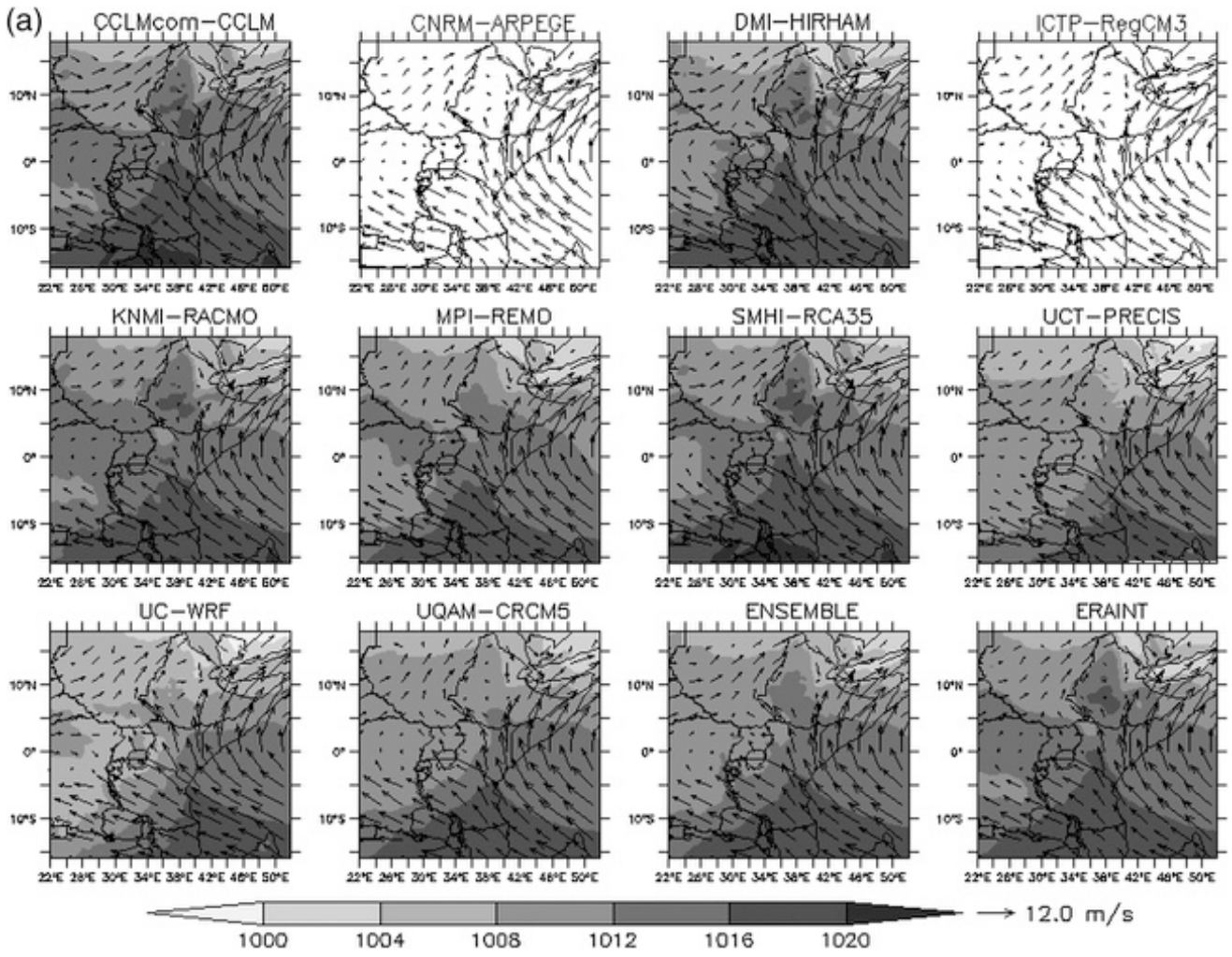

FIG. 3. Climatology of mean sea level pressure (shaded, hPa) and 850-hPa wind (vectors, $m\,s^{-1}$) during (a) JJAS and (b) OND as simulated by (top, middle, and one-half of bottom row) the 10 CORDEX RCMs in comparison with (bottom row, last two panels) ensemble and ERA-Interim. Mean sea level data were not available for ARPEGE and RegCM3.

years of positive–negative IOD, El Niño–La Niña, and co-occurrence events. ENSO and IOD events are analyzed separately to assess the role of each event in modulating rainfall variability over the region. The composites of El Niño, La Niña, positive IOD, negative IOD, and co-occurrence events are formed for the JJAS and OND seasons within the study period for observations and RCMs. The method is based on the difference between average of the seasonal rainfall of the event years and the climatology for the same season.

3. Results and discussion

a. Seasonal averages

1) RAINFALL CLIMATOLOGY

Figures 2a and 2b show the mean seasonal rainfall for JJAS and OND (averaged for 1990–2006) from the 10 CORDEX RCMs, the ERA-Interim reanalysis, and the ensemble mean of the RCMs in comparison with the observed datasets. All RCMs show rainfall band over land concentrated in the northern sector of the region, which is associated with the northward movement of ITCZ (Fig. 2a). Spatially, all the models capture the rainfall maximum over northern East Africa; however, most of the RCMs and ERA-Interim oversimulate rainfall over the Ethiopian highlands, while the ensemble mean has relatively good agreement with our reference dataset GPCC. During this period, most regions below the equator are dry and this is well captured by the RCMs.

During OND (Fig. 2b), the RCMs indicate that the rainfall band is concentrated over the equator and south of equator where the ITCZ is located at this time of the year. The RCMs reproduce most of the spatial structure of OND rainfall, although of higher intensity in the Congo airmass areas.

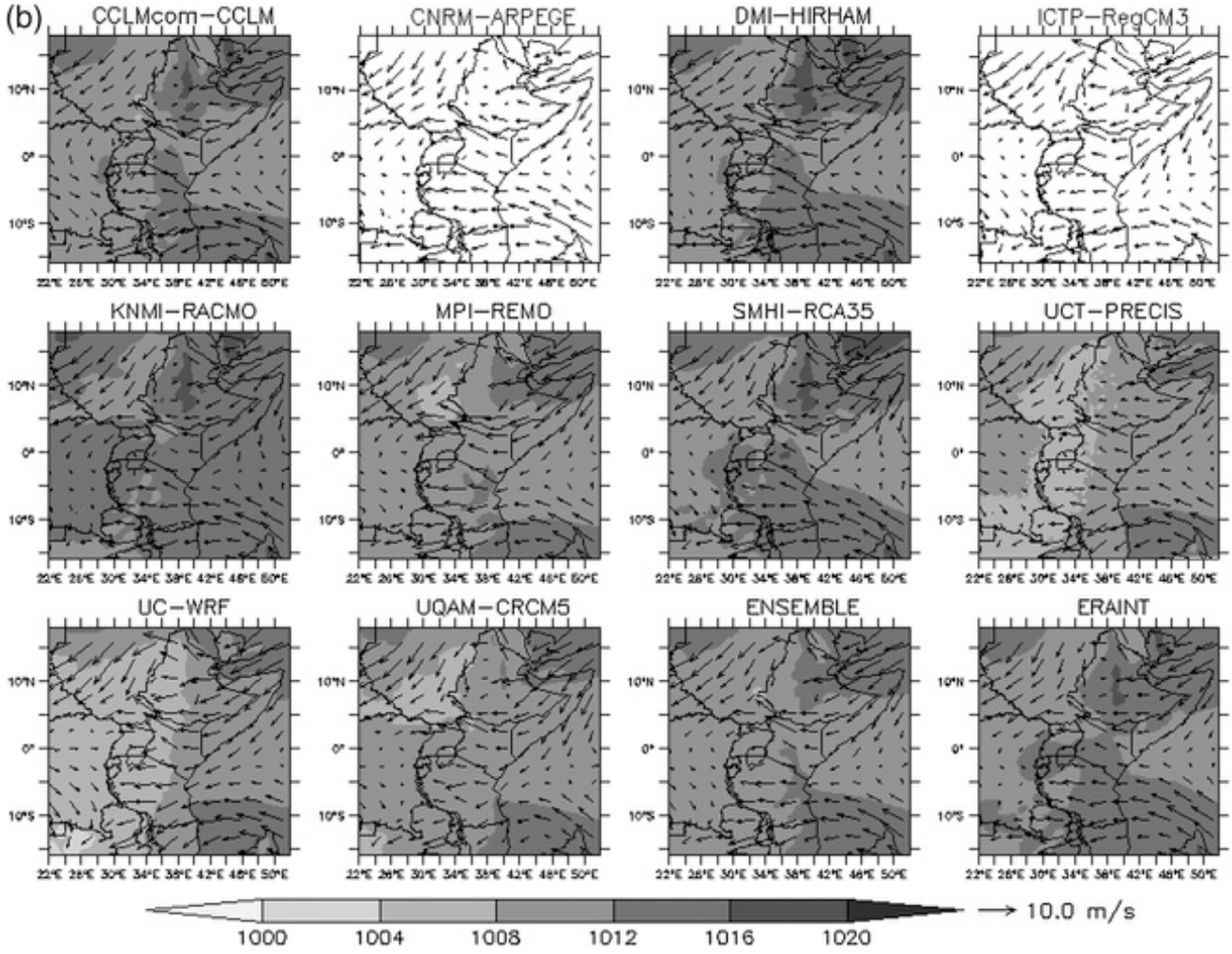

FIG. 3. (*Continued*)

Thus, RCMs capture fairly well the rainfall seasonality, although they overestimate rainfall in some areas, especially over the Ethiopian highlands and Congo Basin during JJAS and OND, respectively.

2) MEAN SEA LEVEL PRESSURE AND WIND FLOW PATTERN CLIMATOLOGY

Figures 3a and 3b show the climatological pattern of mean sea level pressure and 850-hPa wind for JJAS and OND from the 10 CORDEX RCMs and the ensemble mean in comparison with ERA-Interim reanalysis (note that sea level pressure is not available for the CNRM-ARPEGE and ICTP-RegCM3).

During JJAS the northern part of eastern Africa covering most of the Ethiopian highlands is dominated by a meridional ridge of weak high pressure, whereas the southern and south eastern part of the region is dominated by ridge of strong high pressure associated with the extended part of Mascarene high. The spatial extent and intensity of this pressure pattern is well represented by each RCM in comparison with ERA-Interim reanalysis. The intensity of strong westerly winds originate from Atlantic Ocean passes over Sudan, and the East African low-level jet (Somali jet) diverging out of the Mascarene high passes over the coast of eastern Africa are well simulated. These two features are the main source of moisture for the northern part of Ethiopia during JJAS (Segele et al. 2009b; Diro et al. 2011). The weak easterly winds over the Democratic Republic of Congo, Zambia, and Tanzania regions are also well represented. Furthermore, the models capture the role of the Ethiopian and East African highlands that blocks and recurves the circulation around the mountains.

During OND, much of the East African region is dominated by weak high pressure, except the central part of Ethiopia, and this is well represented by each RCM in agreement with ERA-Interim. Furthermore, the four airstreams influencing the regional rainfall patterns are well simulated (Fig. 3b). Two of the airstreams are in association with the Indian Ocean, the southeasterly and

northeasterly components. These airstreams become easterly and converge along the equator. The northerly component climatologically influences Somalia and southern Ethiopia, while the southerly component influences Kenya and Tanzania (Nicholson 1996; Mpeta 2002). The third airstream is associated with the tropical Congo rain forest. This flow is much weaker with a westerly component. This airstream climatologically influences western portion of equatorial eastern Africa, in particular Uganda, Rwanda, and Burundi. The final airstream is associated with dry Saharan air seen over much of Sudan, thus explaining the smaller portions of rainfall received over this area during OND.

b. Model bias

Spatial plots of model bias from the reference field GPCC over the entire domain are analyzed (not shown). However, it is difficult to draw conclusions about the model bias over the entire domain as each model shows a wide variety of bias patterns in different parts of the domain. Therefore, a paired *t* test for difference between mean values of RCMs and observed GPCC for each subregion at the 0.05 significance level is applied. The null hypothesis is that there is no difference between the two means (i.e., the means are equal). The alternative hypothesis is that there is a difference between the two means (the means are different). In fact, our assumption is that the rainfall data follow a normal distribution. Statistically significant biases that pass a Student's *t* test at the 0.05 level are shown in bold (Table 3).

1) JJAS

During JJAS over NEA, all RCMs and observational datasets (GPCP and CRU) show statistically difference values at 0.05 level (Table 3). All RCMs show wet bias, except REMO and CCLM, which show dry bias.

2) OND

The paired *t* test for difference between mean values of RCMs and GPCC shows that all the 10 RCMs indicate wet bias in reproducing the OND rainfall over EEA, whereas CCLM, ARPEGE, HIRHAM, RACMO, and REMO show dry bias in reproducing OND rainfall over SEA (Table 3). All the biases are statistically significant at the 0.05 level. The ensemble mean, ERA-Interim, and the two observed datasets (GPCP and CRU) have a small bias over SEA that is not statically significant.

Using the ensemble mean as a reference (Table 4), CCLM, ARPEGE, RACMO, REMO, and CRCM5 show statically significant dry bias, whereas WRF and RegCM3 show wet bias over NEA during JJAS. Over EEA during OND, CCLM, HIRHAM, RegCM3, and PRECIS show wet bias, whereas REMO, WRF, and CRCM5 show dry bias that is statistically significant at the 0.05 level. All RCMs show statistically significant bias over SEA using the ensemble mean as a reference field.

c. Spatial correlation

The consistency of the models in representing the spatial distribution of rainfall with time for each subregion is evaluated using spatial correlation. Figure 4 depicts the magnitude and variability of spatial correlations of the RCMs, ensemble mean, ERA-Interim, GPCP, and CRU with GPCC over time during JJAS over NEA and during OND over EEA and SEA.

The results for NEA show that CRCM5, RACMO, RegCM3, RCA, and the ensemble mean have high and consistent correlation with the GPCC data during JJAS while CCLM, HIRHAM, REMO, PRECIS, ARPEGE, and WRF are relatively weakly correlated (between 0.7 and 0.4) with the GPCC data. The HIRHAM model has the lowest correlation with GPCC in this region and it is noteworthy that the CCLM model poorly represented the spatial pattern of rainfall during the 1998 La Niña event. The two observed datasets (GPCP and CRU) and ERA-Interim have relatively higher and more consistent correlation with GPCC than the individual models.

Over EEA, most of the models are inconsistent in representing spatial rainfall distribution except RACMO, RegCM3, and the ensemble mean, which have good and consistent rainfall representation. The CCLM, HIRHAM, and REMO models have relatively poor correlation in terms of magnitude and consistency. Again, poor representation is displayed by CCLM during the 1997 cooccurrence of the strong El Niño and positive IOD event, and in REMO during the 1994 IOD event. This shows the shortcoming of the two models in capturing the response from ENSO and IOD events. Over this region, the CRU dataset shows inconsistency in representing the spatial distribution of rainfall.

Over SEA, all RCMs and ERA-Interim had nearly same level of consistency in reproducing spatial patterns of rainfall during OND. Although the two observed datasets have better agreement with GPCC than individual models, inconsistency in spatial distribution is observed for CRU dataset.

d. Annual cycles

Figure 5 illustrates the performance of the CORDEX RCMs in simulating annual rainfall cycle for the three subregions. In NEA and SEA, all of the RCMs capture the shape of the rainfall seasonality well. However, in EEA most of the models poorly reproduce the OND rainfall peak. The GPCP observed data wrongly

TABLE 3. Difference between seasonal mean rainfall between each RCM and GPCC during 1) JJAS in subregion NEA and 2) OND in subregions EEA and SEA. Bold values are significant at the 0.05 level.

Model comparison	JJAS (NEA)	OND (EEA)	OND (SEA)
CCLM–GPCC	**−0.36**	**0.65**	**−1.3**
ARPEGE–GPCC	**0.84**	**1.23**	**−1.02**
HIRHAM–GPCC	**0.99**	**0.53**	**−1.49**
RegCM3–GPCC	**2.28**	**0.44**	**1.29**
RACMO–GPCC	**0.83**	**1.15**	**−0.69**
REMO–GPCC	**−0.76**	**1.37**	**−1.27**
RCA–GPCC	**0.94**	**1.25**	**0.5**
PRECIS–GPCC	**0.98**	**0.71**	**0.96**
WRF–GPCC	**3.01**	**1.68**	**1.62**
CRCM5–GPCC	**0.84**	**1.51**	**0.62**
Ensemble–GPCC	**0.96**	**1.05**	−0.08
ERA-Interim–GPCC	**1.8**	**1.02**	−0.07
GPCP–GPCC	**−0.21**	**0.4**	−0.02
CRU–GPCC	**−0.3**	−0.13	−0.18

TABLE 4. Difference between seasonal mean rainfall between each RCM and the ensemble mean during JJAS in subregion NEA and OND in subregions EEA and SEA. Bold values are significant at the 0.05 level.

RCM comparison	JJAS (NEA)	OND (EEA)	OND (SEA)
CCLM–ensemble	**−1.63**	**−0.4**	**−1.22**
ARPEGE–ensemble	**−0.43**	0.18	**−0.94**
HIRHAM–ensemble	−0.28	**−0.52**	**−1.41**
RegCM3–ensemble	**1.01**	**−0.61**	**1.37**
RACMO–ensemble	**−0.44**	0.09	**−0.61**
REMO–ensemble	**−2.03**	**0.32**	**−1.19**
RCA–ensemble	−0.33	0.2	**0.57**
PRECIS–ensemble	−0.28	**−0.34**	**1.03**
WRF–ensemble	**1.73**	**0.62**	**1.7**
CRCM5–ensemble	**−0.43**	**0.46**	**0.7**

represent the rainfall peak both over NEA and EEA subregions, while GPCC and CRU indicate nearly the same pattern of seasonality in all subregions. The wrong representation of seasonality in GPCP might be due to its coarse resolution. In all the regions, the ensemble mean have been found to have relatively good performance as compared to individual models. The WRF is found to be significantly overestimating rainfall over all three subregions.

In general, there is fairly good agreement between annual rainfall cycle simulated by CORDEX RCMs and the reference field (GPCC). The most notable shortcoming in most RCMs is overestimation of the monthly mean.

e. Taylor diagram

The models' ability to simulate both the pattern and amplitude of the observed interannual variation is provided by a Taylor diagram. Figure 6 summarizes the pattern correlation (r), root-mean-square difference, and the amplitude of variation of seasonal mean rainfall of each RCM, ensemble mean, and ERA-Interim with respect to the reference field (GPCC) for each of the three subregions. To provide an overview of observational uncertainty, GPCP and CRU are also compared to GPCC and plotted in the same diagram. All the statistics are computed for 1990–2006.

Over NEA during JJAS, most of the model show relatively low correlation coefficient compared to the other subregions (i.e., $r < 0.8$). RACMO, PRECIS, REMO, and CRCM5 have relatively high pattern of correlation and low root-mean-square difference and has a variation close to the reference field (GPCC). The ensemble mean has better agreement with GPCC than individual models (i.e., $r = 0.84$) or ERA-Interim-derived data. ERA-Interim shows extremely high variation compared to the GPCC. Regarding the observed datasets, the GPCP agrees best with GPCC. CRU and multimodel ensemble have nearly the same level of correlation coefficient, but the ensemble mean shows lower variation than GPCC, while CRU shows higher variation than GPCC.

Over EEA during OND, most of the models underestimate the magnitude of interannual variation relative to GPCC, while three models (WRF, CRCM5, and RCA) overestimate the variation. CCLM, RACMO, CRCM5, and the ensemble mean have relatively higher correlation and low RMS errors than other RCMs as well as the ERA-Interim reanalysis. It has been also noticed that there is a large spread among observational datasets. GPCP has a standard deviation higher than GPCC, while CRU shows a variation much lower than GPCC. But GPCP has relatively higher correlation and lower root-mean-square difference than CRU.

Over SEA, all RCMs show a variation lower than the observed except the WRF, which shows larger than the observed. ARPEGE, ERA-Interim, and the ensemble mean have a relatively higher pattern of correlation (i.e., $r > 0.8$) and lower root-mean-square difference than the rest of the RCMs. The GPCP agrees best with GPCC.

Generally, some regional climate models have outperformed the derived ERA-Interim (in relation to the observed GPCC) and others have not; however, the multimodel ensemble is found generally closer to the GPCC than individual models as well as the derived ERA-Interim. The WRF Model has showed a variation higher than the observed in all subregions. Even though there is large uncertainty between observational datasets, GPCP has better agreement with GPCC than CRU in all subregions. Particularly over subregion SEA, GPCP has a correlation coefficient of above 0.99 and has a similar interannual variation with GPCC.

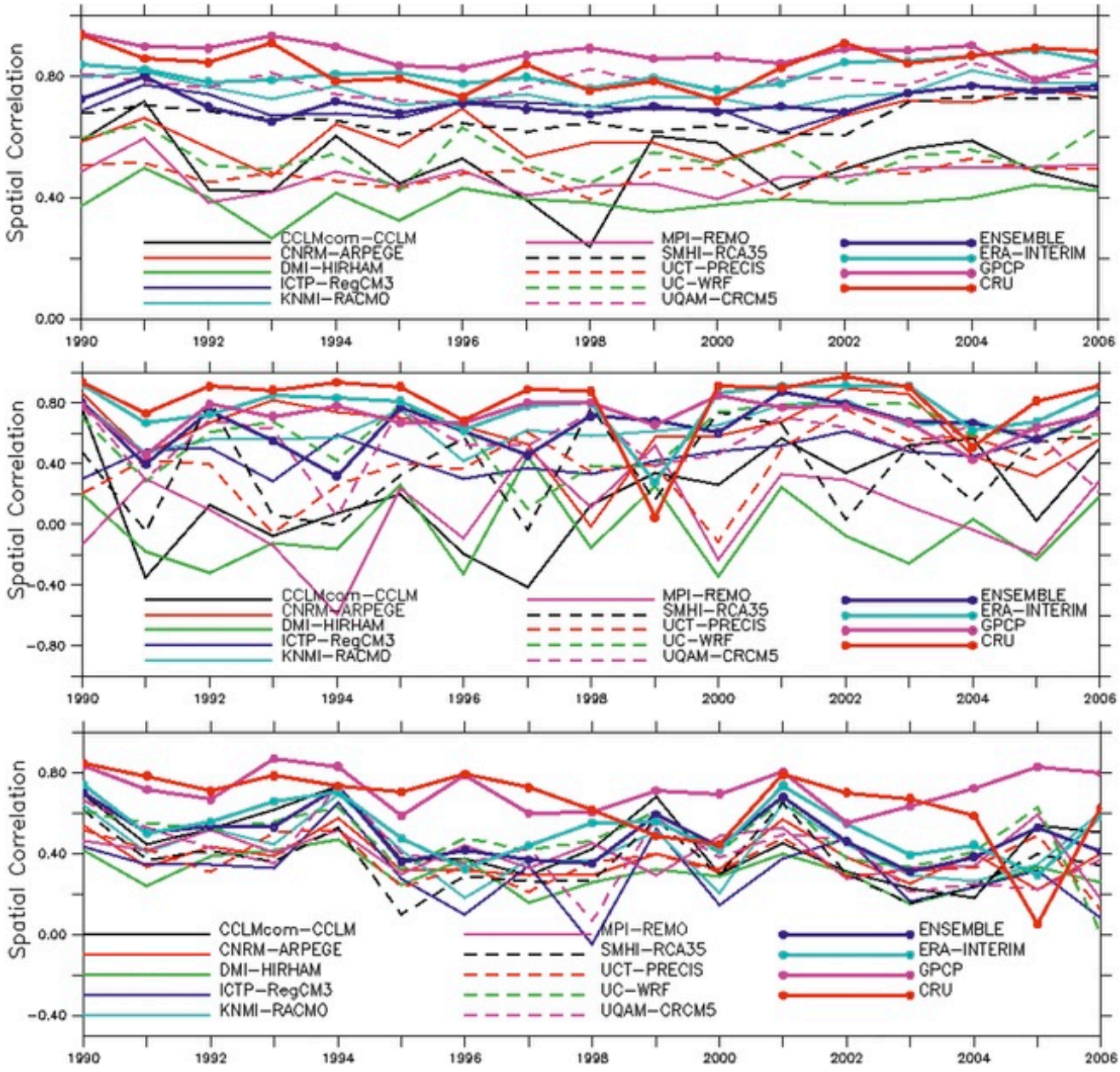

FIG. 4. Spatial correlations between GPCC and the CORDEX RCMs (top) over NEA during JJAS, (middle) over EEA during OND, and (bottom) over SEA during OND.

f. Interannual rainfall variability

The temporal pattern of rainfall over eastern Africa has a strong interannual rainfall variability associated with extreme events such as floods and droughts. Previous studies have shown that the interannual rainfall variability is strongly associated with perturbations in the global SSTs, especially over the equatorial Pacific and Indian Ocean basins (Ogallo 1988; Nicholson and Kim 1997; Indeje et al. 2000; Saji et al. 1999; Black et al. 2003; Clark et al. 2003 Nyakwada 2009; Omondi et al. 2013). The influence of global SST on eastern Africa rainfall depends on the season and the region. Generally, during JJAS El Niño conditions produce deficit rainfall and La Niña conditions produce excess rainfall over the northern parts of East Africa, whereas during OND the equatorial and southern parts of East Africa get below average rainfall during La Niña and above average during El Niño.

Figure 7 shows time series analysis of area averaged seasonal rainfall anomalies of the RCMs, the ensemble, ERA-Interim, and observed (GPCP and CRU) rainfall over the three subregions in comparison to GPCC. During JJAS, the observed rainfall variability is well

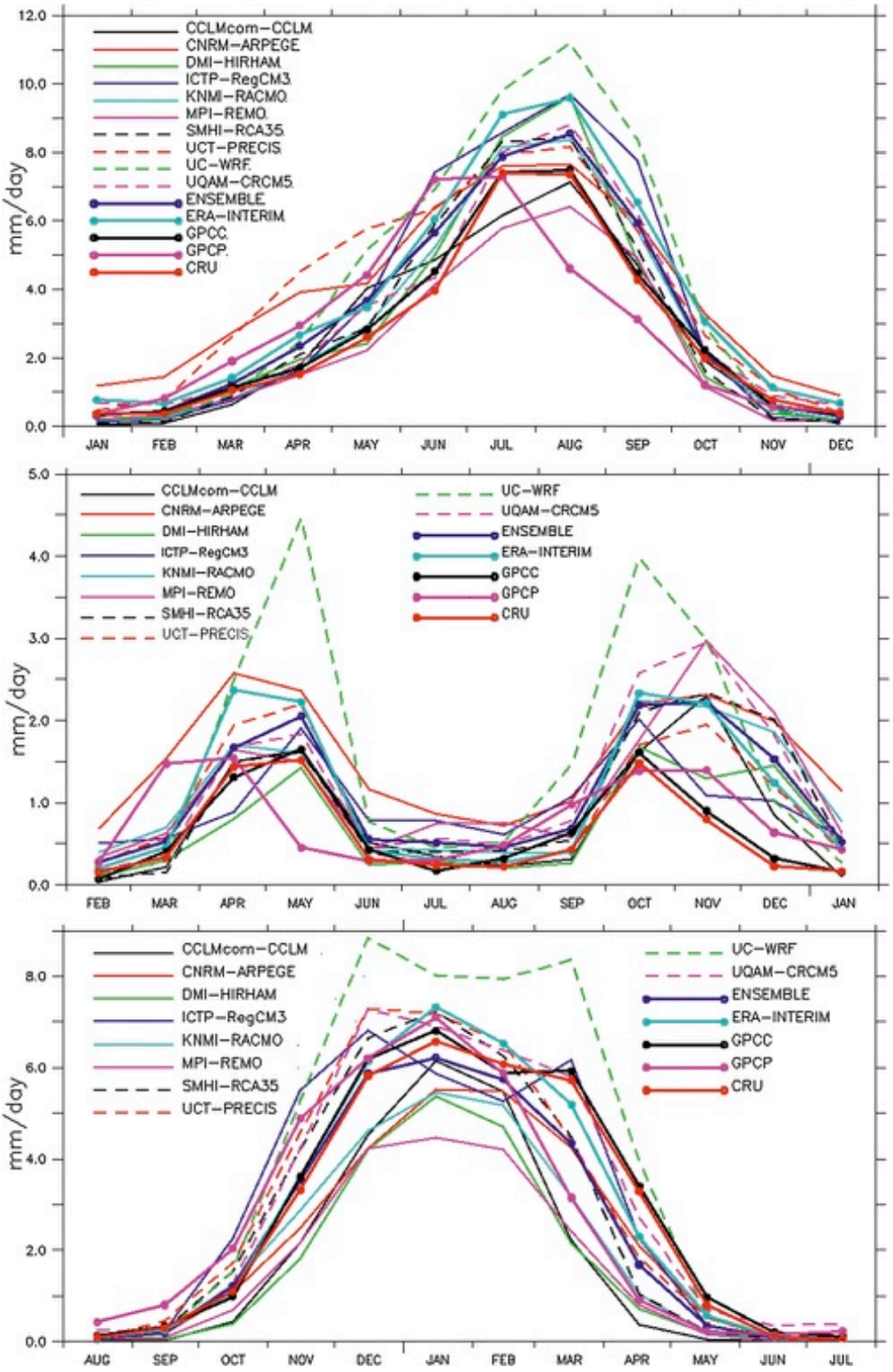

FIG. 5. Mean annual cycle of rainfall over (top) NEA, (middle) EEA, and (bottom) SEA (mm day^{-1}) from the 10 RCMs, ensemble, ERA-Interim reanalysis, and observations.

reproduced by most RCMs over NEA except for ARPEGE, which showed some deviation. ERA-Interim poorly represented the year-to-year variability of rainfall, which also was shown in Fig. 6 over NEA. Most RCMs capture the extreme years such as El Niño years of 1991, 1997, and 2004 with minimum rainfall whereas during La Niña years (1998, 1999) rainfall is above average. In EEA, almost all the RCMs realistically simulate the

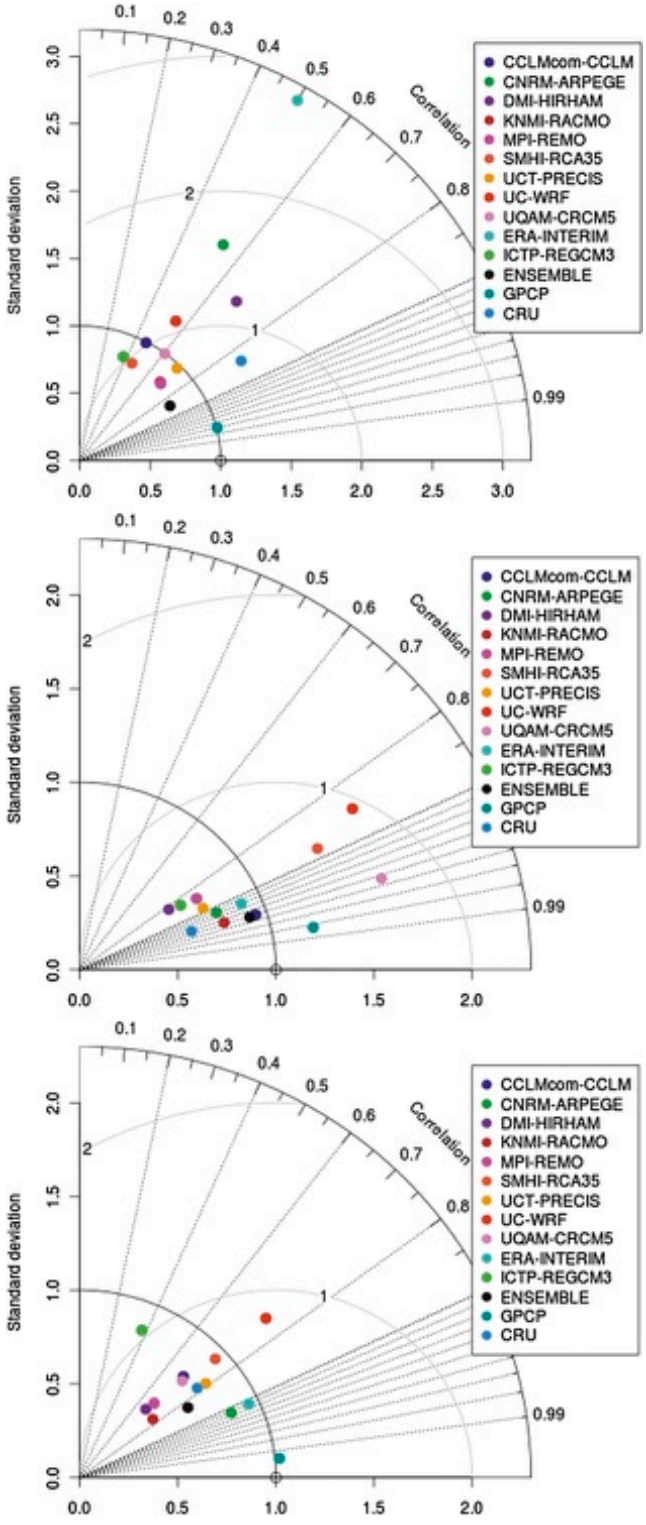

FIG. 6. Taylor diagram displaying normalized statistical comparison of seasonal mean rainfall of the 10 RCMs and ERA-Interim reanalysis with observation over (top) NEA during JJAS, (middle) EEA during OND, and (bottom) SEA during OND.

interannual rainfall variability, notably the 1997 high rainfall event that was associated with strong El Niño in phase with positive IOD. CRU shows low year-to-year variability of rainfall (also shown in Fig. 6 over EEA with low standard deviation value). In SEA, the RegCM3 and WRF do not capture well the interannual rainfall variability. Although the ERA-Interim reanalysis and ARPEGE model did not capture the rainfall variability in the NEA, in the latter two regions they best represented the observed GPCC rainfall during the El Niño of 1997.

g. Teleconnection

The teleconnection associated with East African rainfall is quite complex as several forcings control the rainfall variability for various seasons and regions. In this section, we assess the ability of CORDEX RCMs in capturing teleconnection signals using composite analysis. The composite of each ENSO and IOD event is formed separately to examine how well the models are able to translate the teleconnection signal from the boundary forcing into the interior of the domain and also to understand the relative influence of the events on the rainfall variability over the region.

Figure 8 shows the JJAS rainfall anomaly simulated by CORDEX RCMs and ERA-Interim reanalysis in comparison to the observation when pure La Niña events are composited (refer to Table 2). Most of the RCMs and ERA-Interim show a positive rainfall anomaly over large parts of the Ethiopian highlands and South Sudan in agreement with observation. This indicates that during La Niña events there is an increase of rainfall over the northern parts of eastern Africa during JJAS. This finding is in agreement with previous studies (e.g., Diro et al. 2011; Gissila et al. 2004; Korecha and Barnston 2007; Segele et al. 2009b, and others) that associated the positive rainfall anomalies over the Ethiopian highland during JJAS with La Niña, and the negative rainfall anomalies with El Niño.

It should be noted that in our analysis period there is no pure El Niño event to investigate whether the models can translate the signal into the domain. However, co-occurrence events of El Niño and positive IOD are studied. Figure 9 represents rainfall anomaly for the co-occurrence of El Niño and positive IOD events during JJAS. Both simulated and observed results show negative rainfall anomalies during JJAS over large parts of the Ethiopian highlands and South Sudan. Most of the RCMs simulate the negative rainfall anomaly quite well, which is also a mirror image of La Niña impacts. However, only two models (RCA and WRF) capture the drier anomaly over the northern and eastern parts of the Democratic Republic of Congo, whereas most of the

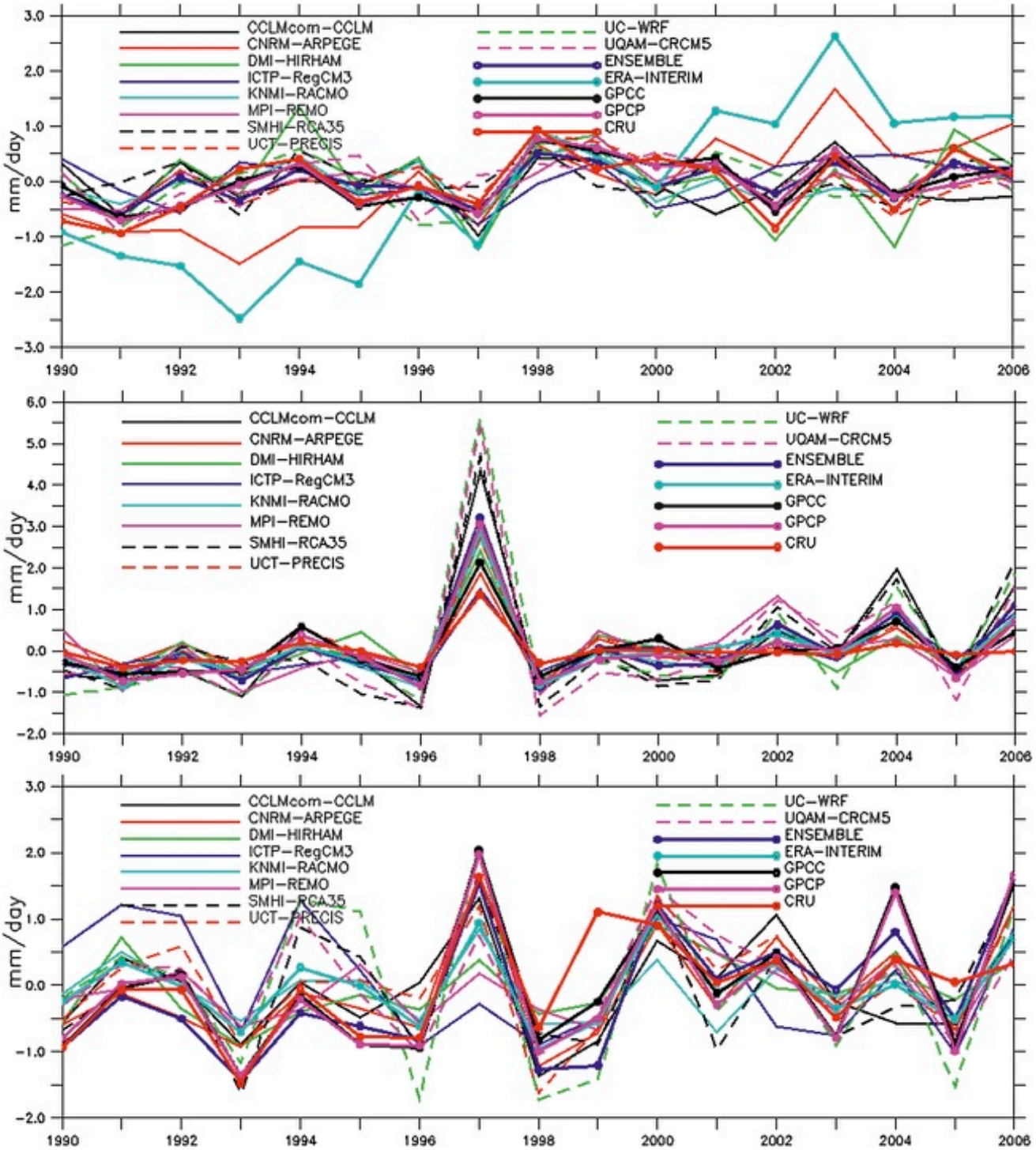

FIG. 7. Time series of CORDEX RCMs, ensemble, and observed rainfall anomalies (mm day^{-1}) over (top) NEA during JJAS, (middle) EEA during OND, and (bottom) SEA during OND.

other models show wetter anomalies and the ensemble mean of this region shows no anomaly.

The rainfall anomalies during pure La Niña and co-occurrence of El Niño with positive IOD events for OND are shown in Figs. 10 and 11. Most of the RCMs correctly simulate negative rainfall anomaly during OND in the equatorial and southeastern parts of the region when La Niña years are composited (Fig. 10). A similar but reverse response is observed in co-occurrence of El Niño with positive IOD composites (Fig. 11), which is associated with increased rainfall during OND. Similar findings have been reported in a number of previous

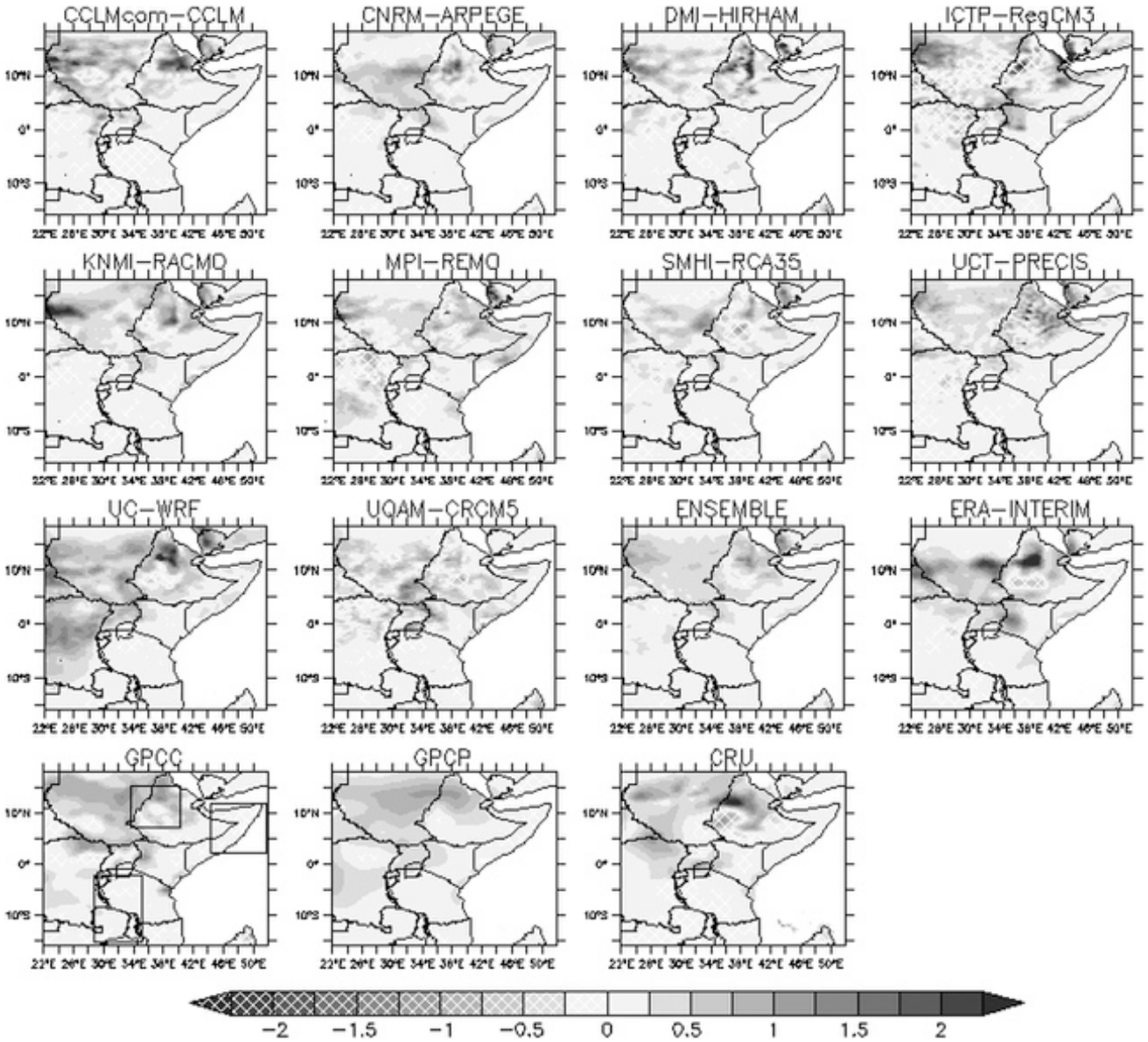

FIG. 8. As in Fig. 2a, but for JJAS rainfall anomaly (mm day^{-1}) during pure La Niña conditions.

studies (e.g., Ropelewski and Halpert 1987; Ogallo 1988; Indeje et al. 2000; Nicholson and Kim 1997). The warm phase of ENSO (El Niño) is associated with excess rainfall and flooding, while the cold phase (La Niña) often coincides with extreme drought conditions during the short rain in much of equatorial East Africa (Ogallo 1988; Nicholson and Kim 1997).

To understand the effects of IOD over the region, the pure positive and negative IOD composites are plotted separately. The positive IOD composites for JJAS, positive IOD composites for OND, and negative IOD composites for JJAS and OND have been analyzed over the region (results not shown), and all of the results show weak and localized rainfall anomalies compared to the ENSO composites.

In general, results from the composite analysis have shown that most of the models capture the response of large-scale signals over eastern Africa during the anomalous events with respect to observations, where the ensemble mean outperforms the individual models. Both the RCMs and observed results show that ENSO has a strong association for rainfall over the region while the effect of IOD is weak and localized.

4. Summary and conclusions

In this study, the performance of 10 CORDEX RCMs was evaluated for their ability to capture and characterize rainfall patterns over East Africa as well as their ability to reproduce the response to large-scale global

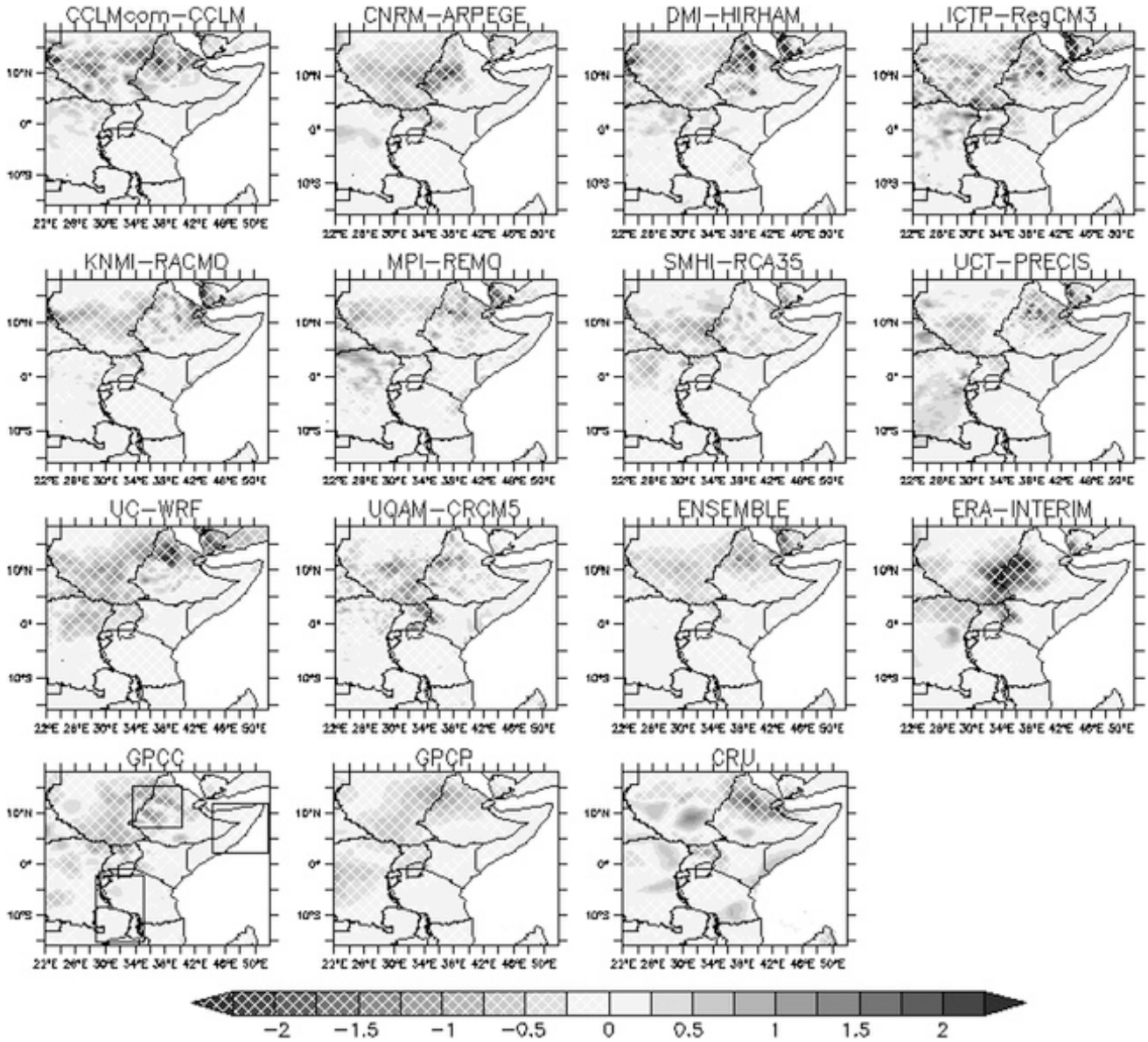

FIG. 9. As in Fig. 2a, but for JJAS rainfall anomaly (mm day^{-1}) during the co-occurrence of El Niño and positive IOD.

signals during the period 1990–2008. In the northern sector of the region, JJAS is considered to be the long rainy season as the region receives the largest fraction of its total annual rainfall in these months. All RCMs realistically simulated the rainfall belt associated with the ITCZ during this season although most of the models show wet bias apart from REMO and CCLM, which showed dry bias. During OND, all RCMs captured well the ITCZ belt. It was noted that 10 RCMs indicated wet bias over EEA while CCLM, ARPEGE, HIRHAM, RECMO, and REMO show dry bias in reproducing OND rainfall over SEA. CRCM5, RACMO, RegCM3, and RCA showed high spatial correlations together with consistency in reproducing spatial patterns of rainfall over time for JJAS in NEA and RACMO and RegCM3 during OND in EEA. The 10 RCMs had nearly same level of consistency in reproducing spatial patterns in SEA sector during OND. Overall, the 10 RCMs considered in the present study represent the correct shape of the mean annual cycle of rainfall over both NEA and SEA, but with a small shift in capturing the correct peak of the dominant bimodal rainfall regimes in EEA. Generally, most of the models capture the regional rainfall anomaly associated with ENSO and IOD in agreement with the observations. Both model and observed results showed that ENSO has a strong association for rainfall over the region while the effect of IOD is weak and localized. Many studies have shown that downscaling

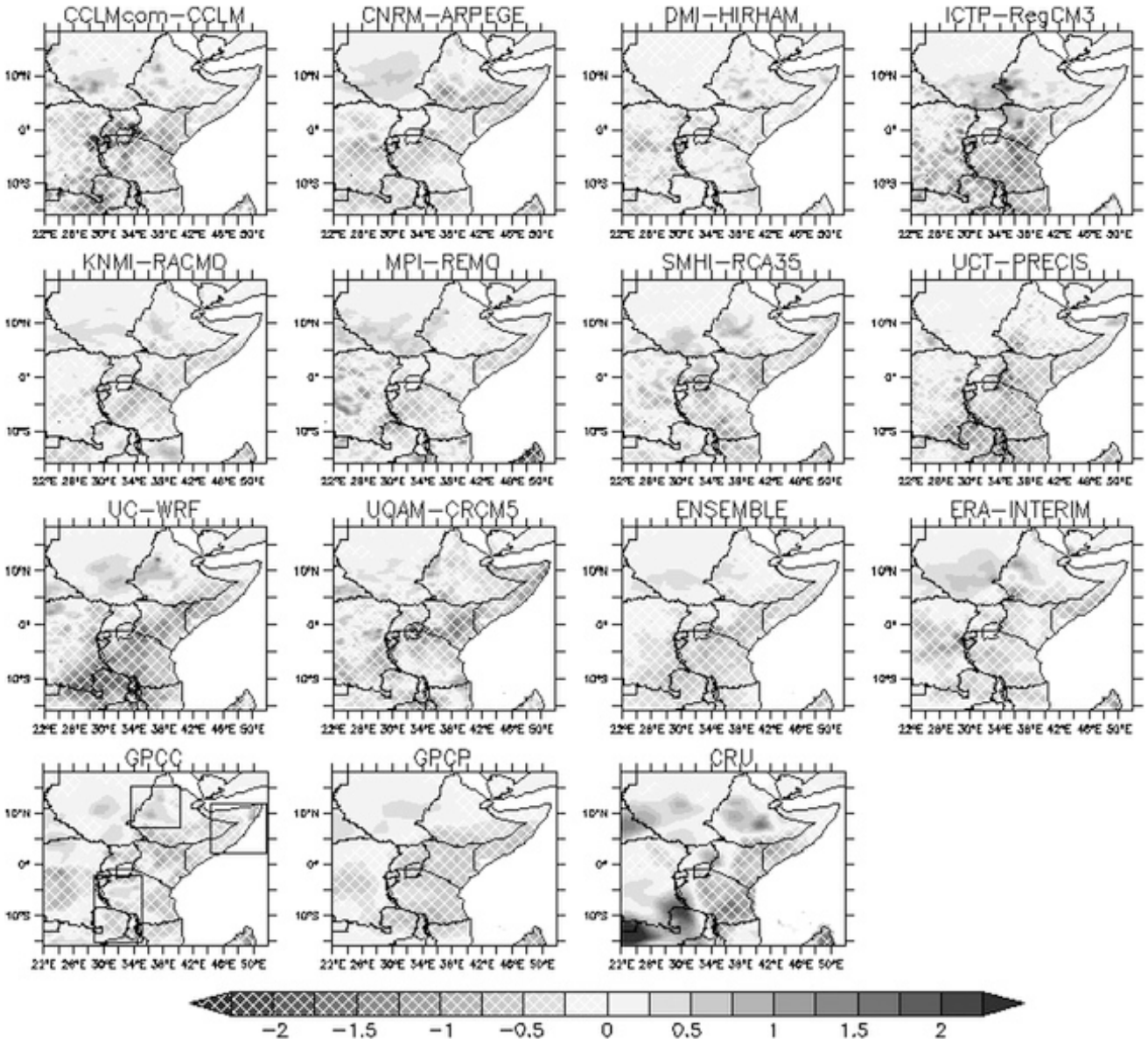

FIG. 10. As in Fig. 8, but for OND.

global models to the regional scale adds value to information at these finer scales (Giorgi and Marinucci 1996; Giorgi and Mearns 1999; Giorgi et al. 1993a,b; Sun et al. 1999a,b; Anyah and Semazzi 2006; Anyah et al. 2006). We have demonstrated that some regional climate models used in CORDEX-Africa have outperformed the ERA-Interim rainfall (in relation to the observed GPCC) and others have not; however, the ensemble mean of the RCM output is mostly closer to the GPCC data than the ERA-Interim. As the CORDEX RCMs are forced by ERA-Interim reanalysis, this would suggest that downscaling coarser model output improves rainfall representation at the regional scale.

In general, most of the RCMs overestimated rainfall in all the three subregions, WRF in particular. The multimodel ensemble mean outperforms the results of individual models, and even ERA-Interim, in most of the areas and time periods as assessed by different criteria. This is likely because of the cancellation of opposite signed biases across the models. Similar results have been shown by Paeth et al. (2011) and in the CORDEX context by Nikulin et al. (2012). At the level of individual models it is of concern that many models produce good results in one region and poor results in another over the same time period. This would suggest that some models may be getting correct results in particular regions for the wrong reasons. It is beyond the

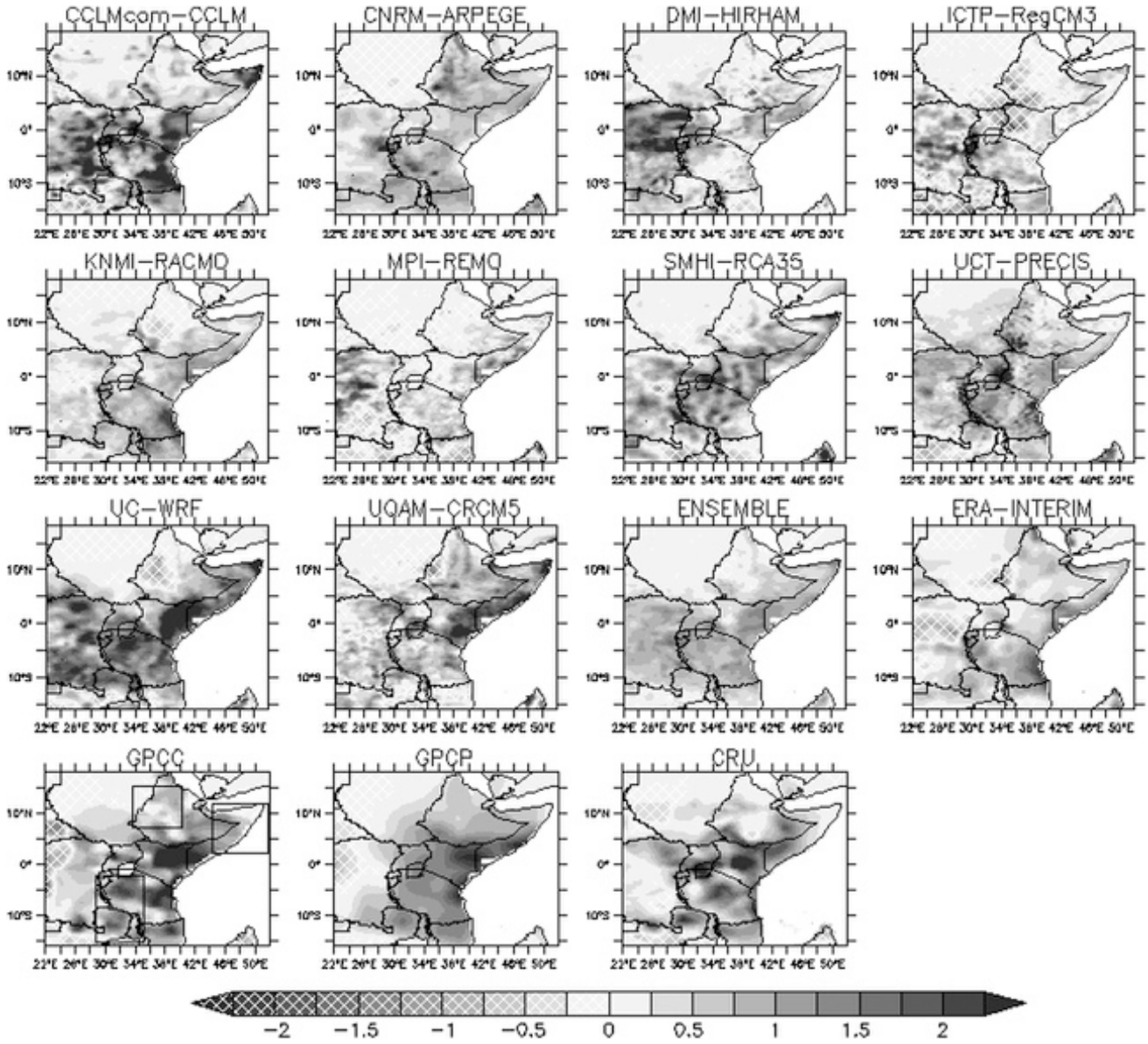

FIG. 11. As in Fig. 9, but for OND.

scope of this paper to investigate the individual models in depth but this is a major caveat in interpreting the results. Despite this, we have demonstrated that the multimodel ensemble mean simulates eastern Africa rainfall adequately and can therefore be used for the assessment of future climate projections for the region.

Acknowledgments. This research was supported by the Global Change System for Analysis, Research, and Training (START) in partnership with the University of Cape Town's Climate Systems Analysis Group, the World Climate Research Program, the Climate and Development Knowledge Network, the International Centre for Theoretical Physics, and the Swedish Meteorological-Hydrological Institute. We would also like to thank the regional downscaling groups who provided the downscaled data used in this analysis (see Table 1). Special thanks to Grigory Nikulin at the Swedish Meteorological and Hydrological Institute whose efforts ensured these data were post-processed to common grids and formats so that they were directly comparable in CORDEX-Africa analyses. We also acknowledge Eastern Africa modeling groups and their respective institutions for their roles in this research.

H. S. Endris would like to thank the SOCOCA project in Department of Geoscience at University of Oslo (DoG/UiO) for the scholarship support for his study at University of Cape Town.

REFERENCES

Alley, R. B., and Coauthors, 2007: Summary for policymakers. *Climate Change 2007: The Physical Science Basis,* S. Solomon et al., Eds., Cambridge University Press, 1–18.

Anyah, R. O., 2005: Modelling the variability of the climate system over Lake Victoria basin. Ph.D. thesis, Department of Marine, Earth and Atmospheric Sciences, North Carolina University, 288 pp.

——, and F. H. M. Semazzi, 2006: Climate variability over the Greater Horn of Africa based on NCAR AGCM ensemble. *Theor. Appl. Climatol.,* **86,** 39–62, doi:10.1007/s00704-005-0203-7.

——, and ——, 2007: Variability of East African rainfall based on multiyear RegCM3 simulations. *Int. J. Climatol.,* **27,** 357–371, doi:10.1002/joc.1401.

——, and W. Qiu, 2012: Characteristic 20th and 21st century rainfall and temperature patterns and changes over the Greater Horn of Africa. *Int. J. Climatol.,* **32,** 347–363, doi:10.1002/joc.2270.

——, F. H. M. Semazzi, and L. Xie, 2006: Simulated physical mechanisms associated with climate variability over Lake Victoria Basin in East Africa. *Mon. Wea. Rev.,* **134,** 3588–3609.

Baldauf, M., 2008: Stability analysis for linear discretisations of the advection equation with Runge–Kutta time integration. *J. Comput. Phys.,* **227,** 6638–6659.

——, and J. P. Schulz, 2004: Prognostic precipitation in the Lokal-Modell (LM) of DWD. *COSMO Newsletter,* No. 4, 177–180. [Available online at http://www.cosmo-model.org/content/model/documentation/newsLetters/newsLetter04/default.htm.]

——, A. Seifert, J. Förstner, D. Majewski, M. Raschendorfer, and T. Reinhardt, 2011: Operational convective-scale numerical weather prediction with the COSMO model: Description and sensitivities. *Mon. Wea. Rev.,* **139,** 3887–3905.

Benoit, R., J. Côté, and J. Mailhot, 1989: Inclusion of a TKE boundary layer parameterization in the Canadian regional finite-element model. *Mon. Wea. Rev.,* **117,** 1726–1750.

Black, E., J. Slingo, and K. R. Sperber, 2003: An observational study of the relationship between excessively strong short rains in the coastal East Africa and Indian Ocean SST. *Mon. Wea. Rev.,* **131,** 74–94.

Bougeault, P., 1985: A simple parameterization of the large-scale effects of cumulus convection. *Mon. Wea. Rev.,* **113,** 2108–2121.

Buzzi, M., M. W. Rotach, M. Raschendorfer, and A. A. M. Holtslag, 2011: Evaluation of the COSMO-SC turbulence scheme in a shear-driven stable boundary layer. *Meteor. Z.,* **20,** 335–350.

Christensen, O. B., M. Drews, and J. H. Christensen, 2006: The HIRHAM regional climate model version 5. DMI Tech. Rep. 06–17, 22 pp.

Clark, C. O., P. J. Webster, and J. E. Cole, 2003: Interdecadal variability of the relationship between the Indian Ocean zonal mode and East African coastal rainfall anomalies. *J. Climate,* **16,** 548–554.

Cuxart, J., P. Bougeault, and J.-L. Redelsperger, 2000: A turbulence scheme allowing for mesoscale and large-eddy simulations. *Quart. J. Roy. Meteor. Soc.,* **126,** 1–30.

Delage, Y., 1997: Parameterising sub-grid scale vertical transport in atmospheric models under statically stable conditions. *Bound.-Layer Meteor.,* **82,** 23–48.

Denis, B., R. Laprise, D. Caya, and J. Côté, 2002: Downscaling ability of one-way nested regional climate models: The Big-Brother Experiment. *Climate Dyn.,* **18,** 627–646, doi:10.1007/s00382-001-0201-0.

Déqué, M., 2010: Regional climate simulation with a mosaic of RCMs. *Meteor. Z.,* **19,** 259–266.

Dickinson, R. E., A. Henderson-Sellers, and P. J. Kennedy, 1993: Biosphere–Atmosphere Transfer Scheme (BATS) version 1E as coupled to the NCAR Community Climate Model. NCAR Tech. Rep. NCAR/TN-387+STR, 72 pp.

Diro, G. T., D. Grimes, and E. Black, 2011: Teleconnections between Ethiopian summer rainfall and sea surface temperature: Part I—Observation and modelling. *Climate Dyn.,* **37,** 103–119, doi:10.1007/s00382-010-0837-8.

——, A. M. Tompkins, and X. Bi, 2012: Dynamical downscaling of ECMWF ensemble seasonal forecasts over East Africa with RegCM3. *J. Geophys. Res.,* **117,** D16103, doi:10.1029/2011JD016997.

Doms, G., J. Förstner, E. Heise, H.-J. Herzog, M. Raschendorfer, R. Schrodin, T. Reinhardt, and G. Vogel, 2007: A description of the nonhydrostatic regional model LM (version 3.20). Part II: Physical parameterization. COSMO Consortium, 154 pp. [Available online at http://www.cosmo- model.org/content/model/documentation/core/cosmoPhysParamtr.pdf.]

Douville, H. S., J. F. Planton, D. B. Royer, S. Stephenson, L. Tyteca, S. Kergoat, R. A. Lafont, and R. A. Betts, 2000: Importance of vegetation feedbacks in doubled-CO_2 climate experiments. *J. Geophys. Res.,* **105,** 14 841–14 861.

Dudhia, J., 1989: Numerical study of convection observed during the winter monsoon experiment using a mesoscale two-dimensional model. *J. Atmos. Sci.,* **46,** 3077–3107.

ECMWF, 2006: IFS documentation—Cy31r1 Operational implementation PART IV: Physical processes. ECMWF, 155 pp. [Available online at http://www.ecmwf.int/research/ifsdocs/CY31r1/PHYSICS/IFSPart4.pdf.]

Edwards, J. M., and A. Slingo, 1996: Studies with a flexible new radiation code. I: Choosing a configuration for a large-scale model. *Quart. J. Roy. Meteor. Soc.,* **122,** 689–719.

Essery, R. L. H., M. J. Best, R. A. Betts, and P. M. Cox, 2003: Explicit representation of subgrid heterogeneity in a GCM land surface scheme. *J. Hydrometeor.,* **4,** 530–543.

Favre, A., D. Stone, R. Cerezo, N. Philippon, and B. Abiodun, 2011: Diagnostic of monthly rainfall from CORDEX simulations over Africa: Focus on the annual cycles. *Proc. Int. Conf. on the Coordinated Regional Climate Downscaling Experiment–CORDEX,* Trieste, Italy, World Climate Research Program. [Available online at http://indico.ictp.it/indico/getFile.py/access?resId=3&materialId=1&confId=a10131.]

FEWS NET, cited 2011: Past year one of the driest on record in the eastern Horn. Famine Early Warning System Network Report, 14 June 2011, U.S. Agency for International Development. [Available online at http://reliefweb.int/report/ethiopia/east-africa-past-year-one-driest-record-eastern-horn-june-14-2011.]

Fouquart, Y., and B. Bonnel, 1980: Computations of solar heating of the earth's atmosphere: A new parameterization. *Beitr. Phys. Atmos.,* **53,** 35–62.

Fritsch, J. M., and C. F. Chappell, 1980: Numerical prediction of convectively driven mesoscale pressure systems. Part I: Convective parameterization. *J. Atmos. Sci.,* **37,** 1722–1733.

Giorgetta, M., and M. Wild, 1995: The water vapour continuum and its representation in ECHAM4. MPI Rep. 162, 38 pp.

Giorgi, F., and M. R. Marinucci, 1996: An investigation of the sensitivity of simulated precipitation to model resolution and

its implications for climate studies. *Mon. Wea. Rev.,* **124,** 148–166.

——, and L. O. Mearns, 1999: Introduction to special section: Regional climate modeling revisited. *J. Geophys. Res.,* **104,** 6335–6352, doi:10.1029/98JD02072.

——, M. R. Marinucci, and G. T. Bates, 1993a: Development of a second-generation regional climate model (RegCM2). Part I: Boundary-layer and radiative transfer processes. *Mon. Wea. Rev.,* **121,** 2794–2813.

——, ——, ——, and G. De Canio, 1993b: Development of a second-generation regional climate model (RegCM2). Part II: Convective processes and assimilation of lateral boundary conditions. *Mon. Wea. Rev.,* **121,** 2814–2832.

——, C. Jones, and G. R. Asrar, 2009: Addressing climate information needs at the regional level: The CORDEX framework. *WMO Bull.,* **58,** 175–183.

Gissila, T., E. Black, D. I. F. Grimes, and J. M. Slingo, 2004: Seasonal forecasting of the Ethiopian summer rains. *Int. J. Climatol.,* **24,** 1345–1358, doi:10.1002/joc.1078.

Gregory, D., and P. R. Rowntree, 1990: A mass flux convection scheme with representation of cloud ensemble characteristics and stability-dependent closure. *Mon. Wea. Rev.,* **118,** 1483–1506.

——, and S. Allen, 1991: The effect of convective downdraughts upon NWP and climate simulations. Preprints, *Ninth Conf. on Numerical Weather Prediction,* Denver, CO, Amer. Meteor. Soc., 122–123.

Grell, G. A., 1993: Prognostic evaluation of assumptions used by cumulus parameterizations. *Mon. Wea. Rev.,* **121,** 764–787.

Hagemann, S., 2002: An improved land surface parameter dataset for global and regional climate models. MPI Rep. 336, 21 pp.

Hastenrath, S., A. Nicklis, and L. Greischar, 1993: Atmospheric-hydrospheric mechanisms of climate anomalies in the western equatorial Indian Ocean. *J. Geophys. Res.,* **98** (C11), 20 219–20 235.

Herzog, H. J., G. Vogel, and U. Schubert, 2002: LLM—A nonhydrostatic model applied to high-resolving simulations of turbulent fluxes over heterogeneous terrain. *Theor. Appl. Climatol.,* **73,** 67–86.

Holtslag, A. A. M., E. I. F. De Bruin, and H. L. Pan, 1990: A high-resolution air mass transformation model for short-range weather forecasting. *Mon. Wea. Rev.,* **118,** 1561–1575.

Hong, S.-Y., J. Dudhia, and S.-H. Chen, 2004: A revised approach to ice microphysical processes for the bulk parameterization of clouds and precipitation. *Mon. Wea. Rev.,* **132,** 103–120.

——, Y. Noh, and J. Dudhia, 2006: A new vertical diffusion package with an explicit treatment of entrainment processes. *Mon. Wea. Rev.,* **134,** 2318–2341.

Indeje, M., H. M. F. Semazzi, and J. L. Ogallo, 2000: ENSO signal in East African rainfall seasons. *Int. J. Climatol.,* **20,** 19–46.

Jacob, D., 2001: A note to the simulation of the annual and inter-annual variability of the water budget over the Baltic Sea drainage basin. *Meteor. Atmos. Phys.,* **77,** 61–73.

——, and Coauthors, 2007: An inter-comparison of regional climate models for Europe: Model performance in present-day climate. *Climatic Change,* **81,** 31–52.

Jones, R. G., M. Noguer, D. Hassel, D. Hudson, S. Wilson, G. Jenkins, and J. Mitchell, 2004: Generating high resolution climate change scenarios using HadRM3P. Met Office Hadley Centre Rep., 40 pp.

Kain, J. S., 2004: The Kain–Fritsch convective parameterization: An update. *J. Appl. Meteor.,* **43,** 170–181.

——, and J. M. Fritsch, 1990: A one-dimensional entraining/detraining plume model and its application in convective parameterization. *J. Atmos. Sci.,* **47,** 2784–2802.

——, and ——, 1993: Convective parameterization for mesoscale models: The Kain–Fritsch scheme. *The Representation of Cumulus Convection in Numerical Models, Meteor. Monogr.,* No. 46, Amer. Meteor. Soc., 165–170.

Kiehl, J. T., J. J. Hack, G. B. Bonan, B. A. Boville, B. P. Briegleb, D. L. Williamson, and P. J. Rasch, 1996: Description of the NCAR Community Climate Model (CCM3). NCAR Tech. Note NCAR/TN-420+STR, 152 pp.

Korecha, D., and A. G. Barnston, 2007: Predictability of June to September rainfall in Ethiopia. *Mon. Wea. Rev.,* **135,** 628–650.

Kuo, H. L., 1965: On formation and intensification of tropical cyclones through latent heat release by cumulus convection. *J. Atmos. Sci.,* **22,** 40–63.

Li, J., and H. W. Barker, 2005: A radiation algorithm with correlated-*k* distribution. Part I: Local thermal equilibrium. *J. Atmos. Sci.,* **62,** 286–309.

Lohmann, U., and E. Roeckner, 1996: Design and performance of a new cloud microphysics scheme developed for the ECHAM general circulation model. *Climate Dyn.,* **12,** 557–572.

Louis, J.-F., 1979: A parametric model of vertical eddy fluxes in the atmosphere. *Bound.-Layer Meteor.,* **17,** 187–202.

Mellor, G. L., and T. Yamada, 1982: Development of a turbulence closure model for geophysical fluid problems. *Rev. Geophys. Space Phys.,* **20,** 851–875.

Meyers, G., P. McIntosh, L. Pigot, and M. Pook, 2007: The years of El Niño, La Niña, and interactions with the tropical Indian Ocean. *J. Climate,* **20,** 2872–2880.

Mitchell, T. D., and P. D. Jones, 2005: An improved method of constructing a database of monthly climate observations and associated high-resolution grids. *Int. J. Climatol.,* **25,** 693–712.

Mlawer, E. J., S. J. Taubman, P. D. Brown, M. J. Iacono, and S. A. Clough, 1997: Radiative transfer for inhomogeneous atmospheres: RRTM, a validated correlated-*k* model for the longwave. *J. Geophys. Res.,* **102,** 16 663–16 682.

Morcrette, J.-J., 1990: Impact of changes to the radiation transfer parameterizations plus cloud optical properties in the ECMWF model. *Mon. Wea. Rev.,* **118,** 847–873.

——, L. Smith, and Y. Fouquart, 1986: Pressure and temperature dependence of the absorption in longwave radiation parametrizations. *Beitr. Phys. Atmos.,* **59,** 455–469.

Mpeta, E., 2002: Mechanisms of inter-annual rainfall variability over tropical highlands of Africa and its predictability potential. Ph.D. thesis, University of Zululand, 198 pp.

Mutemi, J. N., 2003: Climate anomalies over eastern Africa associated with various ENSO evolution phases. Ph.D. thesis, University of Nairobi.

Nicholson, S. E., 1996: A review of climate dynamics and climate variability in eastern Africa. *The Limnology, Climatology and Paleoclimatology of the East African Lakes,* T. Johnson and E. Odada, Eds., CRC Press, 25–56.

——, and J. Kim, 1997: The relationship of the El Niño–Southern Oscillation to African rainfall. *Int. J. Climatol.,* **17,** 117–135.

Nikulin, G., and Coauthors, 2012: Precipitation climatology in an ensemble of CORDEX-Africa regional climate simulations. *J. Climate,* **25,** 6057–6078.

Nyakwada, W., 2009: Predictability of East African seasonal rainfall with sea surface temperature gradient modes. Ph.D. dissertation, University of Nairobi, 265 pp.

Ogallo, L. J., 1988: Relationships between seasonal rainfall in East Africa and the Southern Oscillation. *J. Climatol.,* **8,** 31–43, doi:10.1002/joc.3370080104.

Omondi, P., L. A. Ogallo, R. Anyah, J. M. Muthama, and J. Ininda, 2013: Linkages between global sea surface temperatures and decadal rainfall variability over the eastern Africa region. *Int. J. Climatol.,* **33,** 2082–2104.

Paeth, H., and Coauthors, 2011: Progress in regional downscaling of West African precipitation. *Atmos. Sci. Lett.,* **12,** 75–82, doi:10.1002/asl.306.

Pal, J. S., E. E. Small, and E. A. B. Eltahir, 2000: Simulation of regional-scale water and energy budgets: Representation of subgrid cloud and precipitation processes within RegCM. *J. Geophys. Res.,* **105,** 29 579–29 594.

——, and Coauthors, 2007: Regional climate modeling for the developing world: The ICTP RegCM3 and RegCNET. *Bull. Amer. Meteor. Soc.,* **88,** 1395–1409.

Rasch, P. J., and J. E. Kristjánsson, 1998: A comparison of the CCM3 model climate using diagnosed and predicted condensate parameterizations. *J. Climate,* **11,** 1587–1614.

Rechid, D., T. J. Raddatz, and D. Jacob, 2009: Parameterization of snow-free land surface albedo as a function of vegetation phenology based on MODIS data and applied in climate modelling. *Theor. Appl. Climatol.,* **95,** 245–255.

Ricard, J. L., and J. F. Royer, 1993: A statistical cloud scheme for use in an AGCM. *Ann. Geophys.,* **11,** 1095–1115.

Ritter, B., and J.-F. Geleyn, 1992: A comprehensive radiation scheme of numerical weather prediction with potential applications in climate simulations. *Mon. Wea. Rev.,* **120,** 303–325.

Rockel, B., A. Will, and A. Hense, 2008: The regional climate model COSMO-CLM (CCLM). *Meteor. Z.,* **17,** 347–348.

Ropelewski, C. F., and M. S. Halpert, 1987: Global and regional scale precipitation patterns associated with the El Niño/Southern Oscillation. *Mon. Wea. Rev.,* **115,** 1606–1626.

——, and ——, 1989: Precipitation patterns associated with the high index phase of the Southern Oscillation. *J. Climate,* **2,** 268–284.

Rudolf, B., A. Becker, U. Schneider, A. Meyer-Christoffer, and M. Ziese, 2010: The new ''GPCC Full Data Reanalysis Version 5'' providing high-quality gridded monthly precipitation data for the global land-surface is public available since December 2010. GPCC Status Rep., 7 pp.

Rummukainen, M., 2010: State-of-the-art with regional climate model. *Wiley Interdiscip. Rev.: Climate Change,* **1,** 82–96, doi:10.1002/wcc.8.

Saji, N. H., B. N. Goswami, P. N. Vinayachandran, and T. Yamagata, 1999: A dipole mode in the tropical Indian Ocean. *Nature,* **401,** 360–363, doi:10.1038/43855.

Samuelsson, P., S. Gollvik, and A. Ullerstig, 2006: The land-surface scheme of the Rossby Centre Regional Atmospheric Climate Model (RCA3). Swedish Meteorological and Hydrological Institute Meteorology Rep. 122, 25 pp.

——, and Coauthors, 2011: The Rossby Centre Regional Climate Model RCA3: Model description and performance. *Tellus,* **63A,** 4–23.

Sass, B. H., L. Rontu, H. Savijärvi, and P. Räisänen, 1994: HIRLAM-2 radiation scheme: Documentation and tests. SMHI HIRLAM Tech. Rep. 16, 43 pp.

Savijärvi, H., 1990: Fast radiation parameterization schemes for mesoscale and short-range forecast models. *J. Appl. Meteor.,* **29,** 437–447.

Schulz, J.-P., L. Dümenil, J. Polcher, C. A. Schlosser, and Y. Xue, 1998: Land surface energy and moisture fluxes: Comparing three models. *J. Appl. Meteor.,* **37,** 288–307.

Segele, Z. T., L. M. Leslie, and P. J. Lamb, 2009a: Evaluation and adaptation of a regional climate model for the Horn of Africa: Rainfall climatology and interannual variability. *Int. J. Climatol.,* **29,** 47–65.

——, P. J. Lamb, and L. M. Leslie, 2009b: Large-scale atmospheric circulation and global sea surface temperature associations with Horn of Africa June–September rainfall. *Int. J. Climatol.,* **29,** 1075–1100, doi:10.1002/joc.1751.

Shongwe, M. E., G. J. Van Oldenborgh, B. J. J. M. Van Den Hurk, B. De Boer, C. A. S. Coelho, and M. K. Van Aalst, 2009: Projected changes in mean and extreme precipitation in Africa under global warming. Part I: Southern Africa. *J. Climate,* **22,** 3819–3837.

Skamarock, W. C., J. B. Klemp, J. Dudhia, D. O. Gill, D. M. Barker, W. Wang, and J. G. Powers, 2008: A description of the Advanced Research WRF version 3. NCAR Tech Note NCAR/TN-475+STR, 113 pp.

Smirnova, T. G., J. M. Brown, S. G. Benjamin, and D. Kim, 2000: Parameterization of cold-season processes in the MAPS land-surface scheme. *J. Geophys. Res.,* **105,** 4077–4086.

Smith, R. N. B., 1990: A scheme for predicting layer clouds and their water content in a general circulation model. *Quart. J. Roy. Meteor. Soc.,* **116,** 435–460.

Sun, L., F. H. M. Semazzi, F. Giorgi, and L. Ogallo, 1999a: Application of the NCAR regional climate model to eastern Africa: 1. Simulation of the short rains of 1988. *J. Geophys. Res.,* **104,** 6529–6548.

——, ——, ——, and ——, 1999b: Application of the NCAR regional climate model to eastern Africa: 2. Simulation of interannual variability of short rains. *J. Geophys. Res.,* **104,** 6549–6562.

——, D. F. Moncunill, H. Li, A. D. Moura, F. D. A. D. S. Filho, and S. E. Zebiak, 2006: An operational dynamical downscaling prediction system for Nordeste Brazil and the 2002–04 real-time forecast evaluation. *J. Climate,* **19,** 1990–2007.

Sundqvist, H., E. Berge, and J. E. Kristjansson, 1989: Condensation and cloud parameterization studies with a mesoscale numerical weather prediction model. *Mon. Wea. Rev.,* **117,** 1641–1657.

Sylla, M. B., F. Giorgi, E. Coppola, and L. Mariotti, 2012: Uncertainties in daily rainfall over Africa: Assessment of gridded observation products and evaluation of a regional climate model simulation. *Int. J. Climatol.,* **33,** 1805–1817, doi:10.1002/joc.3551.

Taylor, K. E., 2001: Summarizing multiple aspects of model performance in a single diagram. *J. Geophys. Res.,* **106** (D7), 7183–7192.

Tiedtke, M., 1989: A comprehensive mass flux scheme for cumulus parameterization in large-scale models. *Mon. Wea. Rev.,* **117,** 1779–1800.

——, 1993: Representation of clouds in large-scale models. *Mon. Wea. Rev.,* **121,** 3040–3061.

Tompkins, A. M., 2002: A prognostic parameterization for the subgrid-scale variability of water vapor and clouds in large-scale models and its use to diagnose cloud cover. *J. Atmos. Sci.,* **59,** 1917–1942.

Ummenhofer, C. C., M. H. England, P. C. McIntosh, G. A. Meyers, M. J. Pook, J. S. Risbey, A. Sen Gupta, and A. S. Taschetto, 2009: What causes southeast Australia's worst droughts? *Geophys. Res. Lett.,* **36,** L04706, doi:10.1029/2008GL036801.

UNEP, 2011: The Democratic Republic of the Congo: Post-conflict environmental assessment synthesis for policy makers. United Nations Environment Programme, 72 pp.

van Meijgaard, E., L. van Ulft, W. van den Berg, F. Bosveld, B. van den Hurk, G. Lenderink, and A. P. Siebesma, 2008: The

KNMI regional atmospheric climate model RACMO, version 2.1. KNMI Tech. Rep. TR-302, 43 pp.

Verseghy, D. L., 2000: The Canadian Land Surface Scheme (CLASS): Its history and future. *Atmos.–Ocean,* **38,** 1–13.

Wang, Y., R. L. Leung, J. L. McGregor, D.-K. Lee, W.-C. Wang, Y. Ding, and F. Kimura, 2004: Regional climate modeling: Progress, challenges, and prospects. *J. Meteor. Soc. Japan,* **82,** 1599–1628.

Wilson, C. A., 1992: Vertical diffusion. Unified Model Documentation Paper 21, Met Office, 4 pp. [Available online at http://cms.ncas.ac.uk/documents/vn4.5/p021.pdf.]

World Bank, 2012: Doing business in the East African economies. IFC/World Bank Rep., 116 pp.

Zadra, A., D. Caya, J. Côté, B. Dugas, C. Jones, R. Laprise, K. Winger, and L.-P. Caron, 2008: The next Canadian Regional Climate Model. *Phys. Can.,* **64,** 75–83.

3

Evaluation of CGCM-driven simulations

The previous paper demonstrated that the RCMs are able to capture the seasonal and spatial characteristics of rainfall over eastern Africa when driven by "perfect" reanalysis boundary conditions. This section evaluates how well RCMs capture the statistics of the historical climate when driven by imperfect boundary conditions i.e, using driving data from multiple coupled global climate models (CGCMs). Simulations of the past by CGCMs are not time-synchronize with the observed climate, so the boundary conditions supplied by the CGCM to the RCM are not temporally equivalent to observed boundary conditions. Despite this, over a sufficiently long period of simulation the statistics of climate produced by the CGCM would be expected to be similar to that of the statistics of the observed climate. When RCMs are forced by imperfect driving conditions, error is introduced from two sources: through the RCMs own structural errors (for example in parameterisation schemes) and the error inherited through the CGCM lateral boundary conditions. In this paper results from two RCMs driven by multiple CGCM simulations were analyzed and compared to the observed data as well as to the reanalyses-driven RCM simulations that were analyzed in previous paper. The comparison of CGCM-driven RCM results with reanalysis-driven RCM results help to identify the primary source of the error, i.e, whether from the CGCM or the RCM. The CGCM-driven RCM simulations are compared with the corresponding CGCM simulations to assess how far the RCM results diverge from their corresponding driving CGCM results. The results form this paper provides a basis from which projection information can be assessed, which is the theme of the paper in Chapter 4.

Clim Dyn
DOI 10.1007/s00382-015-2734-7

Teleconnection responses in multi-GCM driven CORDEX RCMs over Eastern Africa

Hussen Seid Endris[1] · **Christopher Lennard**[1] · **Bruce Hewitson**[1] · **Alessandro Dosio**[2] · **Grigory Nikulin**[3] · **Hans-Jürgen Panitz**[4]

Received: 7 October 2014 / Accepted: 29 June 2015

Abstract The ability of climate models to simulate atmospheric teleconnections provides an important basis for the use and analysis of climate change projections. This study examines the ability of COordinated Regional climate Downscaling EXperiment models, with lateral and surface boundary conditions derived from Coupled Global Climate Models (CGCMs), to simulate the teleconnections between tropical sea surface temperatures and rainfall over Eastern Africa. The ability of the models to simulate the associated changes in atmospheric circulation patterns over the region is also assessed. The models used in the study are Rossby Centre regional atmospheric model (RCA) driven by eight CGCMs and COnsortium for Small scale MOdeling (COSMO) Climate Limited-area Modelling (COSMO-CLM or CCLM) driven by four of the same CGCMs. Teleconnection patterns are examined using correlation, regression and composite analysis. In order to identify the source of the errors, CGCM-driven regional climate model (RCM) results are compared with ERA-Interim driven RCM results. Results from the driving CGCMs are also analyzed. The RCMs driven by reanalysis (quasi-perfect boundary conditions) successfully capture rainfall teleconnections in most examined regions and seasons. Our analysis indicates that most of the errors in simulating the teleconnection patterns come from the driving CGCMs. RCMs driven by MPI-ESM-LR, HadGEM2-ES and GFDL-ESM2M tend to perform relatively better than RCMs driven by other CGCMs. CanESM2 and MIROC5, and their corresponding downscaled results capture the teleconnections in most of the sub-regions and seasons poorly. This highlights the relative importance of CGCM-derived boundary conditions in the downscaled product and the need to improve these as well as the RCMs themselves. Overall, the results produced here will be very useful in identifying and selecting CGCMs and RCMs for the use of climate change projecting over the Eastern Africa.

Keywords CORDEX · CMIP5 · Teleconnections · Eastern Africa · Rainfall · RCM

1 Introduction

Rainfall over Eastern Africa shows a high degree of inter- and intra-annual variability. This rainfall variability impacts the economy of the region because of the dependence of important sectors on rainfall (e.g. agriculture, water management, health and energy) and the relatively low adaptive capacity of these economies. For example, the two severe recent droughts 2008/2009 and 2011 in wide regions of Kenya, Ethiopia, Djibouti and Somalia affected food security and subjected millions of peoples to famine (FEWS NET 2011; Slim 2012; UNOCHA 2011). Previous studies have linked the interannual variability of rainfall over the region with sea surface temperature (SST) anomalies over the tropical Oceans (Ropelewski and Halpert 1987; Nicholson and Kim 1997; Clark et al. 2003; Behera et al. 2005).

✉ Hussen Seid Endris
hussen.seid1@gmail.com

[1] Climate System Analysis Group, University of Cape Town, Cape Town, South Africa

[2] European Commission Joint Research Centre, Institute for Environment and Sustainability, Ispra, Italy

[3] Rossby Centre, Swedish Meteorological and Hydrological Institute, Norrköping, Sweden

[4] Karlsruher Institut für Technologie, Institut für Meteorologie und Klimaforschung, Karlsruhe, Germany

Published online: 08 July 2015

Particularly, the El Niño Southern Oscillation (ENSO) (Ogallo 1988; Indeje et al. 2000; Mason and Goddard 2001; Segele et al. 2009a; Diro et al. 2011b) and the Indian Ocean Dipole (IOD) (Saji et al. 1999; Abram et al. 2008; Ummenhofer et al. 2009; Bahaga et al. 2015) are suggested to be the dominant drivers of the rainfall variability over the region. Thus, a better understanding of SST-rainfall teleconnections and their simulation by global and regional climate models (RCMs) is increasingly important to deliver reliable predictions of seasonal to interannual rainfall anomalies for disaster prevention (floods and droughts) and resource planning (agriculture, water and energy).

Global Climate Models (GCMs) are the primary tools for understanding the global climate and its projected change under different forcing scenarios (IPCC 2007, 2013). However, the coarse resolution of GCMs precludes them from capturing the effects of local forcings like terrain effects and land-sea contrasts that modulate the climate signal at finer scales (Giorgi et al. 2001; Wang et al. 2004; Rummukainen 2010). It also limits their ability to reproduce realistic extreme events that are critical to many users of climate information (Giorgi et al. 2009). In order to respond to the strategic, regional demands of society regarding climate variability and climate projection, various downscaling techniques have been developed. These are broadly categorized into statistical and dynamical downscaling techniques. Statistical downscaling develops robust statistical relationships between large-scale climate variables like atmospheric surface pressure and a local climate variable like rainfall at a particular place. This relationship is then mapped to GCM data to obtain the local variable response (Hewitson and Crane 1996). The main drawback of statistical downscaling is that it assumes the derived statistical relationship will not change due to climate change. On the other hand, dynamical downscaling involves the use of numerical models that simulate the climate over a chosen domain based on fundamental conservation laws and receives forcing GCM data at the domain boundaries. Dynamical downscaling include limited-area RCMs (e.g. Giorgi and Mearns 1991, 1999) and stretch-grid atmospheric GCMs (e.g. Déqué and Piedelievre 1995; Fox-Rabinovitz et al. 2006).

RCMs are widely used tool for climate process studies and climate change projection by using boundary conditions from reanalysis or GCMs output (Giorgi and Mearns 1999; Wang et al. 2004). By operating at high spatial resolutions, RCMs have the ability to capture small-scale features and process that influence the regional climate such as topographical influence and small-scale processes. However, accurate simulation of precipitation still remains a major challenge in RCMs as it depends on many processes. For example, Nikulin et al. (2012) show that precipitation is triggered too early during the diurnal cycle in the majority of CORDEX RCMs. Endris et al. (2013) also show that most of the CORDEX models failed to reproduce the October–December (OND) rainfall peak over equatorial part of eastern Africa. Therefore, a process based comparison of models with observations is an important step to understand limitations of the models and to provide guidance for model improvement. Furthermore, the process based evaluation of models provides an important context for the interpretation and use of climate change projections. This is particulary important for CORDEX data users to explore the uncertainity for use of projected data.

Although several works have investigated the capability of RCMs to reproduce several features of African climatology (Segele et al. 2009b; Sylla et al. 2009; Paeth et al. 2011; Nikulin et al. 2012; Endris et al. 2013; Kalognomou et al. 2013 and Kim et al. 2014 among others), very few studies have attempted to evaluate the performance of RCMs in reproducing the large scale processes (e.g. teleconnections). Due to the high computational cost to run multiple RCMs and/or to force RCMs with output from a number of GCMs, those very few studies focused only on evaluating the performance of a single RCM driven by a single GCM and/or reanalysis datasets. For example, Anyah and Semazzi (2007) evaluated the capability of the International Center for Theoretical Physics RCM (ICTP-RegCM3) in reproducing the rainfall variability over east Africa and found that the model preserves the relationships between the regional rainfall and some of the global teleconnections (ENSO and IOD). Boulard et al. (2013) evaluated the performance of the Weather Research and Forecasting (WRF) model in downscaling large-scale climate variability over southern Africa with a particularly attention of ENSO. They showed limited skill in the model's ability to reproduce the seasonal droughts associated with El Ninõ conditions. Over tropical Americas, Tourigny and Jones (2009) evaluated the ability of the Rossby Centre Atmospheric Model (RCA) to downscale SST and large-scale atmospheric anomalies associated with ENSO, and found that the model reproduces the majority of the documented regional responses to ENSO forcing. However, it is well known that each model has its strengths and weaknesses depending on the season and region chosen for the analysis (e.g. Endris et al. 2013; Kalognoumou et al. 2013). Additionally, the boundary conditions provided to the RCMs plays an important role in the model's ability to propagate teleconnective signals into the region of interest. If the GCM is unable to capture, for example, the Walker circulation response to ENSO, it is unreasonable to expect the RCM to propagate the signal into the region of interest.

In this study, our aim is to examine the ability of two RCMs that participated in the COordinated Regional climate Downscaling EXperiment (CORDEX), with lateral and surface boundary conditions derived from reanalysis

and CGCMs, to accurately reproduce the observed spatiotemporal rainfall variability associated with the leading climate modes (like ENSO and IOD) affecting the eastern Africa on interannual time scales. We examine whether or not the downscaling propagates large-scale (teleconnective) forcing present in the reanalysis and CGCMs through the boundaries of the RCMs into the interior of the domain to simulate the local rainfall response. Such study is crucial since the capability of the RCMs to accurately simulate current climatic conditions associated with large-scale features constrains their ability to accurately simulate future climate. Obviously this idea is based on the assumption that current climate teleconnections with ENSO and IOD continue to operate in the same manner under a warming scenario. When RCMs are forced by CGCMs, the RCM simulations are affected by the combination effect of the imperfect driving fields and the RCMs' structural errors. Comparing reanalysis driven and CGCM-driven RCM results with observational data will help to determine whether errors come from the RCMs or driving lateral boundary conditions. To our knowledge, this is the first study assessing the ability of RCMs to simulate the climate impacts associated with ENSO and IOD over eastern Africa using different driving dataset as lateral boundary conditions.

The key research questions that we address in the study are:

1. Which oceanic basins have a strong relationship with Eastern Africa regional rainfall? This will be addressed using observed data.
2. How well the models perform at reproducing the observed teleconnection patterns (amplitudes and spatial patterns)?
3. How do different boundary forcings (from CGCMs) affect the RCM ability to simulate the teleconnections?
4. How well the models represent the anomalous circulation patterns associated with the leading climate modes affecting the rainfall over the region?

2 Data and methods

2.1 Study region and areas of analysis

The study region covers the Eastern Africa region (see Fig. 1). Because of the complexities of rainfall in the region, it is important to categorize the region into homogeneous rainfall subregions. As such we first classified the

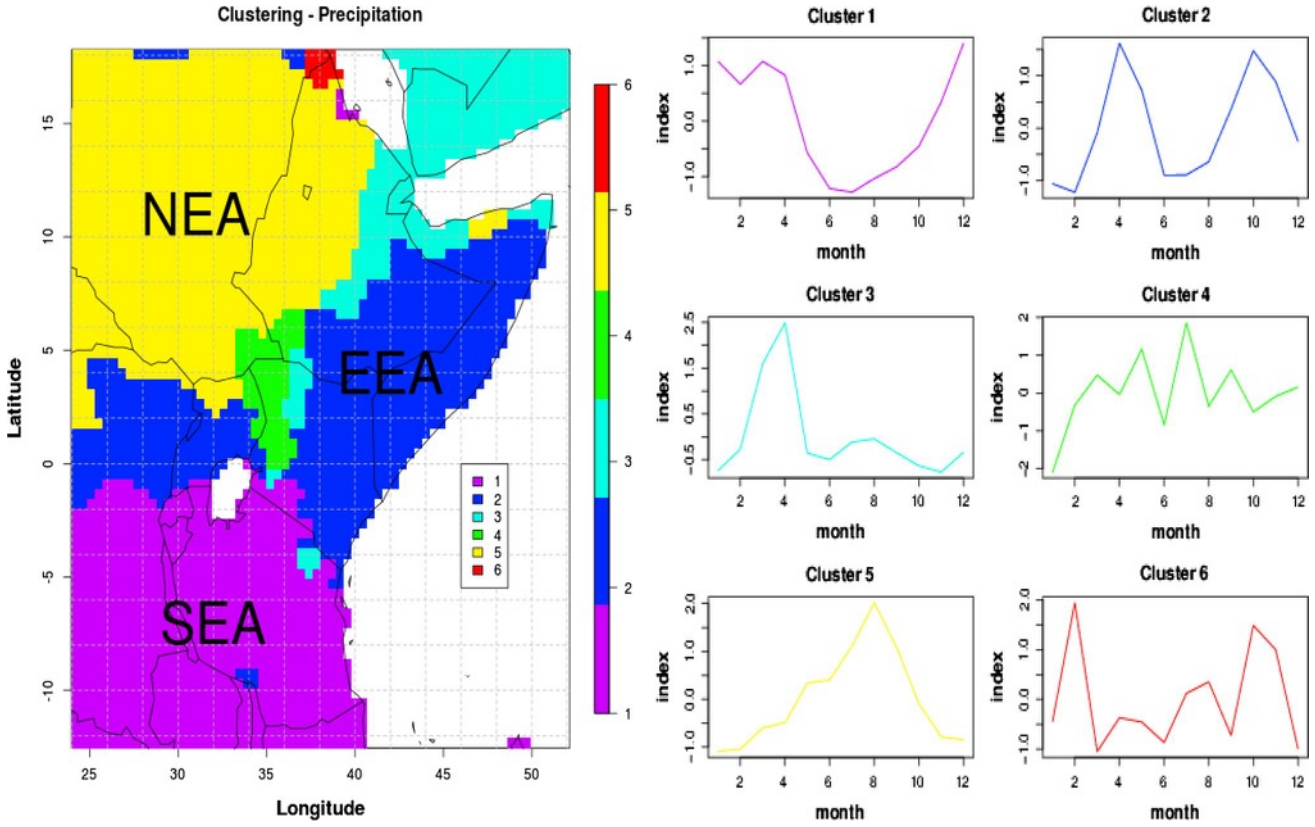

Fig. 1 Homogeneous rainfall regions (*left*) with corresponding annual cycles (*right*) as categorized using hierarchical agglomerative clustering technique

region into six climatically homogeneous rainfall subregions using Global Precipitation Climatology Centre data that has a spatial resolution of 0.5° (GPCC; version 5, 1901–2006; Rudolf et al. 2010). The regionalization was carried out using hierarchical agglomerative clustering technique with average linkage based on the R function *hclust* algorithms of Murtagh (1985). Like any other clustering methods, this method has its own limitations. One of the limitations of this technique is that it requires the analyst to specify the appropriate number of clusters. Since this study focuses on the large-scale forcings, and we also analyze coarse resolution GCM output, we choose to limit the number of clusters to six, however it should be noted that the number of homogeneous rainfall regions could be fewer or greater than this number depending on the objectives of the study. In fact, the result we obtained here is in agreement with previous studies conducted over different time periods using different observational data such as Liebmann et al. (2012) over Africa and Gissila et al. (2004) over Ethiopia.

Our analysis focuses on three subregions, which cover most of eastern Africa, namely: the northern part of Eastern Africa (NEA), Equatorial Eastern Africa (EEA) and the Southern part of Eastern Africa (SEA) (Fig. 1). NEA covers most the Ethiopian highlands and South Sudan, and some parts of Eritrea and Sudan, which has a rainfall maximum during boreal summer (June–September) and a pronounced dry season in boreal winter. EEA covers most of Somalia, Kenya, Uganda, and South Eastern parts of Ethiopia, and is characterized by a bimodal rainfall distribution with the major rainfall season in March–May (MAM) and a shorter rainfall season in October–December (OND). SEA lies south of the equator and is mainly characterized by long unimodal rainfall distribution extending from October to April.

The seasons analyzed in this study are JJAS for NEA, and OND for EEA and SEA. MAM rainfall season is not included in the analysis because rainfall teleconnections (i.e., correlations) with SSTs is much weaker (Indeje et al. 2000) and so is less usefully assessed against model data.

2.2 Data

2.2.1 Observed data

The observed rainfall dataset utilized in this study is the GPCC. This dataset is a gauge-based gridded observational dataset available at a 0.5° spatial and monthly temporal resolution. The observed SST data used in this study is the monthly mean National Oceanic and Atmospheric Administration Optimum Interpolation SST version 2 (NOAA_OI_SST_V2) gridded observational dataset, provided by the NOAA-CIRES Climate Diagnostics Center, Boulder, USA (http://www.esrl.noaa.gov/psd/data/gridded/data.noaa.oisst.v2.html). The NOAA_OI_SST_V2 product integrates both in situ and satellite data from November 1981 to present at a 1° spatial resolution. These SST monthly fields are derived by a linear interpolation of the weekly optimum interpolation (OI) version 2 fields to daily fields and then averaging the daily values over a month (Reynolds et al. 2002). More details about the product can be found in Reynolds et al. (2002). Surface winds and sea level pressure dataset are based on ERA-Interim reanalysis (Dee et al. 2011). We note that reanalysis is essentially model simulations that incorporate all available observations at the time of the processing.

2.2.2 Model data

In this study we used the results from two CORDEX RCMs, namely the Rossby Centre regional atmospheric model (RCA) (Samuelsson et al. 2011) and COnsortium for Small scale MOdeling (COSMO) Climate Limited-area Modelling (COSMO-CLM or CCLM) [Baldauf et al. 2011]. Both models have first been run in an "evaluation" mode, i.e. driven by ERA-Interim for the period 1989–2008 (see Nikulin et al. 2012; Panitz et al. 2014). Thanks to SMHI institution, another RCA model evaluation run is performed and available for the period of 1980–2010. For the historical CGCM driven runs, which cover the period 1950–2005, RCA has been driven by 8 CGCMs and CCLM by 4 of the same CGCMs (see Dosio et al. 2015; Dosio and Panitz 2015 for CGCM driven CCLM runs). All the CORDEX Africa simulations were at spatial grid resolution of 0.44°. Table 1 presents a list of RCMs and driving CGCMs considered in the present study.

The CMIP5 CGCMs have different ensemble members (r1, r2, r3 etc.) different only in initial conditions around 1850, while the physics and the greenhouse gas forcing are the same. For CORDEX Africa simulations only the first member from the CMIP5 CGCMs is used to force the RCMs with the exception of the EC-EARTH model from which the 12th ensemble member was used. All CGCM and RCM rainfall data were interpolated to a common grid, similar to the observed GPCC dataset 0.5° resolution. As mentioned above, ERA-Interim driven RCA model run is available for the period of 1980–2010 as well as 1989–2008. We compared these two RCA evaluation runs with observation to check the sensitivity of teleconnection patterns to the choice of the period and found teleconnection patterns are not sensitive to the choice of the period. We therefore chose the 1989–2008 period for both RCM ERA-Interim downscalings as a common period. The CGCM and downscaled CGCM data were extracted from 1982 to 2005 to maximise the overlap with observed SST data to compute statistical relationships and quantify teleconective

Table 1 List of CORDEX RCMs and the driving CMIP5 CGCMs used

CGCMs	CGCMs Horizontal resolution	RCMs		Institute and country
		RCA	CCLM	
CNRM-CM5	1.4° × 1.4°	✓	✓	CNRM, France
EC-EARTH	1.125° × 1.12°	✓	✓	European Consortium
HadGEM2-ES	1.875° × 1.25°	✓	✓	MOHC, United Kingdom
MPI-ESM-LR	1.9° × 1.9°	✓	✓	MPI, Germany
CanESM2	2.8° × 2.8°	✓		CCCma, Canada
GFDL-ESM2M	2.5° × 2.0°	✓		NOAA/GFDL, United States
MIROC5	1.4° × 1.4°	✓		CCSR/NIES/JAMSTEC, Japan
NorESM1-M	2.5° × 1.9°	✓		NCC, Norway

RCA is driven by 8 CGCMs, while CCLM driven only by 4 CGCMs. All model dataset were obtained from the Earth System Grid Federation (ESGF) web portals

events. Although this period is not identical to that of the downscaled ERA-Interim runs, we again found that the assessment of teleconnection patterns were not sensitive to the choice of the period. Thus in all cases, our analysis focuses on the period of 1982–2005, with the exception of the ERA-Interim driven evaluation downscaling (1989–2008).

2.3 Methods

To assess the models' ability in representing teleconnection patterns, we follow an approach similar to Langenbrunner and Neelin (2013). Spearman's rank correlation and linear regression are used to calculate the seasonal precipitation teleconnections between regional rainfall and SSTs in a number of oceanic regions for the selected time period. The Spearman's rank-order correlation is a non-parametric rank statistic that measures the strength of the association between two variables (Hauke and Kossowski 2011). Unlike Pearson's product-moment correlation, it is a robust method in the presence of outliers, and does not require the assumption of normality. It also does not assume linear relationships, which means it is well-suited for exponential and logarithmic relationships. Linear regression is widely used for assessing the relationship between precipitation and SSTs. One limitation of this method is the assumption that precipitation data follow a Gaussian distribution, but in reality it is zero bounded and demonstrates non-gaussian behavior.

The analysis procedure is constructed in the following way. First, seasonal means have been computed for both precipitation and SST fields. Since teleconnection signals are the main focus of this study, long-term changes/trends were removed from both observed and simulation time series. Thus, all seasonal time series have been detrended linearly at each grid point. Each SST grid-point is then correlated against a spatially averaged rainfall time series to identify the oceanic regions that have robust relationships with the regional seasonal rainfall, as well as to assess the models' ability to simulate the different patterns of teleconnections with each region. Once we have identified regions that have a strong relationship with regional rainfall, precipitation at each grid-point is regressed against a spatially averaged SST time series. The aim is to examine the ability of the model to capture the spatial pattern as well as the amplitude of the teleconnection patterns. Appropriate tests are used in the rank and linear methods to resolve grid-points that meet or pass 5 % significance level. Student's *t* test is used for computing the statistical significance for linear regression by assuming independent normal distributions. The statistical significance for the spearman's rank correlation is computed using z-test.

Finally, composite analysis is used to assess the models' ability to represent the anomalous circulation patterns associated to the dominant modes affecting the rainfall over the region. Details of this method are presented in section "d" under results and discussion part.

3 Results and discussion

Before analyzing how the climate models represent the teleconnection patterns, we first clarify two important points. The first point is that caution needs to be taken when comparing downscaled CGCMs climatologies (the historical runs) as a function of real calendar time, especially in relation to observational dataset. It is not expected the simulation of natural variability in downscaled CGCM simulations to follow the same time evolution as the observations. This is related with the experimental design of the driving CMIP5 CGCM simuations. The CMIP5 CGCMs are the so-called free-running simulations, and natural variability in these models is not constrained to occur in the same phase sequence as the real world (Taylor et al. 2012). In other words, there is no input to the models to control the natural or internal

variability in the simulated climate. To ensure the models to fellow the same phase with the simulated variability of the real world, the models either must be run in a forecast mode (i.e., models must be initialized to the current state of the coupled ocean–atmosphere system) (Yang et al. 2009) or in forced projection mode (i.e., models must be forced with observed SSTs) (Kosaka and Xie 2013). However, this is not the case for the CMIP5 CGCM runs. Therefore, like the driving CGCM simulations, it is not expected the simulated variability in downscaled CGCMs sequence to match in phase with reality. The models can still simulate the statistical properties of climate features. Thus, in our analysis for models driven by CGCMs, SST from the parent CGCM and rainfall from the RCMs is utilized to compute SST-rainfall teleconnections. However, for RCMs driven by reanalysis dataset, it is expected that the simulated variability occur temporally in phase with reality, so an observed SST dataset is used to analyze the teleconnection patterns. For the analysis of CGCM results, we use monthly precipitation and SST data from the CMIP5 CGCMs.

The second point concerns methods of assessing teleconnections for the multi-model ensemble mean. One approach, to obtain the teleconnection of ensemble mean, is by averaging the different model files to form a single file before computing the teleconnections, however, this is misleading as it smoothes the variability. Another approach is by calculating the teleconnections for each ensemble member (RCM realization) individually and average the patterns together later. While this is more widely used, obtaining a test of statistical significance becomes complicated, as one cannot easily take an average of significance tests across different models. A third approach (the option we have chosen) is by concatenating time series of the available models and then compute the teleconnection from the concatenated data as it allows computation of significant values. It is expected that too many significant correlations would emerge from this method, as there are a large number of observations as a result of the concatenation. To reduce the chances of obtaining erroneous/excessive significant correlations, an adjustment has been made to p values using Bonferroni correction (Bland and Altman 1995). Bonferroni correction is a statistical method used to correct p values when several dependent or independent statistical testes are being performed simultaneously on a single dataset. Accordingly, we obtained a new critical value for the concatenated data (**0.0125**) by deviding the critical p value (**0.05**) with the number of hypothsises being tested (**4**), with p value <0.0125 to be significant. We noted that apart from being able to obtain significant correlation in this approach, the teleconnection patterns obtained from the last two methods are almost identical.

Fig. 2 **a** Correlations of JJAS rainfall averaged over NEA, against concurrent grid-point SSTs. *Hatching* indicates regions where the correlation is statistically significant at the 5 % level. **b** Correlations of OND rainfall averaged over EEA, against concurrent grid-point SSTs. *Hatching* indicates regions where the correlation is statistically significant at the 5 % level. **c** Correlations of OND rainfall averaged over SEA; against concurrent grid-point SSTs. *Hatching* indicates regions where the correlation is statistically significant at the 5 % level ▶

3.1 Teleconnection patterns resolved though Spearman rank correlation

In order to identify oceanic regions that have a robust relationship with regional rainfall and also to assess the models' ability to simulate the spatial pattern of the teleconnection, area averaged seasonal rainfall in each homogeneous rainfall subregion is correlated with concurrent grid point SSTs. These relationships are shown in Fig. 2a–c for the models and observation. In each case, the cross-hatches indicate statistically significant correlations at the 5 % level. Here significant correlations are computed using z-test statistic. The test statistics assumed to follow the normal distribution under the null hypothesis (i.e., no correlation). As has been mentioned above, RCA model was driven by 8 CGCMs, whereas CCLM was driven by 4 common CGCMs. For direct inter-comparison of CGCM and downscaled results, each Figure contains two panels (top and bottom). In the top panel, the first column shows the observational dataset, then the 4 common driving CGCMs and finally the CGCM ensemble mean; the second column shows the results of RCA driven by ERA-Interim, 4 common CGCMs and the ensemble mean; and the third column is similar to the second column, but for CCLM. In the bottom panel are the results of the remaining 4 CGCMs (first column) and the downscaled RCA results (second column).

Figure 2a shows the spearman's rank correlations between de-trended JJAS rainfall area-averaged over NEA, against de-trended concurrent grid-point SSTs. Hatching indicates statistically significant correlations at the 5 % level. The observed dataset (GPCC) shows that JJAS rainfall in the northern part of the region has significant correlation with SSTs in Eastern equatorial Pacific—a positive rainfall anomaly tends to occur during the cold phase of ENSO while dry conditions prevail during the warm phase ENSO. This is consistent with previous studies of Segele et al. (2009a) and Diro et al. (2011b), which use rain gauge rainfall data, and observed SST. This signal is also well captured by ERA-Interim driven RCMs. Mixed results are found in the CGCMs and the downscaled CGCM data. In some cases both CGCMs and corresponding downscaled results show similar teleconnection patterns, but in other cases the RCMs either deteriorate or improved the teleconnection signal. For example, EC-EARTH and MPI-ESM-LR and their corresponding downscaled results fail to

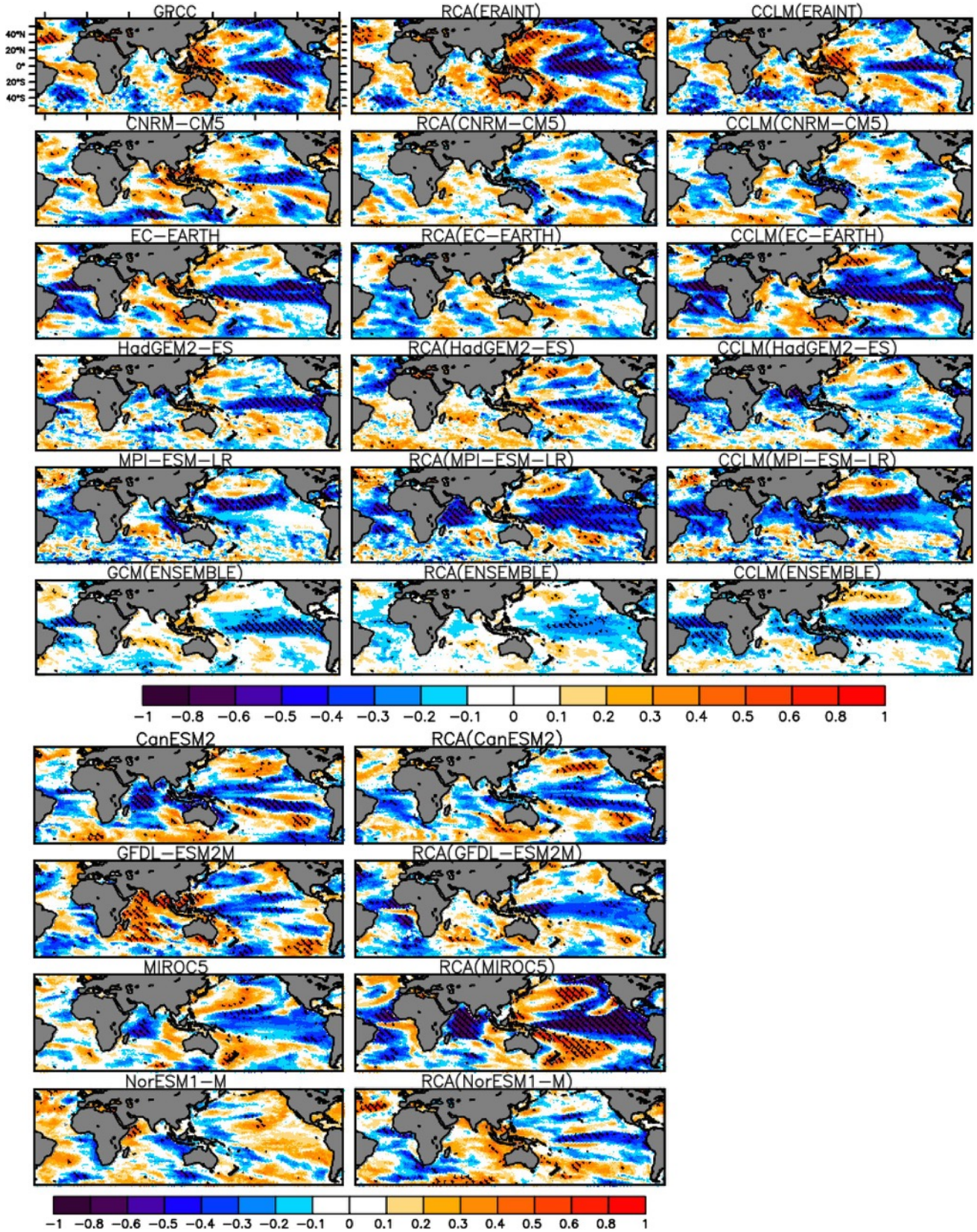
GRCC
RCA(ERAINT)
CCLM(ERAINT)
40°N
20°N
0°
20°S
40°S
CNRM−CM5
RCA(CNRM−CM5)
CCLM(CNRM−CM5)
EC−EARTH
RCA(EC−EARTH)
CCLM(EC−EARTH)
HadGEM2−ES
RCA(HadGEM2−ES)
CCLM(HadGEM2−ES)
MPI−ESM−LR
RCA(MPI−ESM−LR)
CCLM(MPI−ESM−LR)
GCM(ENSEMBLE)
RCA(ENSEMBLE)
CCLM(ENSEMBLE)
−1 −0.8 −0.6 −0.5 −0.4 −0.3 −0.2 −0.1 0 0.1 0.2 0.3 0.4 0.5 0.6 0.8 1
CanESM2
RCA(CanESM2)
GFDL−ESM2M
RCA(GFDL−ESM2M)
MIROC5
RCA(MIROC5)
NorESM1−M
RCA(NorESM1−M)
−1 −0.8 −0.6 −0.5 −0.4 −0.3 −0.2 −0.1 0 0.1 0.2 0.3 0.4 0.5 0.6 0.8 1

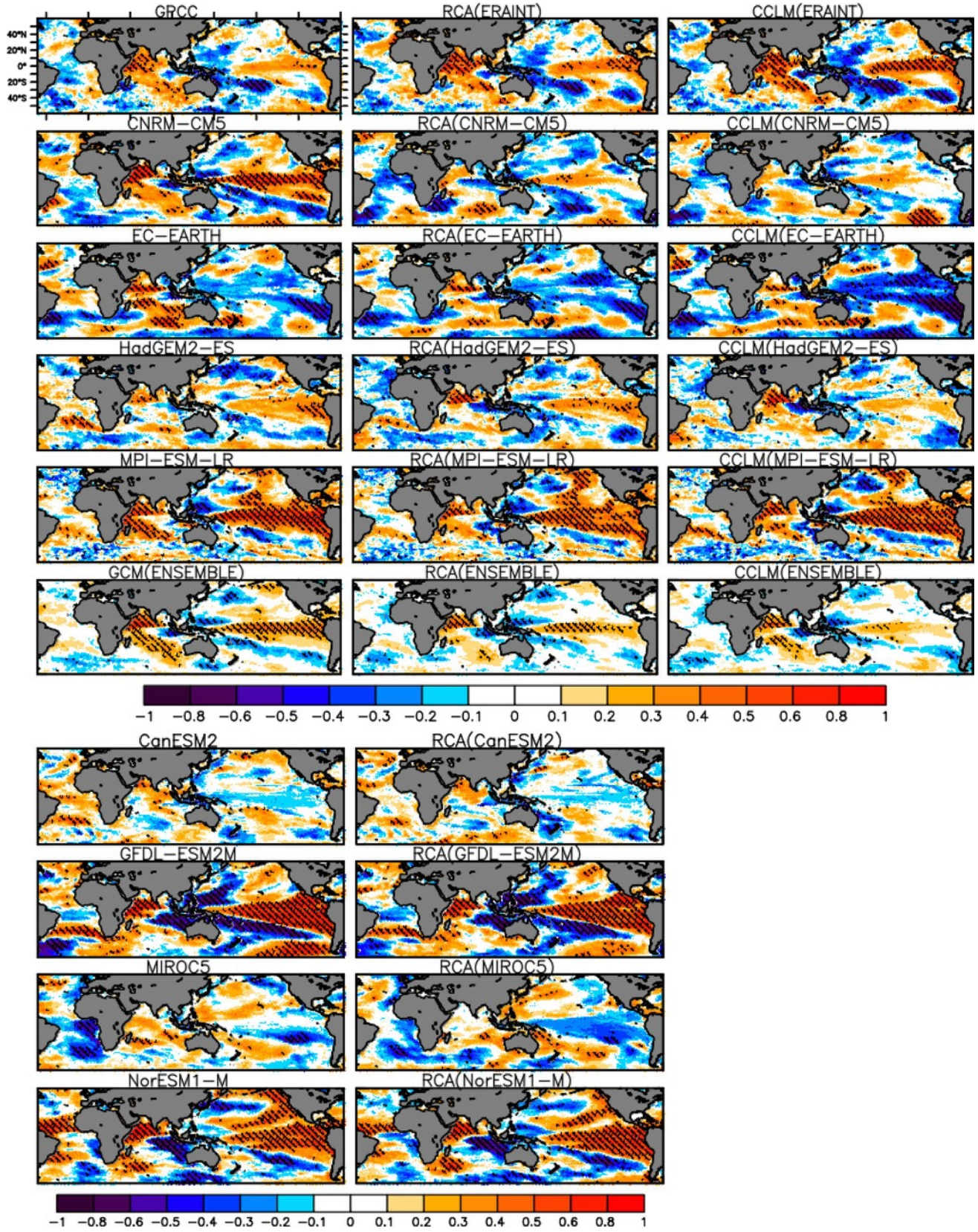

Fig. 2 continued

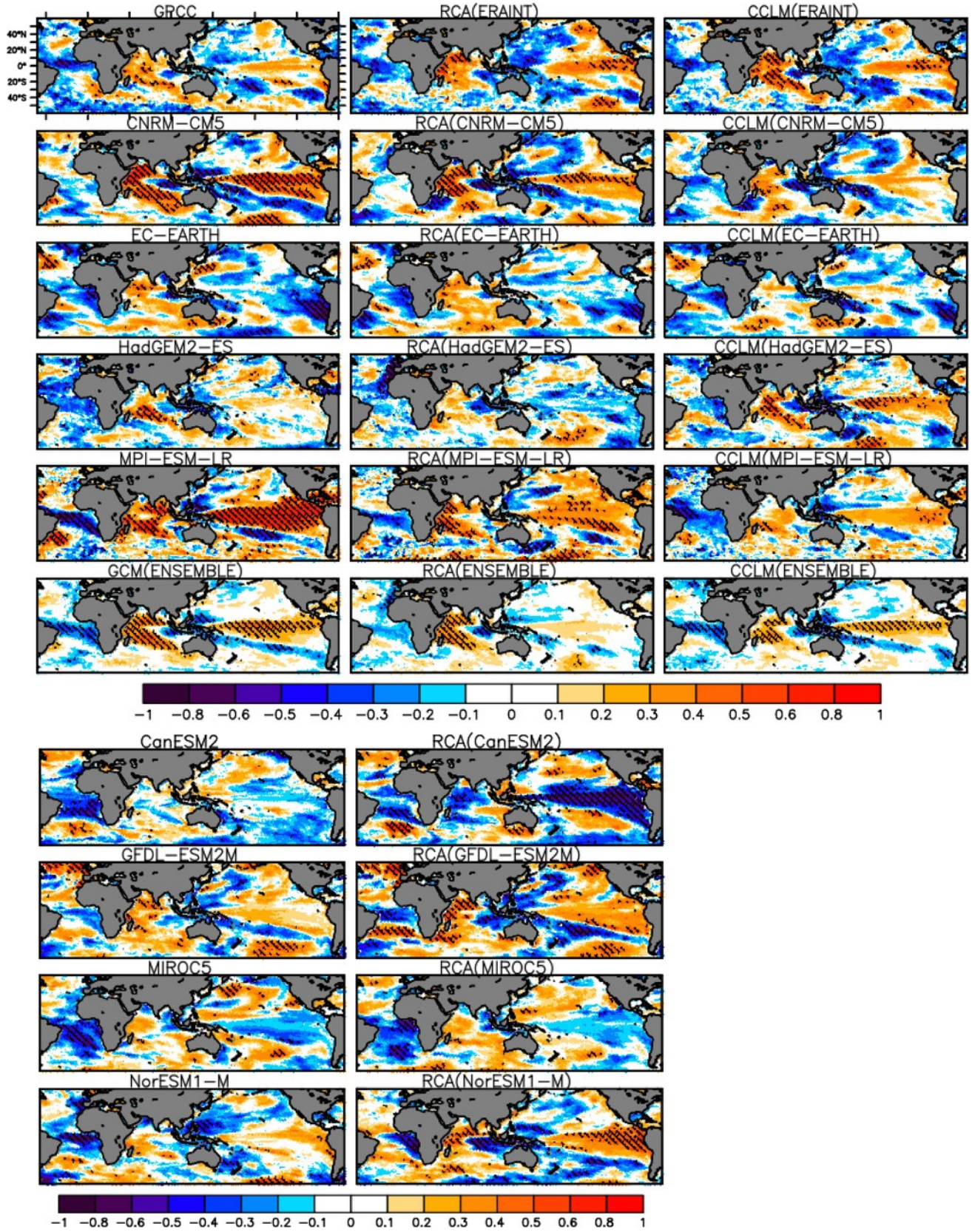

Fig. 2 continued

capture the positive correlation observed in our reference dataset (i.e., GPCC) over tropical Atlantic Ocean. Similarly, CanESM2, MIROC5 and corresponding downscaled results RCA (CanESM2) and RCA (MIROC5) show strong negative correlations with central Indian Ocean, which is not observed in our reference dataset. In those cases it is clear that the errors primarily originated from the driving CGCMs and the RCMs are unable to improve the teleconnection patterns. In few cases the RCMs deteriorated or improved the teleconnection patterns. For instance, NorESM1-M shows positive correlation with eastern equatorial pacific (which is opposite to the observed signal), while the downscaled result RCA (NorESM1-M) reproduced well the observed patterns. Similarly, GFDL-ESM2M shows strong positive correlations over the central Indian Ocean, whereas the corresponding downscaled result exhibit relatively good agreement with the observation (see Fig. 2a lower panel). These improvements in downscaled simulations might be due to the better representation of sub-GCM grid scale forcings by the RCM or because of the possible cancellation of errors produced by the RCM and those from the driving CGCM. Conversely, CNRM-CM5 captured the teleconnection with eastern equatorial Pacific Ocean, while the RCMs deteriorated the signal, especially RCA model.

Figure 2b represents the correlations between de-trended OND area-averaged rainfalls over EEA, against de-trended concurrent grid-point SSTs. During OND, warmer (colder) than average SSTs throughout the western Indian Ocean and equatorial Pacific Ocean are associated with enhanced (decreased) rainfall over the equatorial part of Eastern Africa. The correlations over the equatorial Pacific Ocean, however, are weaker compared to the western part of the Indian Ocean, and this suggest that the IOD is the dominant rainfall driver for the equatorial Eastern Africa region during OND. This is in agreement with the recent study of Bahaga et al. (2015) who indicated that the positive phase of IOD produces more rainfall (compared to the positive phase of ENSO) over the EEA by enhancing the moisture influx from Congo basin. The majority of the models, both CGCMs and the RCMs, simulated positive correlations between western Indian Ocean SST and the rainfall over EEA. Over all, the ERA-Interim driven downscaled results show better agreement with observed spatial teleconnection patterns than the CGCM driven downscaled results. It can be seen that disagreements exist in the CGCM downscaled results in reproducing the observed teleconnection patterns. The most notable feature is that EC-EARTH, CanESM2, MIROC5 and their downscaled results show opposite teleconnection patterns over Eastern equatorial Pacific Ocean. This clearly reflects the impact of the driving CGCM in producing a wrong signal in the downscaled results. MPI-ESM-LR, GFDL-ESM2M, NorESM1-M and their corresponding downscaling results overestimate the strength of the teleconnections over Eastern equatorial Pacific. This overestimation in downscaled results are likely primarily associated with the respective driving CGCMs, however some error is attributable to the RCMs as ERA-Interim driven RCM simulations also overestimate the correlations over the equatorial Pacific Ocean. Unlike NEA (Fig. 2a), there is a similarity between the RCM results and their respective driving CGCM results in reproducing the teleconnection patterns in EEA (Fig. 2b).

Figure 2c is similar to Fig. 2b, but for SEA. Similar teleconnection patterns are observed as EEA, but the highest correlations are shifted to the central Indian Ocean instead of Western part of Indian Ocean and spatially there is less statistical significance in the correlations than the case of EEA. Despite this, we suggest that the central Indian Ocean is an important driver for the rainfall variability over SEA as suggested by Rowell (2013). Overall, the ERA-Interim driven RCM simulations captured the pattern and strength of teleconnections better than the CGCM-driven RCM simulations. CanESM2 and its corresponding simulation failed to reproduce the positive correlation over tropical Indian and Pacific Ocean. Similarly, MIROC5 and its corresponding downscaled result failed to represent the positive relationship between the SSTs over equatorial Pacific Ocean and rainfall over SEA. This again reflects the effect of boundary conditions for the wrong teleconnections in the downscaled results.

It is worth noting that the teleconnections between SSTs and rainfall over EEA and SEA (Fig. 2b, c) are generally very similar in the CGCM simulations and their downscaled results than the case of NEA (Fig. 2a). This might be related with the processes that drive the seasonal rainfall in the respective regions. As suggested by previous studies (Indeje et al. 2000), OND rainfall over EEA and SEA is mainly controlled by large-scale features, while both local and large-scale features control JJAS rainfall over NEA (Diro et al. 2011a; Endris et al. 2013). Thus it is expected that a discrepancy might exist between the RCM and the respective driving CGCM simulations over a region where mesoscale processes have important influence on rainfall, as the CGCMs cannot adequately represent small-scale features.

It is also important to mention that the similarity between the downscaled ERA-Interim and the observed patterns is much greater than the similarity between the downscaled CGCM and the original CGCM patterns (Fig. 2a–c). We further assess this by analyzing and comparing the deviation of the reanalysis-driven teleconnection patterns from observation and/with deviation of CGCM-driven simulations from the CGCMs (not shown). The results show that the RCMs change teleconnection patterns from CGCMs much more than they change patterns when driven by reanalysis dataset. This is particularly true over

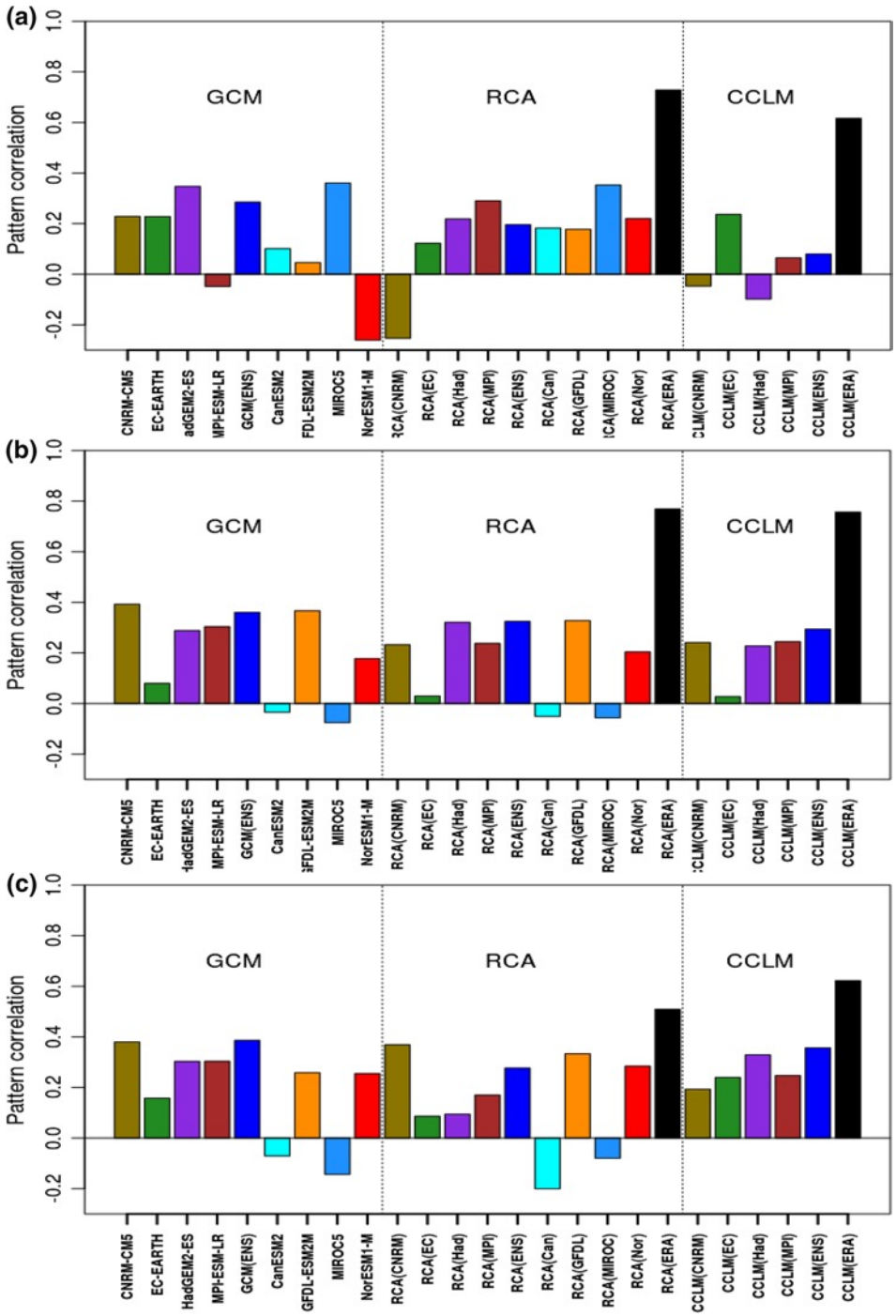

Fig. 3 Pattern correlation of correlation coefficients between the models and observation **a** over NEA (JJAS), **b** EEA (OND) and **c** SEA (OND). Correlations are weighted with respect to latitude

topographically complex region (NEA) where the local rainfall is controlled by both mesoscale and large-scale processes. As noted above, the interaction between small-scale and large-scale features might cancel out or increase the noise when downscaled if there are unrealistic features in the driving fields of the CGCM.

It is, however, difficult to assess the individual model performance since some models capture some teleconnections but not others. Thus an objective and quantitative approach is applied by calculating the spatial (pattern) correlation of temporal correlations. Figure 3 represents the pattern correlation of correlation coefficients between observation and each model. Due to the curvature of the Earth, the actual area represented by a latitude/longitude grid sample decreases with latitude. Thus, to ensure that each grid point is weighted by the area it represents, the correlation values at each grid-point are multiplied by the square root of the cosine of latitude.

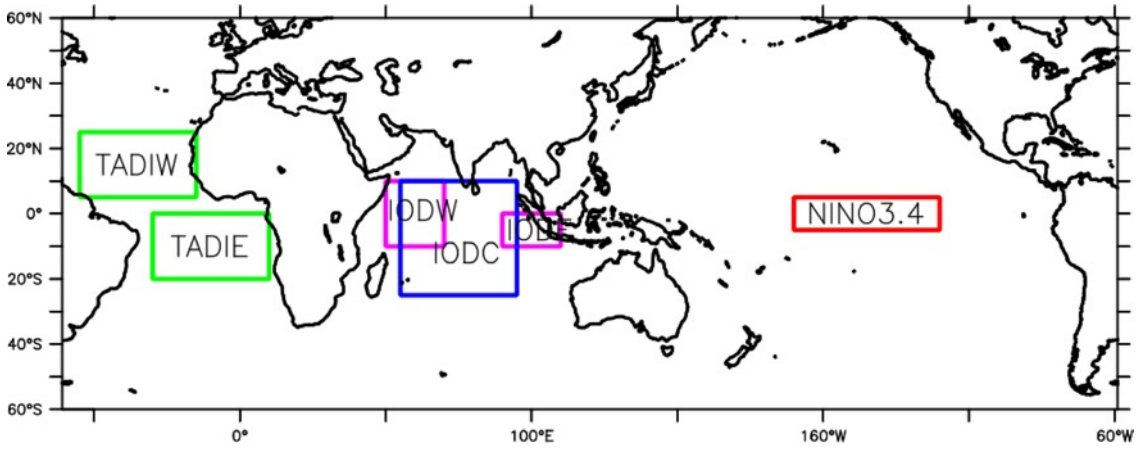

Fig. 4 Location of SST regions used to compute indices in the analysis

The ERA-Interim driven RCM runs perform better than any CGCM runs in reproducing the spatial pattern of teleconnections in every subregion and season, but again there is a wide disagreement in CGCM-driven RCMs between one another and with the observation. There is also no clear improvement by the RCMs of their driving CGCM results. For example, over NEA during JJAS (Fig. 3 top panel), CNRM-CM5 shows a positive pattern correlation with the observed GPCC, but its corresponding downscaled results (both by RCA and CCLM model) show negative pattern correlation i.e. RCMs have deteriorated the teleconnection relationship. In contrast, NorESM1-M and MPI-ESM-LR show a negative correlation, while their downscaled results improve the correlation. Over EEA and SEA during OND (Fig. 3 middle and bottom panel), HadGEM2-ES, MPI-ESM-LR, GFDL-ESM2M and Ensemble Mean captured the pattern correlation better than any other models, while CanESM2 and MIROC5 performed poorly. As it was discussed earlier, there is a similarity between the RCM simulations and their driving CGCMs simulations in reproducing the spatial pattern of teleconnections over EEA and SEA during OND.

In general, results from the correlation analysis have shown that ENSO has a strong association with rainfall over the northern part of the region during JJAS, while the effect of IOD is more evident for equatorial and southern part of the region during OND. It is also clear that the ERA-Interim driven RCMs outperform the CGCM-driven RCMs, suggesting that boundary conditions from the CGCM are indeed is the main contributor to poor skill in representing the response to teleconnections in the RCMs. It is also worth mentioning that similarities in SST-rainfall teleconnection patterns between the RCM simulations and respective driving CGCM simulations are noticeable over regions where the rainfall is primarily controlled by large-scale (synoptic-scale) features, with the RCM simulations conserving the overall regional patterns from the forcing models. Differences in RCM simulations from corresponding driving simulations are noted mainly over northern part of the domain which is most likely related to mesoscale processes that are not resolved by CGCMs.

3.2 Teleconnection pattern resolved through linear regression

To evaluate the ability of individual models to simulate both the patterns and amplitude of rainfall teleconnections, a regression analysis was applied to SST indices in Oceanic regions that have strong correlations with eastern African rainfall. The SST regions used to compute indices are indicated in Fig. 4. These regions have been selected based on Fig. 2a–c and literatures that describe the relationship between Eastern Africa rainfall and SST (e.g. Ogallo 1988; Saji et al. 1999; Ummenhofer et al. 2009; Diro et al. 2011b; Rowell 2013). For the Pacific, the **NINO3.4 index,** which is the average of SST over 5°S–5°N, 170°–120°W, is used to measure ENSO variability. For the Indian Ocean, we use the standard definition of IOD (Saji et al. 1999), which is the difference between the area average SST in the IODW region (10°S–10°N, 50°–70°E) and IODE region (10°S–0°,

90°–110°E). Also the central Indian Ocean Index **(CIOD),** which is the average of SST over 25°S–10°N, 55°–95°E, is used following Rowell (2013). In the Atlantic, a Tropical Atlantic Dipole Index (**TADI**) is defined as the difference between tropical North and South Atlantic indices (averages of 5°–25°N, 55°–15°W minus 20°S–0°, 30°W–10°E), following Enfield et al. (1999).

As discussed earlier, the main advantage of using regression over the Spearman rank correlation is that we can interpret the teleconnections in terms of changes in the magnitude of the physical variables, which in this case is rainfall rate per degree change of SST in the different ocean regions. It is important to note that linear regression makes a few assumptions about the data (e.g. linearity and normality). Thus we checked the sensitivity of teleconnection patterns to the statistical assumptions going into the calculations with Spearman's rank method, which does not make such assumptions (Fig not shown). The test confirmed that teleconnection patterns are not sensitive to the statistical methods employed. As has been noted by Langenbrunner and Neelin (2013), teleconnection patterns defined with linear regression are useful for questions that involve the amplitude of the signal.

Figures 5a shows observed and modeled rainfall teleconnections for the JJAS season against NINO3.4 as estimated by linear regression. Stippled patterns indicate statistically significant regression coefficients at the 5 % level. Here student's t-test is used to resolve grid points that meet or pass 5 % significance level. The test statistics assumed to follow the t-distribution under null hypothesis regression slop of zero. Negative coefficients occur over most of the northern part of the domain indicating that rainfall is above normal when the index is negative, and the rainfall is below normal when the index is positive. The majority of models reproduce these observed features. Both RCMs driven by CNRM-CM5 poorly simulate the teleconnection patterns against Niño3.4 index, while driving CGCM (CNRM-CM) reproduced the pattern better than the downscaled results. GFDL-ESM2M and NorESM1 produced wrong signal over the northern part of the domain. The regression coefficients between JJAS rainfall and TADI were also calculated (not shown). The results show that TADI has week and localized effect over the region during JJAS compared to the influence of ENSO, and there is a disagreement among the models in capturing the teleconnections patterns.

Rainfall teleconnections for the OND season against NINO3.4 and IOD index estimated by linear regression are indicated in Fig. 5b, c, respectively. Both indices have a positive relationship with the regional rainfall, but the IOD rainfall relationships are stronger than the ENSO rainfall relationships, and this indicates the influence of the IOD on regional rainfall during OND is higher than ENSO. The majority of the models reproduced the teleconnection against both indices. Once again there is a clear effect of the CGCM-supplied boundary conditions in simulating the teleconnection patterns. For example, the wrong signal in EC-EARTH, CanESM2 and MIROC5 over NINO3.4 region resulted in wrong teleconnection patterns in their corresponding downscaled results (Fig. 5b). Similarly, the wrong teleconnection signal in CanESM2 and MIROC5 models against IOD affected the teleconnection in their downscaled results (Fig. 5c).

To understand the effect of the central Indian Ocean over the region, regression coefficients between OND rainfall and CIOD were calculated (not shown). The CIOD has a large influence in the southern region of the domain with excess (deficit) rainfall being associated with warming (cooling) of the central Indian Ocean as shown by Rowell (2013). Like the case of ENSO and IOD, differences in regional simulations associated with the CIOD originate mainly from the respective CGCM fields (not shown).

Figure 5a–c provide a spatial assessment of teleconnection patterns over the entire Eastern Africa region, and one can see that there is often disagreement between the CGCMs as well as the downscaled results in different regions. We further assess and summarize the ability of the models to reproduce the spatial pattern of teleconnections and represent the amplitude of these patterns in each homogeneous rainfall sub-regions using Taylor diagrams (Taylor 2001). The Taylor diagrams in Fig. 6 show the spatial root mean square deviation and spatial correlation of regression field (i.e. regression coefficients from Fig. 5a–c, and regression coefficients against TADI and CIOD discussed previously) of models with respect to the reference field in each homogeneous rainfall sub-regions. The spatial root mean square deviations (spatial standard deviation) of the models are normalized against the spatial standard deviation of the observation, and this spatial standard deviation is used as a measure of the teleconnection amplitudes. Examination of spatial patterns of teleconnections based on pattern correlation demonstrated that similarties between the regional simulations and the respective CGCM simulations are evident, with the RCM simulations maintaining the regional patterns from the forcing models. Concering the amplitude of teleconnections, CGCMs generally tend to underestimate the amplitude, while the RCMs overestimate it in most of the subregions against the different indices (Fig. 6a, b). The high amplitude of teleconnection (i.e., higher spatial standard deviation) in the RCM simulations might be directly due to better precipitation capture, enhanced by a better-resolved topography. On the other hand, the low amplitude of teleconnection in CGCMs may be assocaited with a poorly resolved topography and other small-scale features due to coarse resolution. The other possibility for the discrepancy of the amplitude was likely due to the interpolation as we re-gridded the coarse resolution data to a higher resolution (0.44°). However, re-gridding the high resolution dataset into coarse resolution (2°) gave nearly identical results.

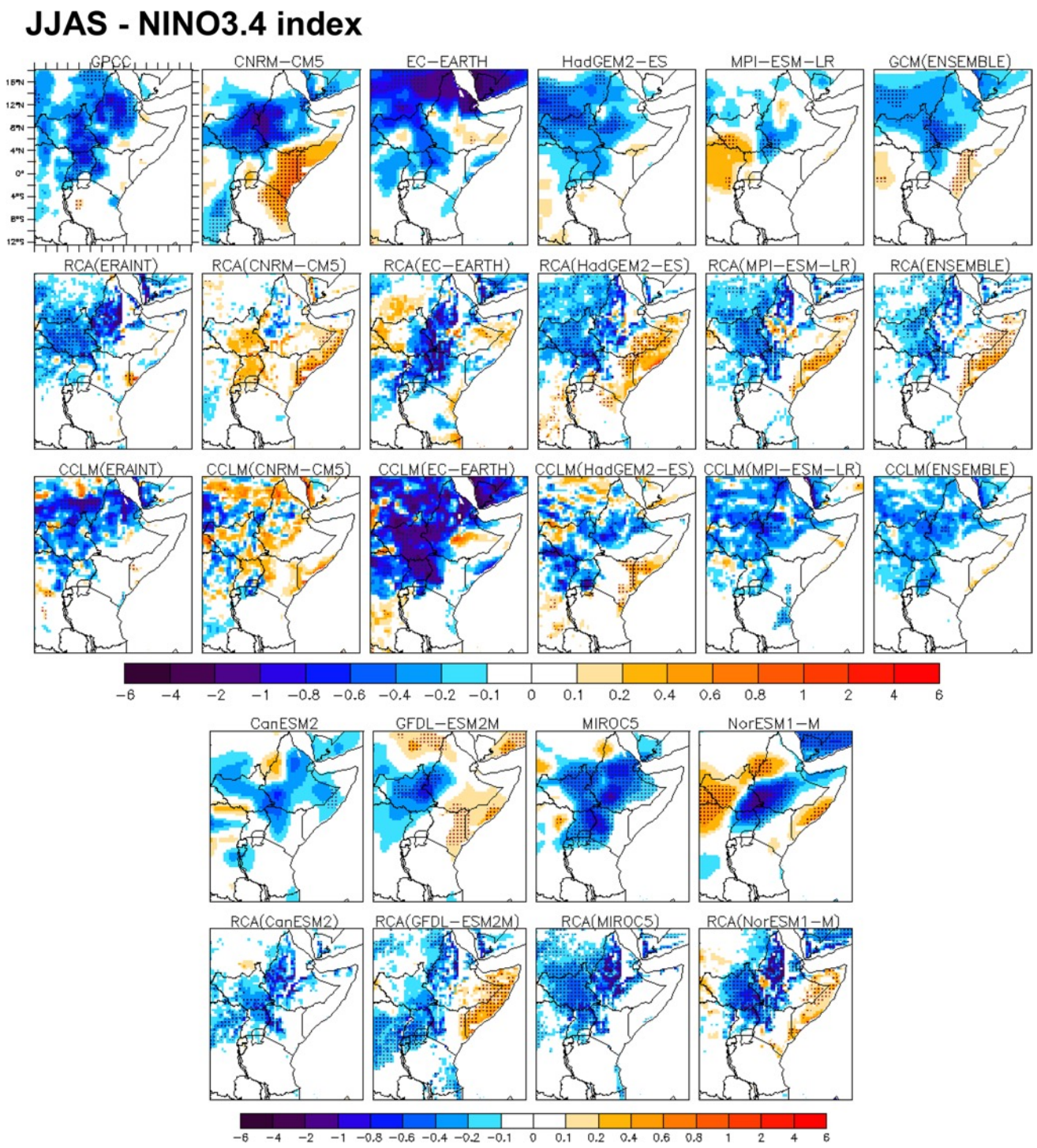

Fig. 5 **a** JJAS rainfall teleconnections, as diagnosed through a linear regression analysis of rainfall against the Nino3.4 index. *Stippling* indicates regions where the regression coefficient is statistically significant at the 5 % level. Units are mm day^{-1} °C^{-1}. **b** OND rainfall teleconnections, as diagnosed through a linear regression analysis of rainfall against the Nino3.4 index. *Stippling* indicates regions where the regression coefficient is statistically significant at the 5 % level. Units are mm day^{-1} °C. **c** OND rainfall teleconnections, as diagnosed through a linear regression analysis of rainfall against the IOD. *Stippling* indicates regions where the regression coefficient is statistically significant at the 5 % level. Units are mm day^{-1} °C^{-1}

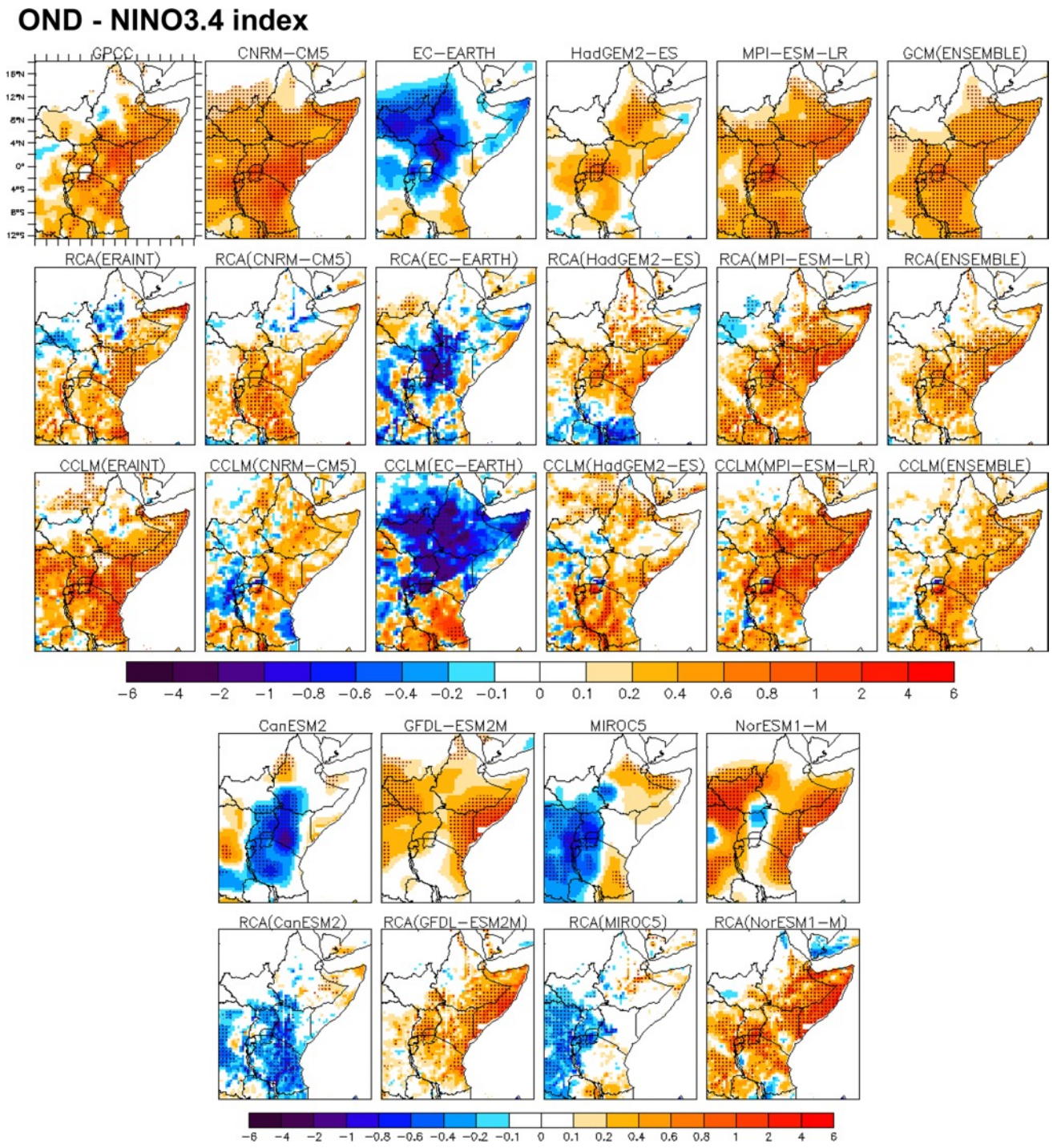

Fig. 5 continued

3.3 Simulating mean climate

Finally, we evaluated the models' performance for simulating the mean climate to check if there is straightforward relationship to their performance in capturing the teleconnections. Taylor diagrams are used to compare model performance for the annual cycle of rainfall with observation in each homogeneous rainfall sub-regions (Fig. 7). Overall, the models produce better annual cycles of rainfall in NEA and SEA (over uni-model rainfall regions) than in EEA (bi-model rainfall region). The ERA-Interim driven RCMs reproduce

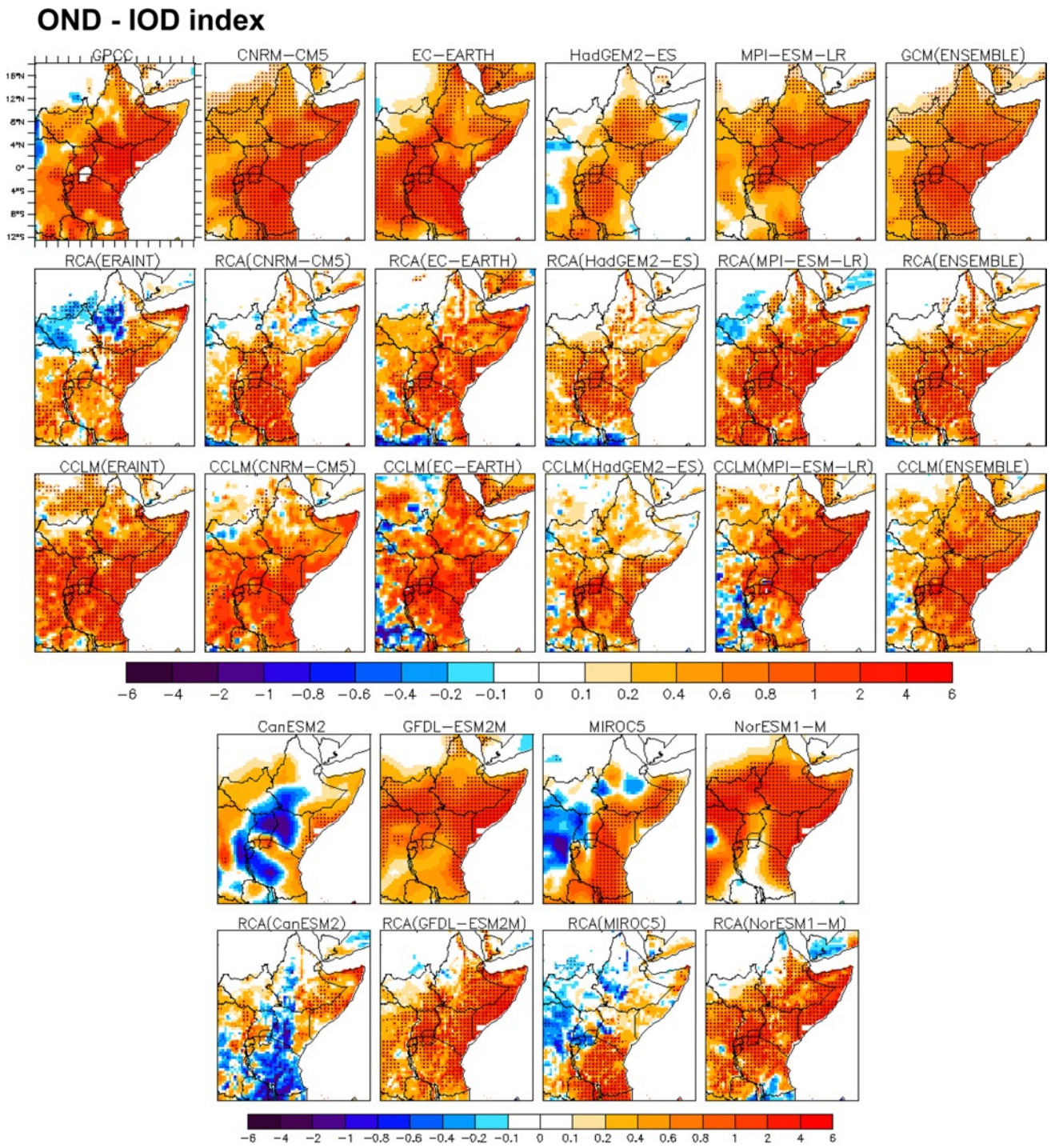

Fig. 5 continued

the annual cycles better than CGCM driven RCMs and parent CGCMs. GFDL-ESM2 and NorESM1-M poorly reproduce the annual cycle in NEA (i.e. correlations less than 0.8). HadGEM2-ES, GFDL-ESM2M, NorESM1-M and their corresponding downscaled results are among poorly performing models in EEA. CanESM2, MIROC5, NorESM1-M and GFDL-ESM2M overestimate the standard deviation over SEA, while CNRM-CM5 underestimates it. From these figures it appears that the ability of the models in reproducing the teleconnections is not directly related to their ability in representing the climatological rainfall pattern.

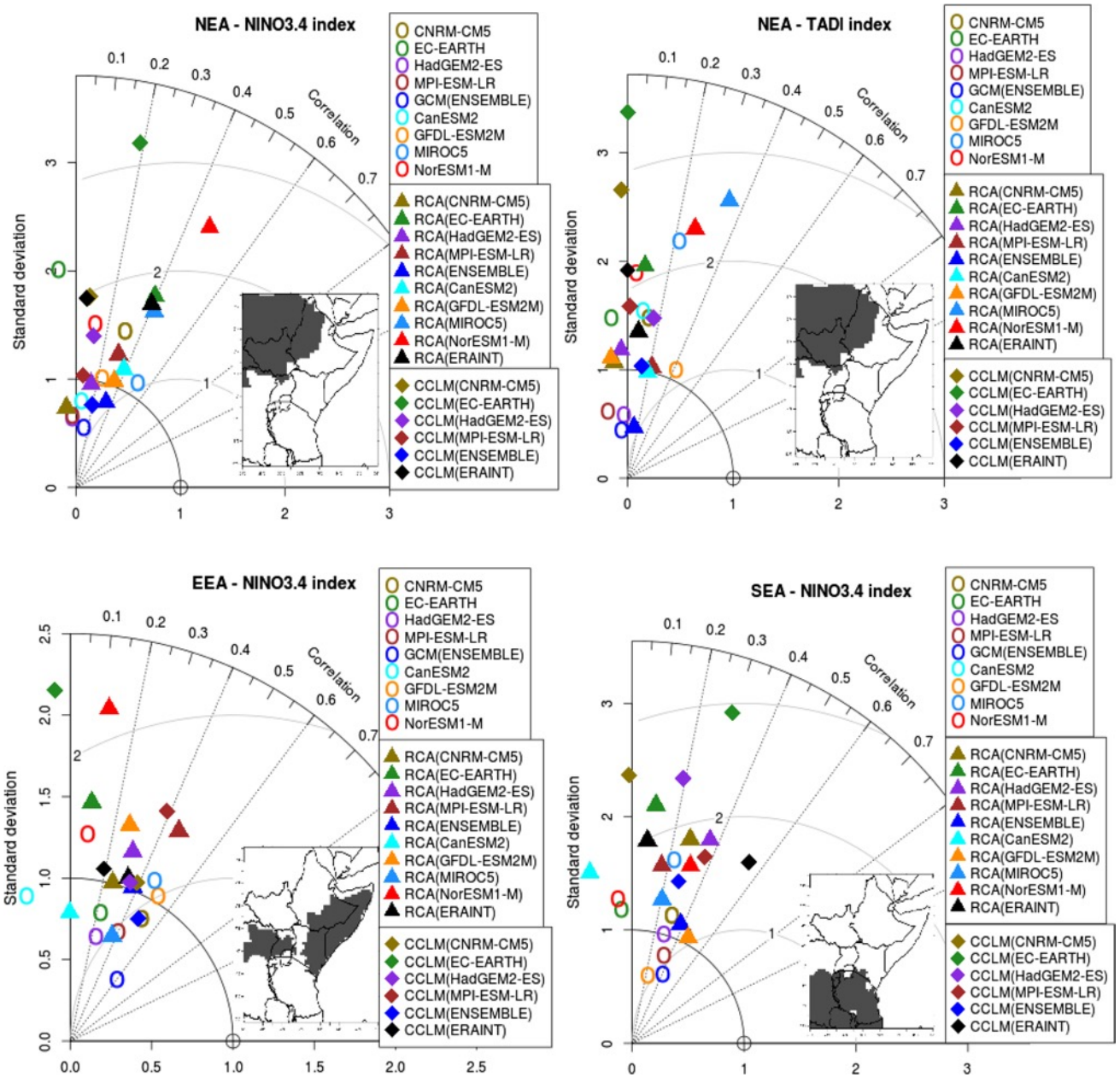

Fig. 6 **a** Taylor diagrams for the standardized amplitude and spatial correlation of precipitation teleconnections in NEA during JJAS against NINO3.4 (*top left*), NEA during JJAS against TADI (*top right*), EEA during OND against NINO3.4 (*lower left*) and SEA during OND against NINO3.4 (*bottom right*). On the Taylor diagrams, *angular axes* show spatial correlations between modeled and observed teleconnections; *radial axes* show spatial standard deviation (root-mean-square deviation) of the teleconnection signals in each area, normalized against that of the observations. *Circles* are for GCMs, triangles are for RCA and diamonds for CCLM model. **b** Taylor diagrams for the standardized amplitude and spatial correlation of OND rainfall teleconnections in EEA against IOD (*top left*), EEA against CIOD (*top right*), SEA against IOD (*lower left*) and SEA against CIOD (*lower right*). On the Taylor diagrams, *angular axes* show spatial correlations between modeled and observed teleconnections; *radial axes* show spatial standard deviation (root-mean-square deviation) of the teleconnection signals in each area, normalized against that of the observations. *Circles* are for GCMs, triangles are for RCA and diamonds for CCLM model

3.4 Circulation anomalies

Composite analysis is used to assess the ability of the models to represent key regional anomalous atmospheric circulation patterns associated with ENSO and IOD variability. ENSO and IOD years are identified from each CGCM and observation, by calculating the Oceanic Niño Index (ONI) and Dipole Mode Index (DMI), respectively.

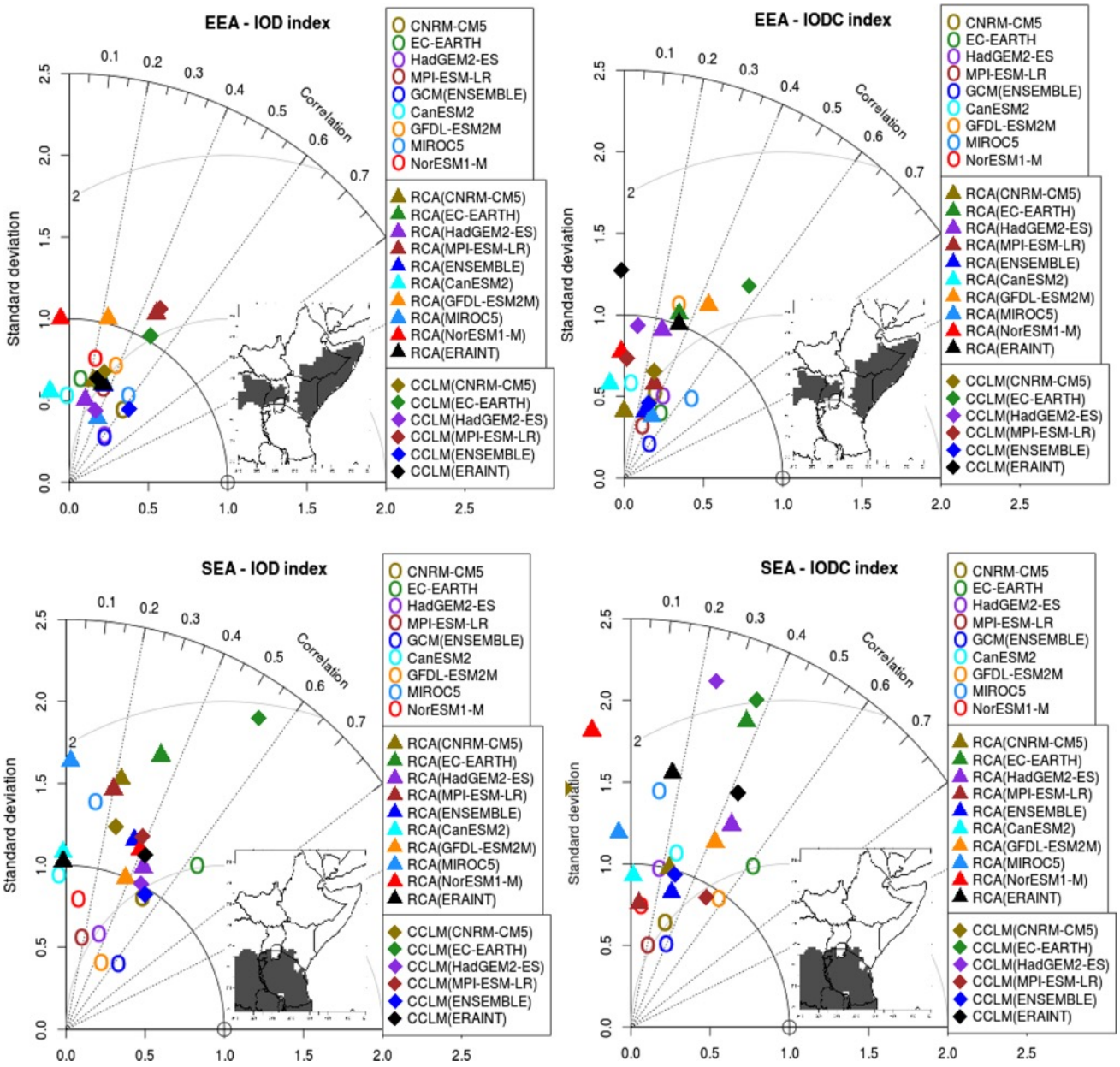

Fig. 6 continued

To identify the ENSO years, we follow an approach similar to da Rocha et al. (2014). The ONI based on the SST anomaly in Niño3.4 region (120°–170°W and 5°S–5°N) is used to identify El Niño and La Niña years. Here the anomaly is calculated relative to a climatological seasonal cycle based on the years 1982–2005. A given year is defined as El Niño or La Niña year when ONI value is higher (lower) than a positive (negative) threshold for at least five consecutive overlapping seasons, defined as the average of three consecutive months of that year. The NOAA Climate Prediction Center (CPC) uses a threshold of ±0.5 °C, while here, similar to da Rocha et al. (2014), the CGCM thresholds are based on their respective ONI standard deviation (Sd). The reason is that some models might show excessive number of El Niño and La Niña years due to the high Sd in Niño3.4 region if a ±0.5 °C threshold is used.

The CGCMs' thresholds for El Niño and La Niña are defined by the following criteria:

$$T_i = Sd_i * C$$

T_i is the threshold of the ith CGCMSd_i is the ONI Sd of the ith CGCMC is a constant (or fixed value) = 0.47, which is the ratio between a threshold used by CPC (**±0.5**) and ONI Sd from NOAA for the period of 1982–2005 (**1.07**).

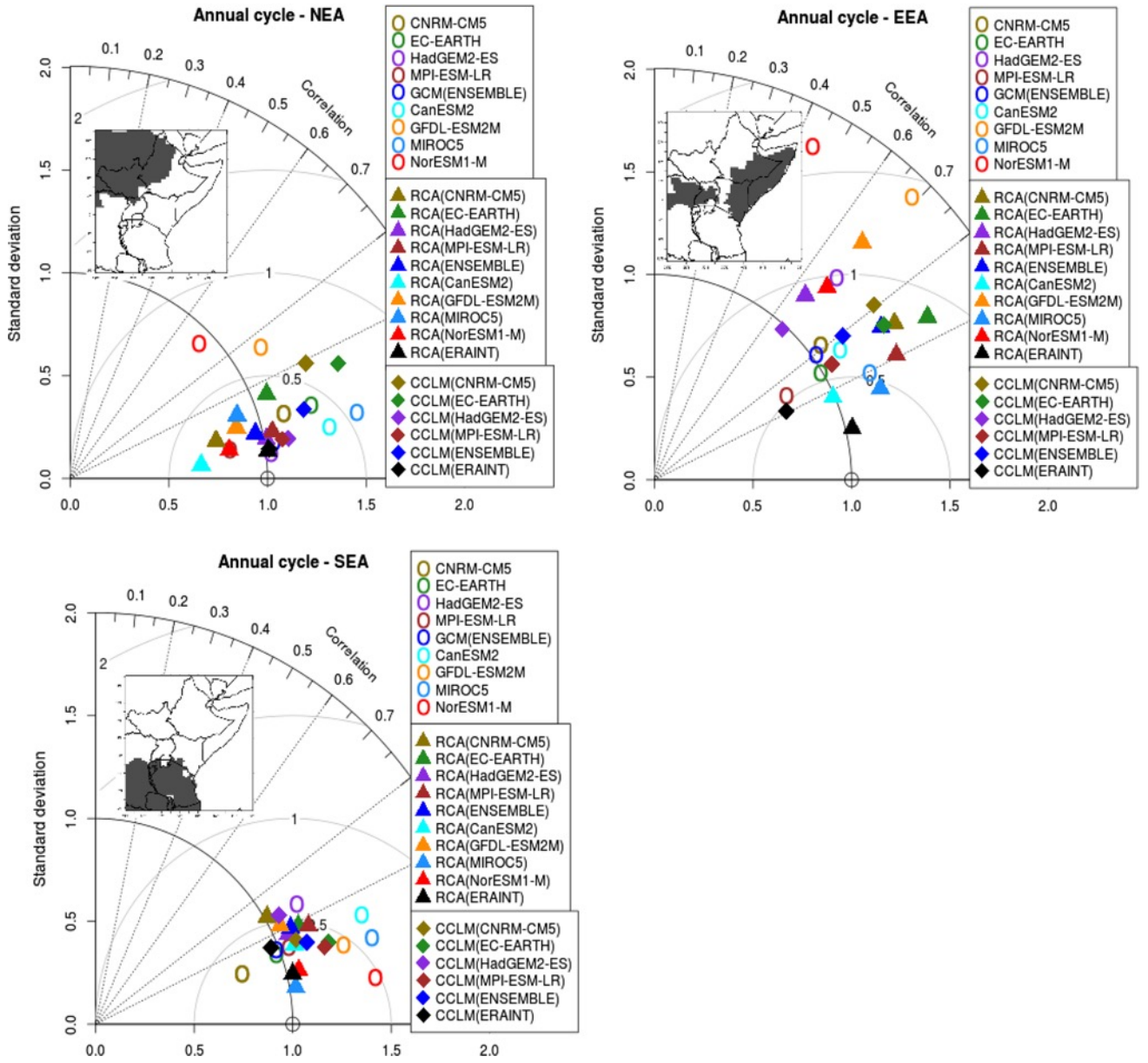

Fig. 7 Taylor diagram quantifying the correspondence between the simulated and observed area-averaged annual cycle of rainfall in each homogeneous rainfall sub-regions. *Circles* are for GCMs, *triangles* are for RCA and *diamonds* for CCLM model

A similar approach is used to identify the IOD years. IOD years are identified using the DMI (Saji et al. 1999), which is calculated as the SST anomaly difference between the western equatorial Indian Ocean (50°–70°E and 10°S–10°N) and south-eastern equatorial Indian Ocean (90°–110°E and 10°–0°S). Like ONI, this index oscillates between positive and negative values. A given year is defined as positive IOD or negative IOD year when DMI index is higher (lower) than a positive (negative) threshold for at least three consecutive overlapping seasons including OND, defined as the average of three consecutive months of that year. Note that for IOD we used 3 consecutive seasons including OND, since an IOD usually starts in May or June, peaks between August and November and then rapidly decays. For observation, a threshold ±0.5 °C is used to identify positive IOD and negative IOD years, while for CGCMs (similar to the ENSO) the thresholds are based the their respective Sd of DMI. Number of ENSO and IOD years for an observation dataset (NOAA_OI_SST_V2) and each CGCM and the corresponding standard deviation (SD) of ONI and DMI indices are presented in Table 2.

The rainfall anomalies over the region associated with ENSO and IOD from composite analysis are similar to

Table 2 Number of ENSO (El Niño and La Niña) and IOD (Positive IOD and Negative IOD) years, and the corresponding standard deviations (Sd) in the 1982–2005 period

Obs and CGCMs	ONI Sd	El Niño	La Niña	DMI Sd	+ve IOD	−ve IOD
NOAA_OI_SST_V2	1.07	8	6	0.62	4	7
CNRM-CM5	0.98	9	7	0.62	8	8
EC-EARTH	0.72	6	7	0.45	5	9
HadGEM2-ES	0.87	8	6	0.58	8	6
MPI-ESM-LR	1.27	5	6	0.65	3	5
CanESM2	1.13	6	8	0.49	7	8
GFDL-ESM2M	1.66	5	8	0.76	5	7
MIROC5	1.42	7	7	0.63	4	8
NorESM1-M	0.88	7	9	0.57	6	7

those obtained using regression analysis (Fig. 5), so our subsequent analyses will concentrate only on circulation anomalies associated with ENSO and IOD. Moreover, the climatological pattern of SLP and 850 hPa wind over eastern Africa for JJAS and OND are discussed in part I of our paper (see Endris et al. 2013). Figure 8a shows the El Niño anomalies of SLP and 850 hPa wind vectors for RCMs and their driving CGCMs in comparison with ERA-Interim reanalysis. ERA-Interim (our reference data in this case) shows strong positive SLP anomalies over the Arabian Peninsula. The positive SLP anomalies over Arabian Peninsula reflect the weakening of the monsoon through during El Niño. As Diro et al. (2011b) described, the weakening of monsoon trough over Arabian Peninsula might reduce the east–west pressure gradient, and consequently reduce the westerly winds from Atlantic/Congo, and leads to reduction of rainfall over the northern part of the region during JJAS. It also become evident that there is a reduction of the Somali Low Level Jets (SLLJ) diverging out of the Mascarene high, and the strength of westerly winds from the South Atlantic high, which are the main sources of moisture over the northern part of the domain during JJAS. The reduction of these winds is manifested by the presence of north-easterly wind anomaly vectors off the coast of East Africa, and easterly wind anomaly vectors over western part of Eastern Africa. In contrast, during La Niña (figure not shown) most part of the study region is dominated by negative SLP anomalies particularly with deepening of the trough over the Arabian Peninsula. The deeper monsoon trough over the Arabian area is strongly associated with greater rainfall over the eastern Africa during JJAS. In addition, there are anomalies of strong westerly wind vectors as result of SLP intensification over the Atlantic basin, and south-easterly wind vectors as a result of SLP intensification over the Indian Ocean, which produce abundant rainfall over the region. These finds are consistent with findings of other studies such as Segele and Lamb (2005), Segele et al. (2009a, b), Diro et al. (2011b).

Some models represent the intensity as well as the spatial pattern of circulation anomalies associated with El Niño and La Niña; particularly the ERA-Interim driven RCMs, Ensemble mean, HadGEM2-ES and its corresponding downscaled results. Consistent with the rainfall results shown in Fig. 5, the two RCMs driven by CNRM-CM5 show opposite anomaly circulation patterns in comparison with the reanalysis. These models show negative SLP anomalies over east coast of Africa and zero SLP anomalies over the Arabian Peninsula (Fig. 8a). They also show an easterly and south-easterly wind vector anomalies, opposite to the reanalysis. Even though these patterns were not observed in the forcing CGCM (CNRM-CM5), analysis of the CNRM-CM5 model patterns over the large domain (15°W–120°E and 35°S–35°N) showed strong negative (positive) SLP anomalies during El Niño (La Niña) over the northern part of Africa (over Algeria, Tunisia and Libya), which has not been observed in the reanalysis. We expect that this wrong signal in the driving CGCM might be transferred to the RCMs, which leads the RCMs to generate a wrong anomalous circulation patterns over the domain. MPI-ESM-LR and its corresponding downscaled results show more intense SLP and wind field anomalies than ERA-Interim over the Arabian area extended down to western part of the Indian Ocean, while EC-EARTH model shows strong positive anomalies of SLP over western part of the Indian Ocean rather than over the Arabian Peninsula. The anomalous troughs over south Sudan represented by NorESM1-M, RCA (MIROC5) and RCA (NorESM1-M) are not seen in the reanalysis.

During OND, interannual rainfall variability over Eastern Africa is linked to both ENSO and IOD (Fig. 5b, c; Clark et al. 2003; Hasternrath 2007; Bahaga et al. 2015 and others). In general, the southern and equatorial part of Eastern Africa receives above normal rainfall during El Niño and positive IOD, and below normal during La Niña and negative IOD. To highlight the underlining mechanisms linking the ENSO and IOD with Eastern African rainfall, and also to evaluate the ability of the models to reproduce the anomalous circulation patterns, the composite SLP and 850 wind fields are analyzed. The regional patterns for La Niña (negative IOD) are generally opposite-signed anomalies to

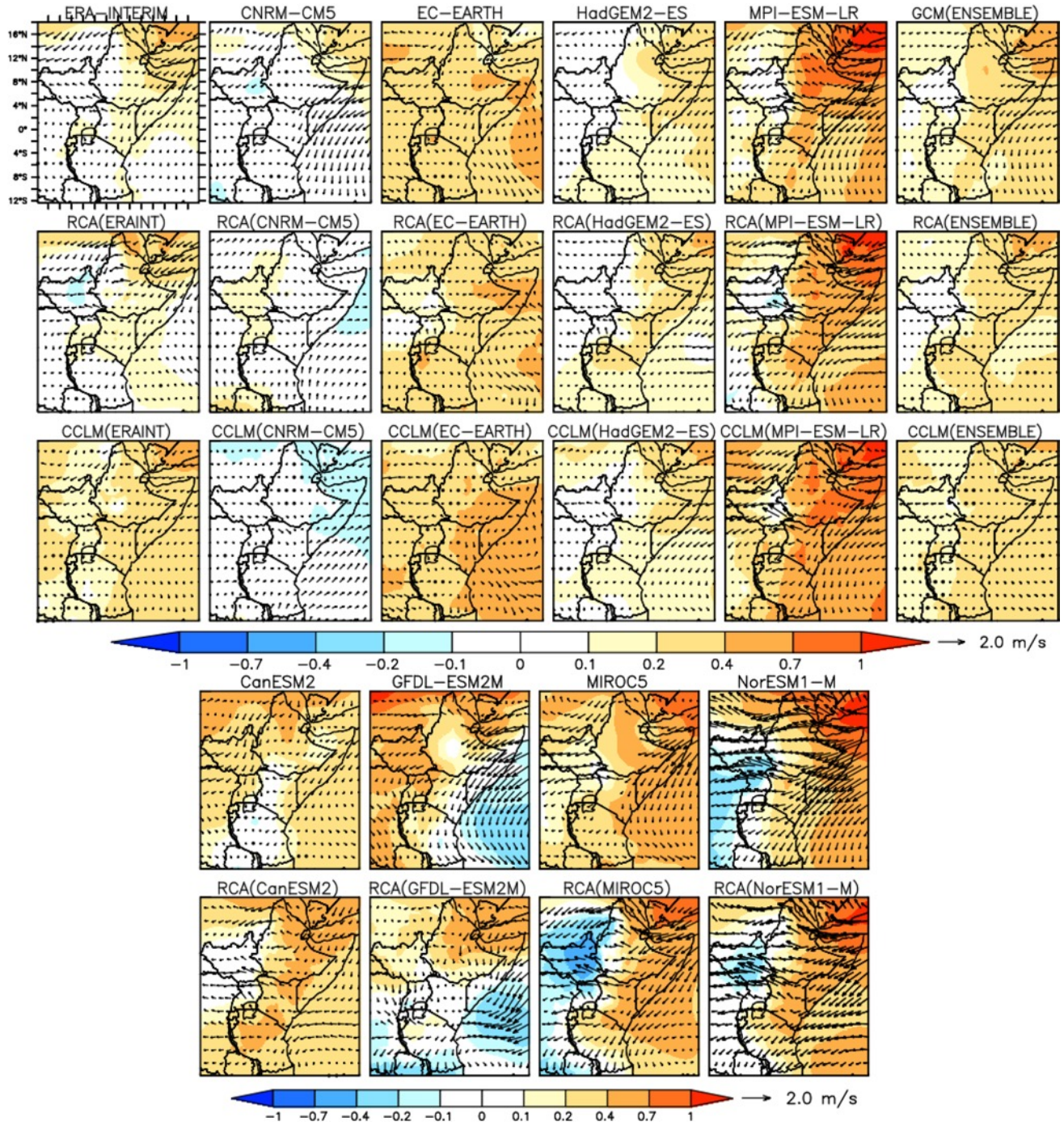

Fig. 8 **a** JJAS El Nino anomalies of SLP (*shaded* in hPa) and 850 hPa winds (*vectors* in m/s). **b** OND El Nino anomalies of SLP (*shaded* in hPa) and 850 hPa winds (*vectors* in m/s). **c** OND positive IOD anomalies of SLP (*shaded* in hPa) and 850 hPa winds (*vectors* in m/s)

El Niño (positive IOD), thus our analysis will concentrate only on anomalous circulation patterns associated with El Niño and positive IOD events. Figure 8b shows the SLP and 850 hPa wind vector anomalies associated with El Niño. Positive surface pressure anomalies are observed over the western part of Eastern Africa, and negative surface pressure anomalies are observed over the south-western part of the Indian Ocean. Moreover, westerly wind anomalies observed over the western part of the domain, and easterly anomalies over the western equatorial Indian Ocean. Kijazi and Reason (2005) link the wet conditions during El Niño events to easterly anomalies over the western equatorial Indian Ocean, while other studies (e.g. Latif et al. 1999; Black et al. 2003) have proposed that the relationship

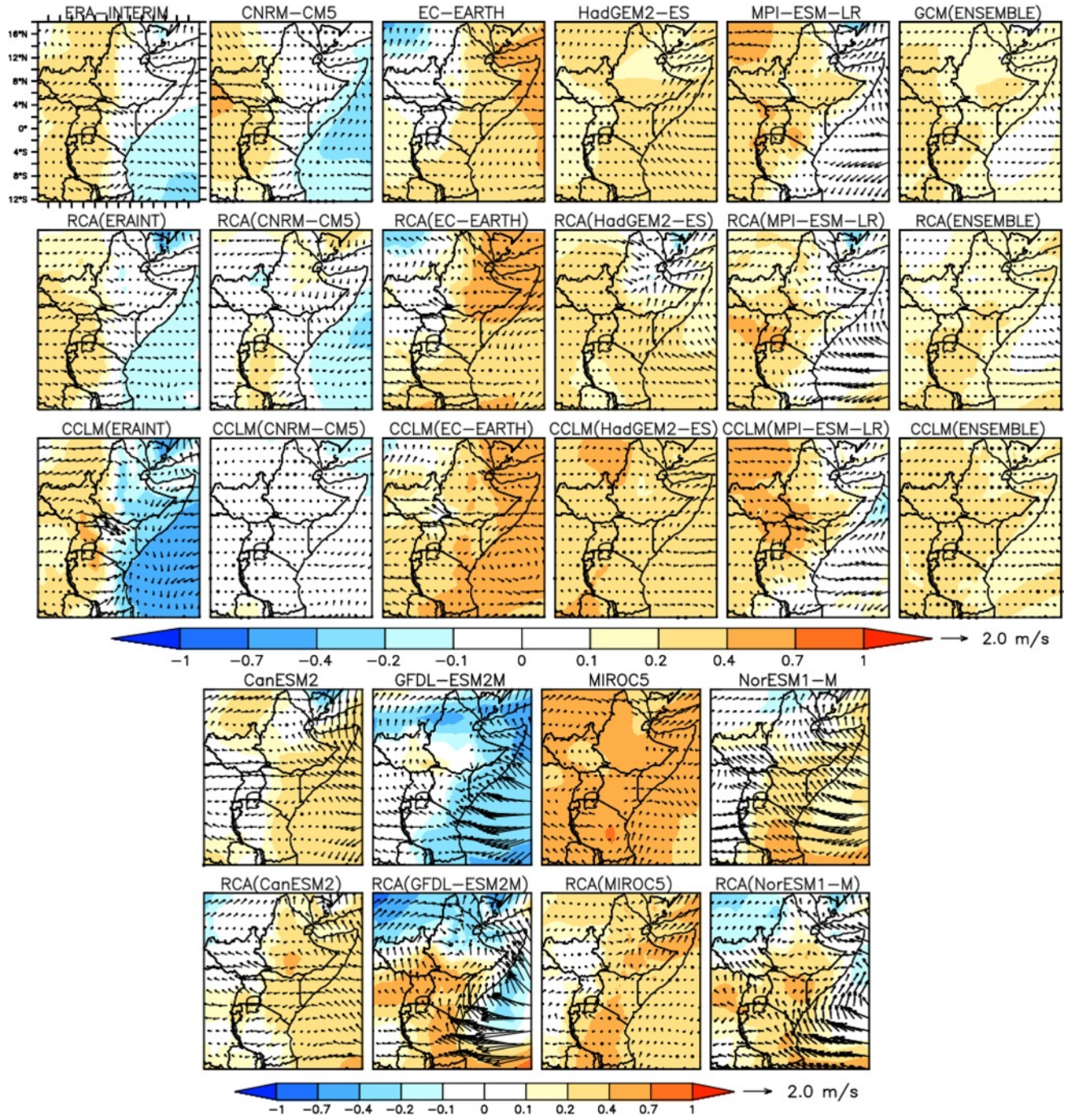

Fig. 8 continued

between East African rainfall and ENSO as the result of an indirect forcing by ENSO on the Indian Ocean. Some of the models are able reproduce the observed anomaly circulation patterns. However, consistent with the rainfall anomalies in Fig. 5b, EC-EARTH, CanESM2, MIROC5 and their corresponding downscaled results fail to represent the negative SLP anomalies over the western tropical Indian Ocean. The models GFDL-ESM2M and NorESM1-M and their corresponding downscaled results show more intense easterly wind anomalies towards Eastern Africa. Overall, there is a clear effect of the CGCM-supplied boundary conditions in simulating the local anomalous circulation patterns, and the error from boundary conditions can be summarized as the "garbage in/garbage out problem".

During positive IOD, there are positive SLP anomalies over the west of Eastern Africa and negative anomalies over

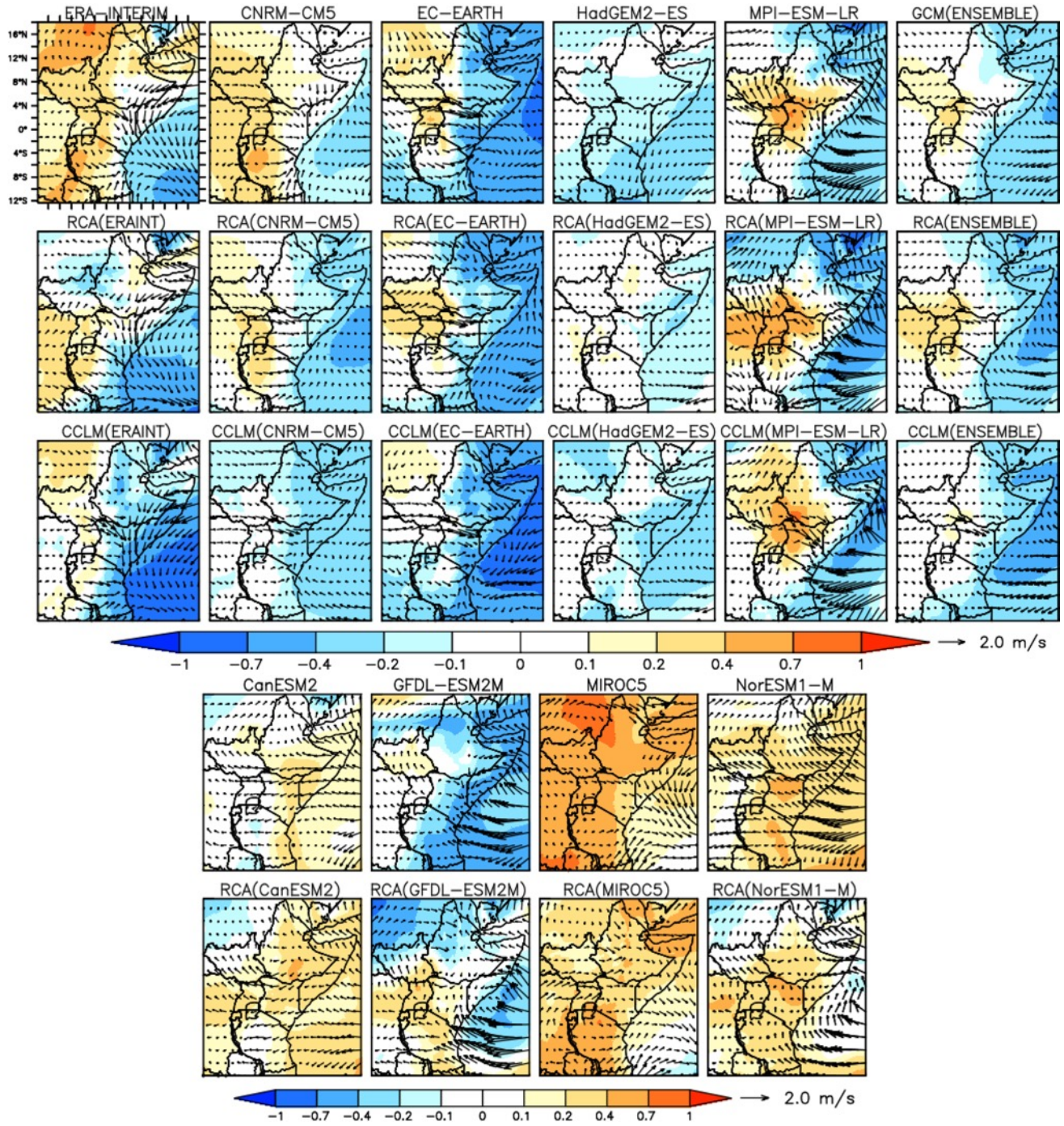

Fig. 8 continued

the western part of the Indian Ocean (see Fig. 8c). The negative SLP anomalies are associated with the warming of the western part of the Ocean during its positive phase. Consistent with the surface pressure response, there are westerly 850 hPa wind anomalies over west of Eastern Africa, and strong easterly anomalies (associated with the cold SST over eastern tropical Indian Ocean) off the east coast of Somalia. These two anomalies converge along the equator and generate north-westerly wind anomalies moving towards the south-east Indian Ocean. Even though the positive (negative) IOD events are linked with above (below) normal rainfall over equatorial and southern part of eastern Africa during OND, the mechanisms for this teleconnection (response of rainfall to anomalous circulation) are not quite clear yet. Ummenhofer et al. (2009) suggested that a reduction in sea level pressure over the western half of the Indian Ocean and

converging wind anomalies over Eastern Africa lead to moisture convergence and increase convective activity over the region during its positive phase. However, Begeha (2014) emphasizes the role of the westerly flows from Congo air mass and the Atlantic region as the main moisture sources for the increase on rainfall over the region. We focus on the ability of the models in reproducing the observed anomalous circulation features. It appears that most models capture the observed broad-scale anomalous circulation characteristics associated with a positive IOD using ERA-Interim as reference, though some models exhibit some variations from the patterns observed. Particularly, CanESM2, MIROC5 and NorESM2-M again misrepresent the negative SLP anomalies associated with warm SST over western tropical Indian Ocean. We argue that this significant short-coming from these CGCMs suggests strongly that these three models are unable to represent the potential implications of circulation pattern change in Eastern Africa.

4 Summary and conclusions

Climate variability is an important aspect of regional climate so assessing the ability of climate models to simulate the natural climate variability of a region is an essential task of evaluating these models. An important component/driver of climate variability over many regions of the world is the SST-rainfall teleconnection. This study examines the ability of two CORDEX RCMs and their driving CGCMs to capture SST-rainfall teleconnection patterns over Eastern Africa. The regional models used in the study are RCA driven by eight CGCMs and CCLM driven by four of common CGCMs. The reanalysis-driven simulations from the two RCMs are also analyzed to estimate error produced by the RCMs and those transmitted from driving CGCMs. We conduct the assessment over three homogeneous rainfall sub-regions, which cover most of Eastern Africa, namely: NEA, EEA and SEA. The analysis period is from 1982 to 2005, which is the period that observed data are available.

Spearman's rank correlation, linear regression and composite analysis were used to examine the teleconnections patterns. The Spearman's rank correlation is used to identify oceanic regions that have a robust relationship with regional rainfall, and also to assess the models' ability to simulate the spatial pattern of the teleconnection patterns. Linear regression is applied to evaluate the ability of models to simulate both the patterns and the amplitude of rainfall teleconnections over the region against different SST indices in Oceanic regions that have strong correlations with Eastern African rainfall. Composite analysis was employed to assess the models' ability to represent the anomalous circulation patterns associated with the dominant modes affecting the rainfall over the region.

The results show that some models reproduce the observed teleconnective SST-rainfall patterns (spatial patterns and amplitudes) better than others. The downscaled RCM-reanalysis runs are in better agreement with observation than RCM–CGCM runs in most of the examined sub-regions and seasons. Generally, RCMs driven by MPI-ESM-LR, HadGEM2-ES and GFDL-ESM2M performed better than RCMs driven by other CGCMs. CanESM2 and MIROC5, and their corresponding downscaled results capture the teleconnections in most of the sub-regions and seasons poorly. CGCMs generally underestimate the amplitude of teleconnection patterns while RCMs tend to overestimate it. The overestimation of amplitude by the RCMs is likely because of enhanced precipitation due to a better-resolved topography. It is also demonstrated that both the CGCMs and corresponding downscaled results exhibit a similar teleconnection pattern over regions where the rainfall is primarily controlled by large-scale features, with the RCMs maintaining the overall regional patterns from the forcing models. Differences in RCM simulations from corresponding driving simulations are noted mainly over northern part of the domain which is most likely related to mesoscale processes that are not resolved by CGCMs.

The models' performance in reproducing the large-scale anomalies in SLP and low-level winds are consistent with their performance at representing the rainfall anomalies. The ERA-Interim driven simulations produce a more realistic representation in the magnitude of these fields. Consistent with the rainfall anomalies, CanESM2 and MIROC5 and their corresponding downscaled results fail to represent anomalous circulation patterns associated with ENSO and IOD in most of the examined regions and seasons. So we suggest that it's not only the parameterizations in the RCMs that are the cause of the errors in the downscaled rainfall fields, the driving circulation states were not captured, as CGCM-derived boundary conditions were incorrect. We would also like to note that the simulation domain is much bigger than the study region giving the RCMs gives a lot of freedom to develop its own climate. Despite this the RCMs cannot improve on the CGCM results over the region if the CGCM boundary conditions are poor.

In conclusion, the results of this study demonstrate that differences in reproducing SST-rainfall teleconnection patterns arise mainly from the driving CGCMs. In other words, the relative contribution of teleconnection errors from boundary forcing is bigger than the choice of RCM or RCM configuration, implying that the choice of the forcing CGCM is more important than the choice of the RCM for the regional application. We suggest that more work should be targeted towards improving the boundary forcing given to the RCMs. We further suggest that the analysis presented here is helpful in selecting the appropriate models for regional applications over the Eastern Africa region. In

future work, we aim to investigate whether the current teleconnection patterns between the large scale climate modes (ENSO and IOD) and rainfall over Eastern Africa will persist in the future under anthropogenic climate change.

Acknowledgments This study forms part of the PhD thesis of Mr. Endris, and he gratefully acknowledge the Socioeconomic Concequences of Climate Change in Sub-equatorial Africa (SoCoCA) project in Department of Geoscience at University of Oslo (DoG/UiO) for financial support to do his PhD at University of Cape Town. All authors would like to thank the World Climate Research Program's Working Group for their role in producing the CORDEX and CMIP5 multi-model datasets, and make it accessible through Earth System Grid Federation (ESGF) web portals. We also would like to acknowledge the two anonymous reviewers for helpful comments and suggestions. The NOAA_OI_SST_V2 data were provided by the NOAA CIRES Climate Diagnostics Center, Boulder, USA, from their Web site at http://www.esrl.noaa.gov/psd/data/gridded/data.noaa.oisst.v2.html.

References

Abram NJ, Gagan MK, Cole JE, Hantoro WS, Mudelsee M (2008) Recent intensification of tropical climate variability in the Indian Ocean. Nat Geosci 1(12):849–853

Anyah RO, Semazzi FH (2007) Variability of East African rainfall based on multiyear RegCM3 simulations. Int J Climatol 27(3):357–371

Bahaga TK, Mengistu Tsidu G, Kucharski F, Diro GT (2015) Potential predictability of the sea-surface temperature forced equatorial East African short rains interannual variability in the 20th century. Quarterly J R Meteorol Soc 141(686):16–26

Baldauf M, Seifert A, Förstner J, Majewski D, Raschendorfer M, Reinhardt T (2011) Operational convective-scale numerical weather prediction with the COSMO model: description and sensitivities. Mon Weather Rev 139(12):3887–3905

Behera SK, Luo JJ, Masson S, Delecluse P, Gualdi S, Navarra A, Yamagata T (2005) Paramount impact of the Indian Ocean dipole on the East African short rains: A CGCM study. J Clim 18(21):4514–4530

Black E, Slingo J, Sperber KR (2003) An observational study of the relationship between excessively strong short rains in coastal East Africa and Indian Ocean SST. Mon Weather Rev 131(1):74–94

Bland JM, Altman DG (1995) Multiple significance tests: the Bonferroni method. BMJ 310(6973):170

Boulard D, Pohl B, Crétat J, Vigaud N, Pham-Xuan T (2013) Downscaling large-scale climate variability using a regional climate model: the case of ENSO over Southern Africa. Clim Dyn 40(5–6):1141–1168

Clark CO, Webster PJ, Cole JE (2003) Interdecadal variability of the relationship between the Indian Ocean zonal mode and East African coastal rainfall anomalies. J Clim 16(3):548–554

Da Rocha RP, Reboita MS, Dutra LMM, Llopart MP, Coppola E (2014) Interannual variability associated with ENSO: present and future climate projections of RegCM4 for South America-CORDEX domain. Clim Change. doi:10.1007/s10584-014-1119-y

Dee DP, Uppala SM, Simmons AJ, Berrisford P, Poli P, Kobayashi S, Andrae U, Vitart F (2011) The ERA-Interim reanalysis: configuration and performance of the data assimilation system. Q J R Meteorol Soc 137(656):553–597

Déqué M, Piedelievre JP (1995) High resolution climate simulation over Europe. Clim Dyn 11(6):321–339

Diro GT, Grimes DIF, Black E (2011a) Large scale features affecting Ethiopian rainfall. In: Williams CJR, Kniveton DR (eds) African climate and climate change, Springer, Netherlands pp 13–50

Diro GT, Grimes DIF, Black E (2011b) Teleconnections between Ethiopian summer rainfall and sea surface temperature: part I—observation and modelling. Clim Dyn 37(1–2):103–119

Dosio A, Panitz H-J (2015) Dynamically downscaling of CMPI5 CGMs over CORDEX-Africa with COSMO-CLM: analysis of the climate change signal and differences with the driving GCMs. Clim Dyn. doi:10.1007/s00382-015-2664-4

Dosio A, Panitz H-J, Schubert-Frisius M, Luethi D (2015) Dynamical downscaling of CMIP5 global circulation models over CORDEX-Africa with COSMO-CLM: evaluation over the present climate and analysis of the added value. Clim Dyn 44:2637–2661. doi:10.1007/s00382-014-2262-x

Endris HS, Omondi P, Jain S, Lennard C, Hewitson B, Chang'a L, Awange JL, Tazalika L (2013) Assessment of the performance of CORDEX regional climate models in simulating East African rainfall. J Clim 26(21):8453–8475

Enfield DB, Mestas-Nuñez AM, Mayer DA, Cid-Serrano L (1999) How ubiquitous is the dipole relationship in tropical Atlantic sea surface temperatures? Journal of Geophysical Research: Oceans (1978–2012) 104(C4):7841–7848

FEWS NET (2011) Past year one of the driest on record in the eastern Horn. Famine early warning system network report, June 14, 2011, U.S. Agency for International Development, Washington, DC

Fox-Rabinovitz M, Côté J, Dugas B, Déqué M, McGregor JL (2006) Variable resolution generalcirculation models: Stretched-grid model intercomparison project (SGMIP). J Geophys Res 111:D16104. doi:10.1029/2005JD006520

Giorgi F, Mearns LO (1991) Approaches to the simulation of regional climate change: a review. Rev Geophys 29(2):191–216

Giorgi F, Mearns LO (1999) Introduction to special section: regional climate modeling revisited. J Geophys Res Atmos (1984–2012) 104(6):6335–6352

Giorgi F, Christensen J, Hulme M, Von Storch H, Whetton P, Jones R, Mearns L, Semazzi F (2001) Regional climate information-evaluation and projections. In: Houghton JT et al (eds) Climate change 2001: the scientific basis. Contribution of working group to the third assessment report of the intergovernmental panel on climate change. Cambridge University Press, Cambridge

Giorgi F, Jones C, Asrar GR (2009) Addressing climate information needs at the regional level: the CORDEX framework. World Meteorol Organ (WMO) Bull 58(3):175

Gissila T, Black E, Grimes DIF, Slingo JM (2004) Seasonal forecasting of the Ethiopian summer rains. Int J Climatol 24(11):1345–1358

Hastenrath S (2007) Circulation mechanisms of climate anomalies in East Africa and the equatorial Indian Ocean. Dyn Atmos Oceans 43(1):25–35

Hauke J, Kossowski T (2011) Comparison of values of Pearson's and Spearman's correlation coefficients on the same sets of data. Quaest Geogr 30(2):87–93

Hewitson B, Crane R (1996) Climate downscaling: techniques and application. Clim Res 7:85–95. doi:10.3354/cr007085

Indeje M, Semazzi FH, Ogallo LJ (2000) ENSO signals in East African rainfall seasons. Int J Climatol 20(1):19–46

Intergovernmental Panel on Climate Change (IPCC) (2007) Climate change 2007-the physical science basis: Working group I contribution to the fourth assessment report of the IPCC (S Solomon et al (eds)). Cambridge University Press

Intergovernmental Panel on Climate Change (IPCC) (2013) Climate change 2013: the physical science basis. In: Contribution of working group i to the fifth assessment report of the intergovernmental panel on climate change, T F Stocker, D Qin, G-K Plattner, M Tignor, S K Allen, J Boschung, et al (eds) (Cambridge, New York: Cambridge University Press), p 1535

Kalognomou EA, Lennard C, Shongwe M, Pinto I, Favre A, Kent M, Büchner M (2013) A diagnostic evaluation of precipitation in

CORDEX models over Southern Africa. J Clim 26:9477–9506. doi:10.1175/JCLI-D-12-00703.1
Kijazi AL, Reason CJC (2005) Relationships between intraseasonal rainfall variability of coastal Tanzania and ENSO. Theor appl climatol 82(3–4):153–176
Kim J, Waliser DE, Mattmann CA, Goodale CE, Hart AF, Zimdars PA, Favre A (2014) Evaluation of the CORDEX-Africa multi-RCM hindcast: systematic model errors. Clim dyna 42(5-6):1189–1202
Kosaka Y, Xie SP (2013) Recent global-warming hiatus tied to equatorial Pacific surface cooling. Nature 501(7467):403–407
Langenbrunner B, Neelin JD (2013) Analyzing enso teleconnections in cmip models as a measure of model fidelity in simulating precipitation. J Clim 26:4431–4446. doi:10.1175/JCLI-D-12-00542.1
Latif M, Dommenget D, Dima M, Grötzner A (1999) The role of Indian Ocean sea surface temperature in forcing east African rainfall anomalies during December-January 1997/98. J Clim 12(12):3497–3504
Liebmann B, Bladé I, Kiladis GN, Carvalho LMV, Senay GB, Allured D, Funk C (2012) Seasonality of African precipitation from 1996 to 2009. J Clim 25:4304–4322. doi:10.1175/JCLI-D-11-00157.1
Mason SJ, Goddard L (2001) Probabilistic precipitation anomalies associated with ENSO. Bull Am Meteorol Soc 82(4):619–638
Murtagh F (1985) Multidimensional clustering algorithms. In: Chambers JM, Gordesch J, Klas A, Lebart L, Sint PP (eds) Compstat lectures, Würzburg: Physica-Verlag, Vienna
Nicholson SE, Kim J (1997) The relationship of the El Nino-Southern oscillation to African rainfall. Int J Climatol 17(2):117–135
Nikulin G, Jones C, Giorgi F, Asrar G, Büchner M, Cerezo-Mota R, Hänsler A, Sushama L (2012) Precipitation climatology in an ensemble of CORDEX-Africa regional climate simulations. J Clim 25(18):6057–6078
Ogallo LJ (1988) Relationships between seasonal rainfall in East Africa and the Southern oscillation. J Climatol 8(1):31–43
Paeth H, Hall NM, Gaertner MA, Alonso MD, Moumouni S, Polcher J, Ruti PM, Rummukainen M (2011) Progress in regional downscaling of West African precipitation. Atmos Sci Lett 12(1):75–82
Panitz HJ, Dosio A, Büchner M, Lüthi D, Keuler K (2014) COSMO-CLM (CCLM) climate simulations over CORDEX-Africa domain: analysis of the ERA-Interim driven simulations at 0.44 and 0.22 resolution. Clim Dyn 42(11–12):3015–3038
Reynolds RW, Rayner NA, Smith TM, Stokes DC, Wang WQ (2002) An improved in situ and satellite SST analysis for climate. J Clim 15:1609–1625
Ropelewski CF, Halpert MS (1987) Global and regional scale precipitation patterns associated with the El Niño/Southern Oscillation. Mon Weather Rev 115(8):1606–1626
Rowell DP (2013) Simulating SST teleconnections to Africa: What is the state of the art?. J Clim 26(15):5397–5418
Rudolf B, Becker A, Schneider U, Meyer-Christoffer A, Ziese M (2010) The new "GPCC full data reanalysis version 5" providing high-quality gridded monthly precipitation data for the global land-surface is public available since December 2010. GPCC status report December
Rummukainen M (2010) State-of-the-art with regional climate models. Wiley Interdiscip Rev Clim Change 1(1):82–96
Saji NH, Goswami BN, Vinayachandran PN, Yamagata T (1999) A dipole mode in the tropical Indian Ocean. Nature 401(6751):360–363
Samuelsson P, Jones CG, Willén U, Ullerstig A, Gollvik S, Hansson U, Kjellström E, Nikulin G, Wyser K (2011) The Rossby centre regional climate model RCA3: model description and performance. Tellus A 63:4–23
Segele ZT, Lamb PJ (2005) Characterization and variability of Kiremt rainy season over Ethiopia. Meteorol Atmos Phys 89(1–4):153–180
Segele ZT, Lamb PJ, Leslie LM (2009a) Large-scale atmospheric circulation and global sea surface temperature associations with Horn of Africa June–September rainfall. Int J Climatol 29(8):1075–1100
Segele ZT, Leslie LM, Lamb PJ (2009b) Evaluation and adaptation of a regional climate model for the Horn of Africa: rainfall climatology and interannual variability. Int J Climatol 29(1):47–65
Slim H (2012) IASC real-time evaluation of the humanitarian response to the horn of africa drought crisis in Somalia, Ethiopia and Kenya. Available from: http://reliefweb.int/sites/reliefweb.int/files/resources/RTE_HoA_SynthesisReport_FINAL.pdf
Sylla MB, Gaye AT, Pal JS, Jenkins GS, Bi XQ (2009) High-resolution simulations of West African climate using regional climate model (RegCM3) with different lateral boundary conditions. Theoret Appl Climatol 98(3–4):293–314
Taylor KE (2001) Summarizing multiple aspects of model performance in a single diagram. J Geophys Res 106(D7):7183–7192
Taylor KE, Stouffer RJ, Meehl GA (2012) An overview of CMIP5 and the experiment design. Bull Am Meteorol Soc 93(4):485–498
Tourigny E, Jones CG (2009) An analysis of regional climate model performance over the tropical Americas. Part I: simulating seasonal variability of precipitation associated with ENSO forcing. Tellus A 61(3):323–342
Ummenhofer CC, Sen Gupta A, England MH, Reason CJ (2009) Contributions of Indian Ocean sea surface temperatures to enhanced East African rainfall. J Clim 22(4):993–1013
United Nations Office for the Coordination of Humanitarian Affairs (UNOCHA) (2011) Eastern Africa drought humanitarian report 4, 15 July, New York, NY
Wang Y, Leung LR, McGREGOR JL, Lee DK, Wang WC, Ding Y, Kimura F (2004) Regional climate modeling: progress, challenges, and prospects. J Meteorol Soc Jpn 82:1599–1628
Yang SC, Keppenne C, Rienecker M, Kalnay E (2009) Application of coupled bred vectors to seasonal-to-interannual forecasting and ocean data assimilation. J Clim 22(11):2850–2870

4

Assessment of future projections

The previous two papers present the results of RCM downscaling over Eastern Africa in the historical period when driven by "perfect" reanalysis data and "imperfect" CGCM data at the boundaries. Particular emphases have been given to examine the propagation of large-scale teleconnection controls from the reanalysis or CGCM across the boundary and into the domain of the RCMs. Results shown that RCMs adequately simulate the main features of the rainfall climatology over the region and also able to reproduce the observed teleconnective SST-rainfall patterns. It was demonstrated that errors in sea-surface temperature and lateral boundary conditions from the CGCMs are the primary reason for poor reproduction of the regional teleconnection rainfall patterns by the RCMs. In this part, the climate change projections for the twenty-first century under the RCP4.5 and RCP8.5 emission scenarios are presented. The two RCM simulations (RCA driven by 8 CGCMs, and CCLM driven by 4 of the common CGCMs) and the corresponding CGCM simulations that were analyzed in the historical period are used to investigate the changes in teleconnection patterns in projection of the future climate. The period 1976 - 2005 is considered as reference for present climate while projected analysis is performed for far future (2070 - 2099). The results suggest two important projected changes in teleconnection signals in the future that have impact on regional East African rainfall. Over eastern part of the domain (Eastern horn of Africa), the ENSO/IOD related rainfall anomaly is stronger, whereas over the southern part of the regions the ENSO/IOD signal is weaker compared to the present climate.

Future changes in rainfall associated with ENSO and IOD over Eastern Africa

Hussen Seid Endris[1*], Christopher Lennard[1], Bruce Hewitson[1], Alessandro Dosio[2], Grigory Nikulin[3]

[1]) Climate System Analysis Group, University of Cape Town, Cape Town, South Africa

[2]) European Commission Joint Research Centre, Institute for Environment and Sustainability, Ispra, Italy

[3]) Rossby Centre, Swedish Meteorological and Hydrological Institute, Norrköping, Sweden

Abstract

El Niño Southern Oscillation (ENSO) and Indian Ocean Dipole (IOD) are the two dominant modes of climate variability over the tropics controlling the eastern Africa rainfall at inter-annual time scales. Therefore, investigating the future changes in regional rainfall patterns associated with ENSO and IOD is of great importance for the region. This study examines the projected changes in the characteristics of ENSO and IOD (mean state, intensity and frequency), and the associated rainfall anomalies over eastern Africa. Two regional climate models (RCA, nested in 8 Coupled Global Climate Models, and CCLM, nested in 4 of the common CGCMs) and the corresponding CGCM simulations are used to investigate the changes in teleconnection patterns in projection of the future climate. The period 1976-2005 is considered as reference for present climate, and projected analysis is performed for the far-future climate (2070-2099) on two-concentration pathways (RCP4.5 and RCP8.5).

Analyses of projections based on CGCMs indicate an El Niño-like (positive IOD-like) warming pattern over the tropical Pacific (Indian) Ocean. However, large uncertainties remain in projecting future changes in ENSO/IOD frequency and intensity. Some models show increase of ENSO/IOD frequency and intensity, but others show a decrease or even no/small change. An increase of OND mean rainfall over Eastern horn of Africa is projected under both RCPs (RCP4.5 and RCP8.5), which might be linked with a faster warming rate in the western parts of the Indian Ocean. During ENSO and IOD years, we find two important changes in the teleconnection signals in future; 1) over eastern part of the domain (Eastern horn of Africa), the ENSO/IOD related rainfall anomaly is stronger compared to the present, and 2) over the southern part of the regions the ENSO/IOD signal is weak. This signal is consistent in all global and regional model simulations.

Key words: CORDEX, CMIP5, Teleconnections, Eastern Africa, Rainfall, RCM

*Corresponding author address: Hussen Seid Endris

E-mail: hussen.seid1@gmail.com

1 Introduction

This is the part of a series of three papers investigating Eastern African climate using data from the COordinated Regional climate Downscaling EXperiment (CORDEX) and analyze the projections of twenty-first-century climate under two representative concentration pathways. The first work (Endris et al., 2013) evaluated the ability of 10 Regional Climate Models (RCMs) driven by reanalysis data in simulating the characteristics of rainfall patterns over eastern Africa. The study showed that most RCMs reasonably simulate the main features of the rainfall climatology over the region, and in most of the areas and time periods, the multimodel ensemble mean outperforms the results of individual models, even the forcing ERA-Interim. The second work (Endris et al., 2015) examined the ability of two RCMs, with lateral and surface boundary conditions from Global Climate Models (GCMs) participating to the phase 5 Coupled Model Intercomparison Project (CMIP5), to propagate the teleconnective forcing of tropical sea surface temperatures (SSTs) on rainfall over East Africa. The study showed that RCMs are capable of reproducing the observed teleconnective SST-rainfall patterns. It also demonstrated that most errors in simulating the regional teleconnection patterns arise mainly from the driving GCMs.

In this analysis we have used the same models that were used in Endris et al. (2015) to look at the projected changes in rainfall associated with El Niño Southern Oscillation (ENSO) and Indian Ocean Dipole (IOD). These are the dominant modes of climate variability over the tropics that control the eastern Africa rainfall at inter-annual time scales.

As a result of increased greenhouse gas concentrations, climate process behaviors and associations are understood to be potentially non-stationary and as a consequence it is possible that ENSO/IOD characteristics could change overtime. Several studies have examined the future state of the tropical Oceans and the associated teleconnections under warming scenarios. There is a general agreement that the mean state in tropical Pacific will shift towards a permanent El Niño-like state, meaning greater surface warming over central and eastern equatorial Pacific than western Pacific, with a corresponding mean eastward shift of precipitation (IPCC, 2007; Müller and Roeckner, 2008; IPCC, 2013). However, considerable disagreements remain in the model-projected changes in ENSO characteristics particularly in amplitudes and frequencies. Using the National Center for Atmospheric Research Community Climate System Model (CCSM; version 1.4), Zelle et al. (2005) looked at the changes in ENSO pattern due to an increase in greenhouse gases. They found that there were no significant changes in ENSO amplitude, period and spatial patterns in future. Merryfield (2006) using 15 CGCMs gathered for the IPCC Fourth Assessment Report (AR4) showed a decrease of El Niño amplitude in some models, but an increase or little change in others models. Collins et al. (2010) further suggested that it is not yet possible to say whether ENSO activity will be enhanced or damped (or whether the frequency of events will change), despite considerable progress in the understanding of the impact of climate change on many of the processes that contribute to El Niño variability. Recently, Cai et al. (2014a) suggested evidence for a doubling in the occurrences of extreme El Niño events in the future in

response to greenhouse warming by aggregating results from CMIP3 and CMIP5 multi-model datasets. The study stated that the increased frequency in extreme El Niño events arises from a projected sea surface temperature warming over the eastern equatorial Pacific that occurs faster than in the surrounding Ocean waters, facilitating more occurrences of atmospheric convection in the eastern equatorial region.

In terms of changes in tropical Indian Ocean, some studies have shown that greenhouse-warming leads to a mean state change in the equatorial Indian Ocean with an easterly wind trend and a faster warming rate in the western parts of the Ocean without a noticeable change in overall frequency or amplitude of IOD events (Vecchi and Soden, 2007; Zheng et al., 2013; Cai et al., 2013). However, Cai et al. (2014b) used a suite of distinct process-based indicators to show a significant increase in the frequency of the extreme positive IOD events under greenhouse warming. The study reported that a mean state change with weakening of both equatorial westerly winds and eastward ocean currents in association with a faster warming in western than the eastern equatorial Indian Ocean facilitates more frequent occurrences of wind and Oceanic current reversal.

The reason for the lack of consensus in future changes ENSO/IOD characteristics is not clear whether it is due to model deficiencies or that the changes to ENSO/IOD characteristics will likely be small (Steinhoff et al., 2015). However, even without significant changes in ENSO/IOD characteristics (i.e. intensity and frequency), the long-term trend in tropical SST (change in the mean state) and the associated changes in the mid-latitude basic state (e.g., convergence zones, mid-latitude jets, storm tracks, etc.) may result in substantial changes in ENSO/IOD-related teleconnections (Meehl et al., 2006; Meehl and Teng, 2007; Lau et al., 2008; Kug et al., 2010; Stevenson et al., 2012; IPCC, 2013). This means if teleconnective forcings associated with ENSO and IOD change, even if ENSO and IOD characteristics do not, rainfall characteristics are likely to change in regions with strong ENSO/IOD responses. Investigating the future changes in regional rainfall patterns associated with ENSO and IOD is therefore crucial in understanding the region changing vulnerability to extreme climate. This will likely help to build appropriate risk management and adaptation strategies for the region. This is particularly crucial for the Eastern Africa region because the economy of the region is highly dependent on agro-based activities such as farming and livestock, which are sensitive to the fluctuations of rainfall.

The main aim of this study is to examine projected changes in the characteristics of ENSO and IOD (such as the mean state, intensity and frequency), and identify whether the current rainfall anomalies associated with ENSO and IOD are projected to change in the twenty-first century. Simulations from two RCMs driven by multiple CGCMs and the corresponding CGCMs are analyzed to quantify the change in teleconnection patterns under two representative concentration pathways (RCP4.5 and RCP8.5).

Section 2 provides a brief introduction to CORDEX and CMIP5 models as well as the primary climate change experiments (RCP4.5 and RCP8.5). The main results are presented in section 3. Summary and conclusions are presented in section 4.

2 Data and methodology

2.1 Models and experiments

We have used monthly output of two RCMs in the on-going CORDEX project. The two RCMs are the Rossby Center regional atmospheric model (RCA4) and the COnsortium for Small-scale MOdeling (COSMO) Regional Climate Limited-area Modelling (COSMO-CLM or CCLM). Choices of the models were based on the availability of the model outputs at the time of the analysis. RCA was driven using eight CMIP5 CGCMs (CNRM-CM5, EC-EARTH, HadGEM2-ES, MPI-ESM-LR, CanESM2, GFDL-ESM2M, MIROC5, NorESM1-M), whereas CCLM was driven using four of common CGCMs (CNRM-CM5, EC-EARTH, HadGEM2-ES, and MPI-ESM-LR). Details of the driving CGCMs and their resolution have been described in the previous paper (Endris et al., 2015).

The two models were integrated in CORDEX-Africa domain [see Nikulin et al. (2012) and Endris et al. (2013)] with a horizontal grid spacing of 0.44 degrees. The historical simulations, covering the period 1950-2005, are forced by observed natural and anthropogenic atmospheric composition changes. Twenty-first century simulations (2006-2100) are forced by Representative Concentration Pathways (RCPs), which are based on radiative forcings (globally radiative energy imbalance) measured in $Wm^{-}2$ by the year 2100 (Moss et al., 2010). For CORDEX-Africa projections, two RCPs are applied, namely, RCP4.5 and RCP8.5. RCP4.5 is a medium level concentration pathway that stabilizes radiative forcing at 4.5 $Wm^{-}2$ by 2100 without exceeding this value. The RCP8.5 experiment represents a high concentration pathway in which radiative forcing reaches 8.5 $Wm^{-}2$ by 2100, and then continues to rise thereafter (Meinshausen et al., 2011). In terms of CO2 concentration, RCP4.5 and RCP8.5 are roughly corresponding to the B1 and A1B scenarios used in the IPCC AR4, respectively (IPCC, 2007).

In this analysis, the period 1976-2005 is considered as reference for present climate while projected analysis is performed for far future (2070-2099). As mentioned, the historical performance of the models was reported in Endris et al. (2015), and therefore it is not presented here. However, there was no sufficient discussion on the characteristics of ENSO and IOD events in Endris et al. (2015), therefore, adequate discussion about the models performance in reproducing the frequency and intensity of ENSO and IOD events has been presented in this analysis. Note that the observed Oceanic Niño index (ONI) and Dipole Mode Index (DMI) indices in this analysis are calculated using the Extended Reconstructed Sea Surface Temperature-ERSST.v3b (Smith et al., 2008). Our analysis focuses on two seasonal time periods that are important for rainfall over the region, the JJAS and OND seasons. JJAS is the main rainfall season for the northern part of Eastern Africa (NEA), and OND for the equatorial part of Eastern Africa (EEA) and Southern part of Eastern Africa (SEA).

2.2 Methodology

Linear regression and composite analysis are applied to evaluate the changes in teleconnection patterns in projection of the future climate. It is known that linear regression is commonly used to diagnose the relationship between SSTs and rainfall. Particularly it is important to examine the amplitude of rainfall teleconnections as has been shown by Langenbrunner and Neelin (2013) and Endris et al. (2015). One limitation of regression analysis, is that it assumes the response to SST (e.g. ENSO) is linear. This means, that the anomalies in the El Niño phase are depicted as the opposite of those in the La Niña phase. Compostie analysis is a useful alternative that can diagnose the asymmetry or nonlinearty of rainfall response to SST anomalies.

In this study, statistics are calculated over thirty years periods, 1976-2005 for historical and 2070-2099 for future. Linear regression is applied to analyze the association of spatial and amplitude of rainfall teleconnection with ENSO and IOD in historical and future periods. For ENSO, Niño3.4 index (Trenberth, 1997), an average of SST over 5^oS-5^oN and 170^o-120^oW, is used to compute the teleconnections. For IOD, Dipole Mode Index (DMI) [Saji et al. (1999)] is used, which is the difference between the area average SST in the western equatorial Indian Ocean (50^o-70^oE and 10^oS-10^oN) and southeastern equatorial Indian Ocean (90^o-110^oE and 10^o-0^oS).

Composite analysis is used to investigate the circulation mechanisms associated with the positive and negative phases of ENSO and IOD, and also to confirm the results obtained from regression analysis. The Oceanic Niño Index (ONI) is used to identify El Niño and La Niña events from the driving model SST fields. ONI is defined as the 3-month running mean SST anomaly in Niño 3.4 region. The NOAA Climate Prediction Center (CPC) uses a threshold of $\pm 0.5\ ^oC$ to define ENSO phases. A year is defined as El Niño or La Niña year when ONI value is higher (lower) than +0.5 (-0.5) for at least five consecutive overlapping seasons, which is the average of three consecutive months of that year. Note that the anomalies are calculated relative to their climatological seasonal cycle based on the respective periods, historical (1976-2005) and far future (2070-2099).

IOD years are identified using the DMI, which is calculated as the SST anomaly difference between the western equatorial Indian Ocean (50^o-70^oE and 10^oS-10^oN) and south-eastern equatorial Indian Ocean (90^o-110^oE and 10^o-0^oS). For observation and models, a threshold of $\pm 0.5\ ^oC$ is used to identify positive IOD and negative IOD years, respectively. A year is defined as positive IOD (negative IOD) year when DMI index is higher (lower) than +0.5 (-0.5) for at least three consecutive overlapping seasons, defined as the average of three consecutive months of that year.

The 3-month running mean SST anomalies of ONI and DMI for observation and models for the historical (1976-2005) and future (2070-2099) are presented in the supplementary material (Fig S1). It is important to mention that the simulated ENSO and IOD events do not synchronize with observed sequence of ENSO and IOD events since the models are free-running CGCMs.

3 Results and Discussions

3.1 Projected changes in mean rainfall

It is important to assess the projected changes in mean rainfall over the region prior to the analysis of changes in rainfall variability associated with ENSO and IOD. To this end we analyzed the projected changes as simulated by the RCMs and the corresponding driving CGCMs in the mean rainfall field, and present results from the ensemble means only in most of the analyses for sake of clarity. For consistency, only the four common CGCMs were used to calculate the ensemble means. Fig. 1 shows the JJAS (top panel) and OND (bottom panel) rainfall change signal of the ensemble mean during the far future (2070-2099) for RCP4.5 and RCP8.5 relative to the reference period (1976-2005) for the CGCMs and two RCMs. Although there is a general similarity in rainfall pattern across the CGCM and RCM simulations, noticeable disagreements exist. During JJAS, the CGCM and RCA runs project a weak positive rainfall change signal over the central part of Ethiopia. However, this is not evident in the CCLM model, which shows strong wet anomaly in the eastern horn of Africa. Both RCM ensembles project a dry anomaly over the south-Sudan and western part of Ethiopia, whereas the CGCM show no signal. Another notable feature is that the RCA model projects a wet anomaly around the Victoria Lake basin, but this is not seen in the CCLM and driving CGCM simulations. All simulations agree in a projected decrease of rainfall over the southern and southeastern part of the region. It is important to note that JJAS is a dry season for southern and southeastern part of the region.

During OND (Fig. 1 bottom panel) the CGCM and RCA ensembles show a more pronounced and widespread positive signal throughout the entire region. The CCLM model, however, shows a negative signal over the northwestern and southern part of the domain. The existence of this contradiction may be related to the physical parametrization in CCLM (i.e not related to the resolution or the boundary forcing) as the coarse resolution CGCM has the same signal as the RCA model. This contradiction feature between CCLM and forcing GCM is also noted in Dosio and Panitz (2015). All the models agree on the projected increase in OND rainfall over eastern horn of Africa region (Somalia, Djibouti, and eastern Ethiopia). The projected increase in OND rainfall over the eastern horn of Africa is similar to other studies (Shongwe et al., 2011; IPCC, 2007) using CMIP3 GCMs, and (Otieno and Anyah, 2013; IPCC, 2013) using the latest CMIP5 models.

To further explore the uncertainty in the models' results, rainfall changes are analyzed and demonstrated for each individual models area-averaged for three homogeneous rainfall sub-regions, namely, Northern East Africa (NEA), Equatorial East Africa and Southern East Africa (SEA) [Fig. 2]. The selection of the regions has been discussed in Endris et al. (2015). There is a general model agreement in projecting positive rainfall changes during OND over EEA (middle panel). However, there are considerable differences between the models over NEA during JJAS (top panel) and SEA during OND (bottom panel). The CGCMs show both increases and decreases in rainfall under both RCPs with the amplitude of the change being greater in RCP8.5,

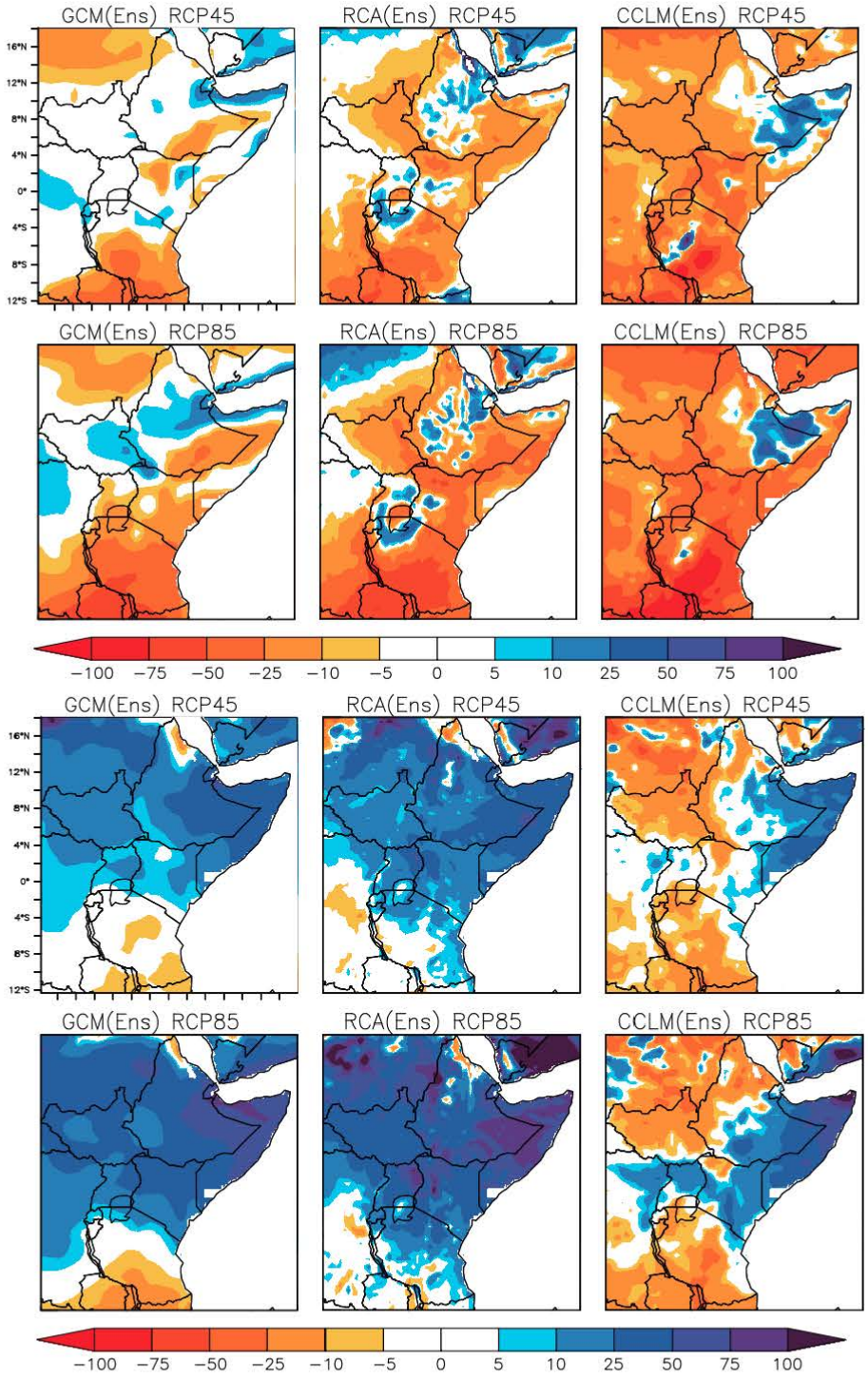

Figure 1: Projected rainfall changes (%) over the region during JJAS (top panel) and OND (bottom panel) under RCP4.5 and RCP8.5 as simulated by the ensemble mean of the RCMs and driving GCMs. Each row corresponds to emission scenarios to each panel: RCP4.5 (first row) and RCP8.5 (bottom).

a pattern that is also seen in the RCA4 results. The CCLM projects a drying in both regions under both RCPs and here the difference in magnitude of change in rainfall between RCPs is larger in NEA under RCP8.5, but similar in SEA. The other interesting feature is that the results

from the RCA4 model simulations follow the patterns of the results of their respective driving GCM simulations.

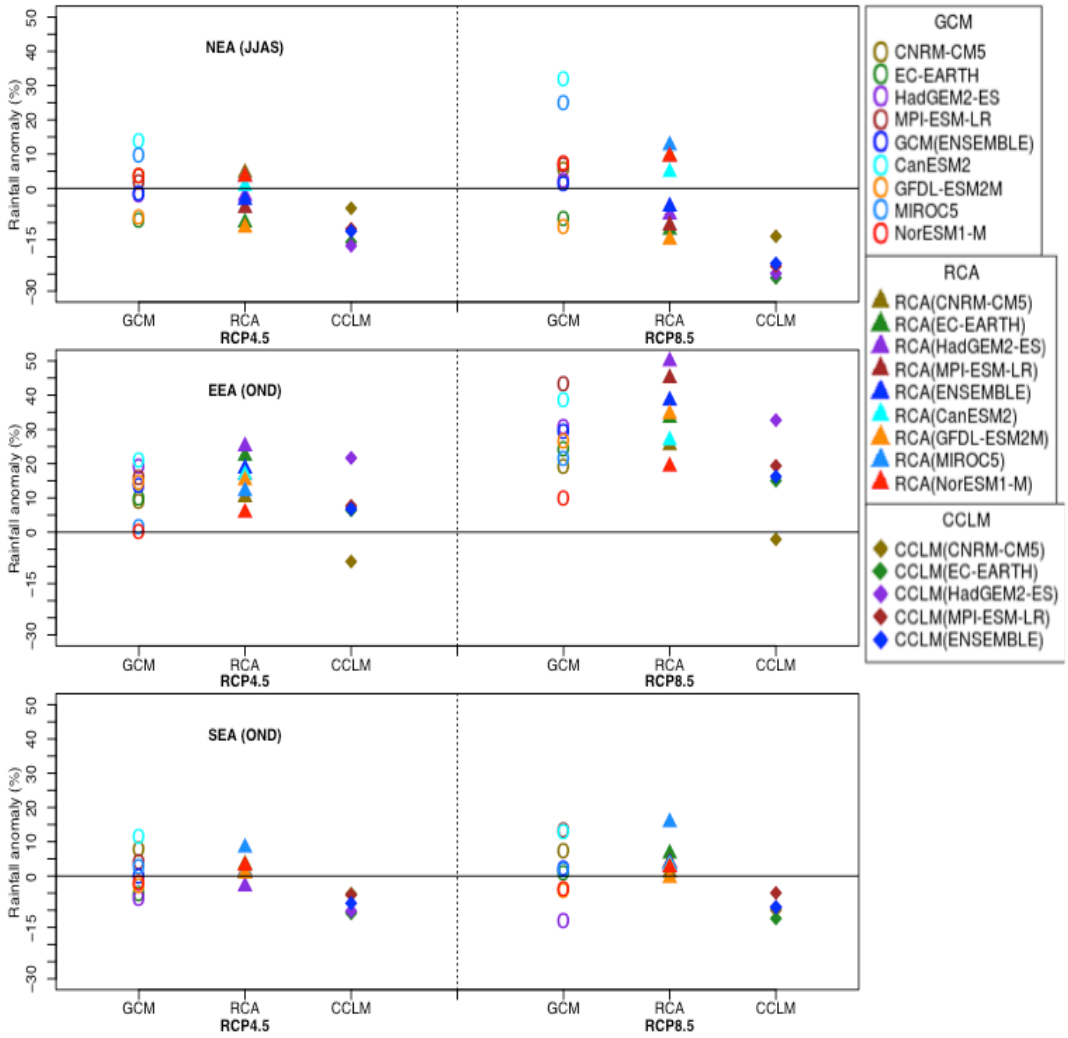

Figure 2: Future changes in rainfall (%) from individual models in three homogeneous rainfall sub-regions. Over NEA during JJAS (top), EEA during OND (middle) and SEA during OND (bottom). Refer Fig. 1 from Endris et al. (2015) for the three homogeneous rainfall sub-regions.

In general, analysis of projected changes in the mean rainfall over the region indicates that there is a decrease in rainfall over the northern part of the region during JJAS (though model consistency is not locally high), and increase in rainfall over equatorial and southern part of the region during OND, with the greatest changes in equatorial region. Results for the RCP4.5 and RCP8.5 exhibit similar patterns, however the magnitudes of change are generally larger in the RCP8.5.

3.2 Projected changes in the characteristics of ENSO and IOD

Changes in the mean state

Fig. 3 illustrates the changes in annual mean SST between the future and the present climate from the ensemble mean of the driving CGCMs. There is a clear SST warming pattern over the whole tropics and an El Niño-like pattern over tropical Pacific. A pIOD-like warming pattern over Indian Ocean is also evident. This is consistent with other studies (e.g., Müller and Roeckner, 2008) that indicated greater surface warming over central and eastern equatorial Pacific than western Pacific, and also greater surface warming over western part of Indian Ocean than the surrounding Ocean. It is possible that the increase in rainfall over EEA during OND is linked with the increase of SST over the western part of the Indian Ocean.

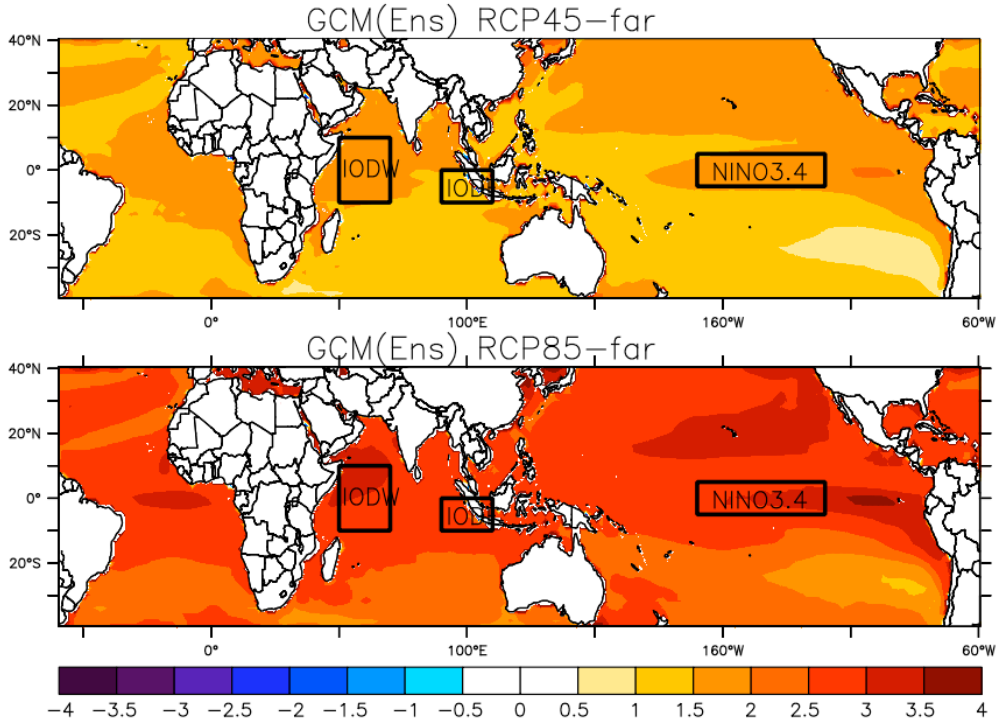

Figure 3: Difference in mean SST (^{o}C) between the future and reference period from the ensemble of the forcing CGCMs (a) RCP4.5 and b (RCP8.5).

Changes in the frequency and intensity ENSO and IOD events

The frequency and intensity of ENSO and IOD events are analyzed for historical and future periods. Fig. 4 presents the frequency and intensity of El Niño, La Niña, pIOD and nIOD events for historical period as well as the projected changes (middle and bottom panels). Frequency is calculated as the number of occurrence of ENSO and IOD events, computed from the 3-month SST anomalies of ONI and DMI for historical (1976-2005) and far future (2070-2099). Thus, the larger the number indicates the more active occurrence of ENSO/IOD events. To estimate ENSO/IOD intensity, we computed the average of the maximum ONI (DMI) for all ENSO (IOD)

events during 1976-2005 and 2070-2099 (similar to the definition used by Zhang et al. (2012)). Larger absolute values represent stronger ENSO/IOD events. For the present climate (1976-2005), 8 El Niño events with an average intensity of 1.62 and 7 La Niña events with an average intensity of 1.52 are shown in the observation (ERSST.v3b). Only one GCM (NorESM1-M) shows the same number of El Niño as observed, but no other model shows the same number of La Niña as observed. The majority of models overestimate the frequency of El Niño and La Niña events. GFDL-ESM2M, MIROC5, CNRM-CM5 and CaESM2 overestimate both the frequency of El Niño and La Niña events, particularly GFDL-ESM2M and MIROC5. In particular, GFDL-ESM2M simulates 15 La Niña events in 30 years period, whereas the observation shows 7 La Niña events. On the other hand, EC-EARTH model underestimate both the frequency of El Niño and La Niña events, with only one El Niño event in 30 years. In terms of the intensity, most models underestimate the intensity of El Niño and La Niña events. Only one model (CNRM-CM5) reports the same intensity as observed. GFDL-ESM2M overestimates both intensity of El Niño and La Niña.

For IOD, three pIOD events with average intensity of 0.89 and four nIOD events with average intensity of 0.61 are reported in ERSST.v3b for the period of 1976-2005. It is worth to mention that the number of pIOD and nIOD events identified in this analysis does not agree with the one reported in Endris et al. (2015), which reported four pIOD and seven nIOD events for the period of 1982-2005 using the NOAA Optimum Interpolation (OI) Sea Surface Temperature (SST) V2 (NOAA_OI_SST_V2) available at one degree resolution. The discrepancy is due to the use of a different SST dataset. Taking ERSST.v3b as a reference, it appears that all the models overestimate the frequency and intensity of pIOD and nIOD events, except HadGEM2-ES, which shows the same intensity of pIOD as observed. Although, the two datasets disagree in producing the frequency and intensity of IOD events, the frequencies and intensities of ENSO events obtained from the two datasets are similar for the same period.

For the future climate (2070-2099), there is no clear indication that the frequencies and intensities of ENSO and IOD will increase or decrease in this period. As is evident in Fig. 4, some of the models project an increase of ENSO and IOD events, whilst others a decrease. In the RCP8.5, all the models agree that there will be an increase in the frequency of El Niño. Under RCP4.5, five out of eight GCMs project an increase in frequency of El Niño, and the rest shows a decrease. Six (four) of out of eight GCMs under RCP4.5 (RCP8.5), show an increase in the intensity of El Niño events, while in the remaining models, there is a decrease in the intensity of El Niño. This is consistent with SST warming in eastern tropical Pacific, the GCMs project more El Niño events in the far future compared to the present. In the case of the IOD there is no clear signal either in the frequency or intensity of IOD events both in RCP4.5 and RCP8.5 scenarios. Almost half of the models project an increase and half the models a decrease.

In general, the above analyses suggest that future changes in ENSO and IOD frequency and intensity are model dependent, as it has been also reported by Stevenson et al. (2012) and Steinhoff et al. (2015). Despite the agreement in increase in the frequency of El Niño in RCP8.5,

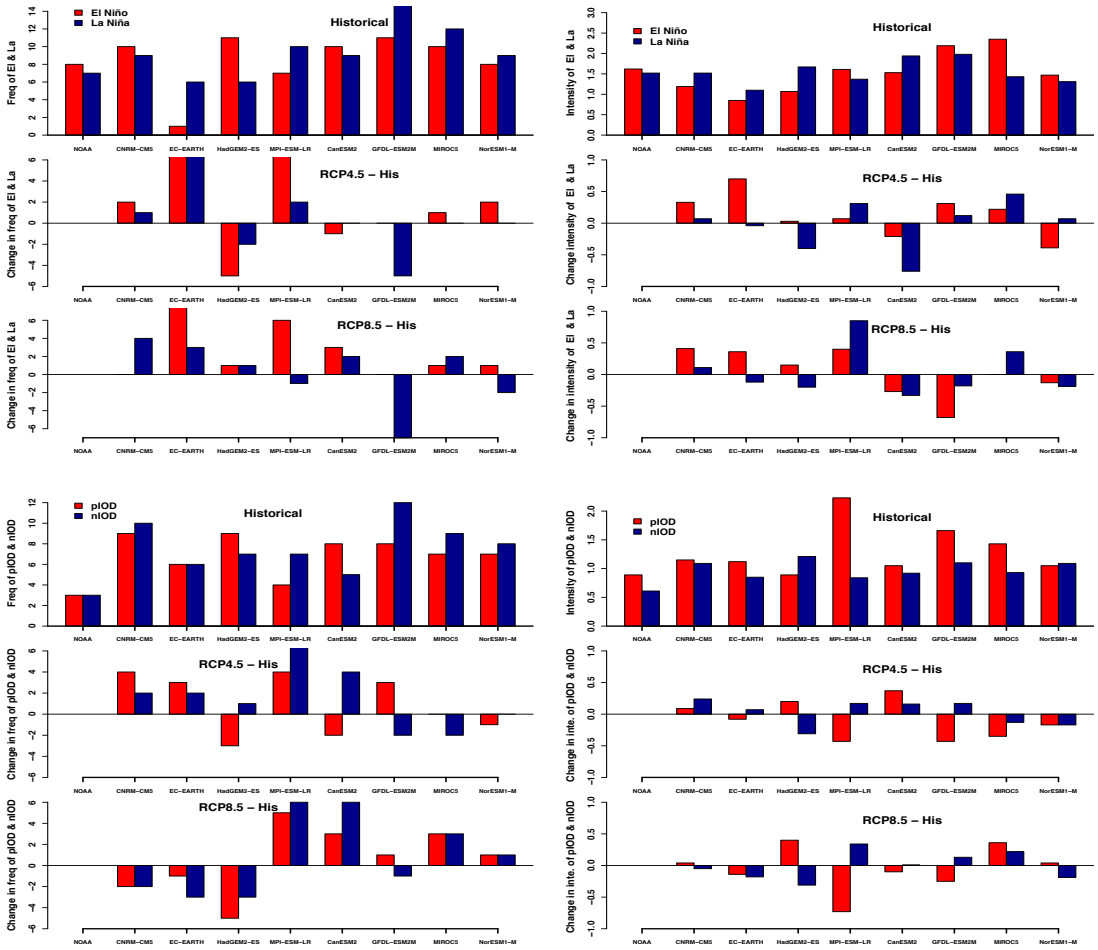

Figure 4: Frequency of ENSO (top left), intensity of ENSO (top right), frequency of IOD (bottom left) and intensity of IOD (bottom right) events in the present climate and changes in the future relative to the present period.

there is no consensus among models on future changes to ENSO/IOD intensity and frequency.

3.3 Teleconnection patterns in present and future period associated with ENSO and IOD

Rainfall patterns associated with ENSO and IOD

Endris et al. (2015) have examined the ability of regional and global models to reproduce historical teleconnection patterns. In this analysis, we used the same GCMs and RCMs to analyses the future teleconnection patterns. Results of the historical simulations are also assessed for the purpose of interpretation future teleconnection patterns. Fig. 5 shows the rainfall teleconnection for the JJAS season against Niño3.4 index in the historical (1976-2005) and future (2070-2099) periods as estimated by linear regression. The top row shows the results from observation, GCMs and the corresponding downscaled ensemble means in the historical period. The second and third rows represent the projected teleconnection in the RCP4.5 and RCP8.5 scenarios respectively.

In the present climate, negative coefficients are observed over the northern part of the domain

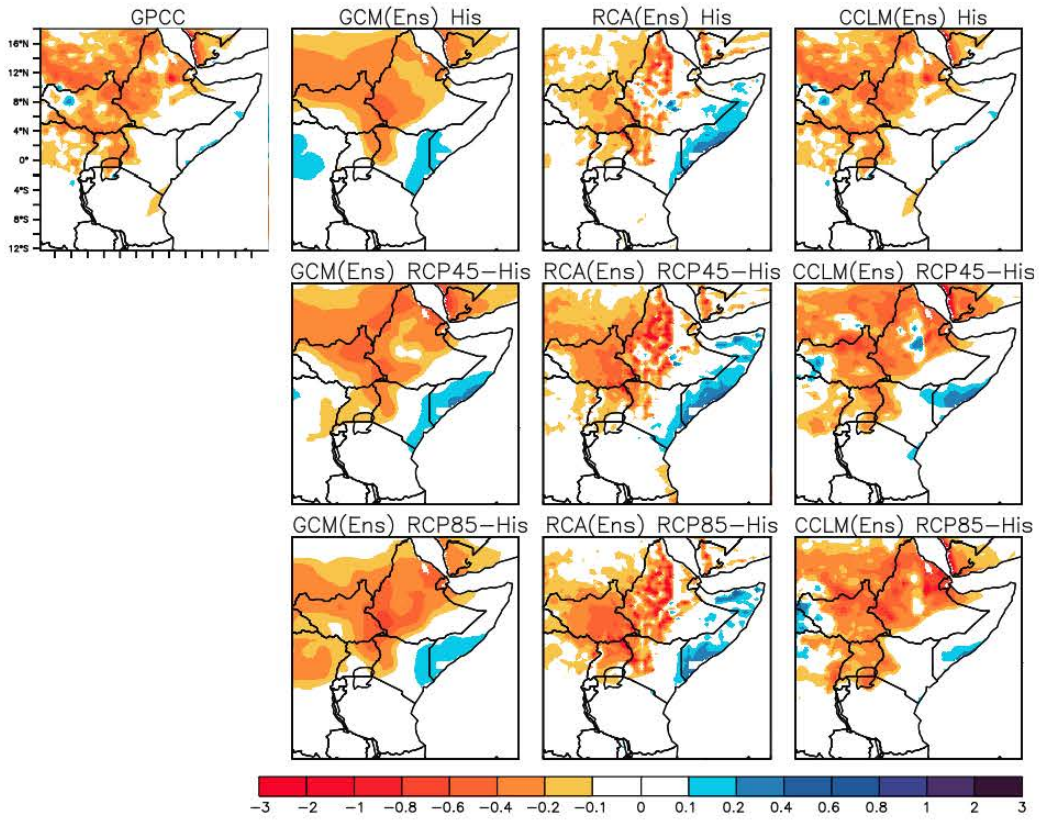

Figure 5: JJAS teleconnections computed using linear regression against Niño3.4 index for historical and future periods. The first row indicates the historical teleconnection patterns from observation, global ensemble mean, and corresponding downscaled regional ensemble means. The second and third rows show the future teleconnection patterns in the RCP4.5 and RCP8.5, scenarios. Units are mm/day/deg ^{o}C.

(top row), which demonstrates the association between tropical Pacific SST and summer (JJAS) rainfall. Warm (cold) SSTs over the tropical Pacific Ocean leads to a dry (wet) summer in the northern part of eastern Africa. Looking at the teleconnection patterns in the historical period (Fig. 5, first row), both the global and regional ensembles correctly represent the negative relationship between ENSO and rainfall over northern part of the region. On the basis of the results from the historical run, we further examine teleconnection patterns under the future climate scenario. The spatial pattern teleconnections in future period are similar to those of the historical period (Fig. 5, second and third rows). The negative coefficients over the northern part of the domain are still simulated by global and regional simulations. This suggests that the spatial pattern of the teleconnections will persist under the global warming scenario. However, the degree/magnitude of the relationship differ compared to the historical period. This will be further discussed in the next section under changes in teleconnection patterns.

It is widely established that rainfall anomaly during short rain season (OND) is associated with both ENSO and IOD (Hastenrath, 2007; Bahaga et al., 2015; Endris et al., 2015). As such, our analysis assesses both influence of ENSO and IOD during OND season. Fig. 6 and 7 show

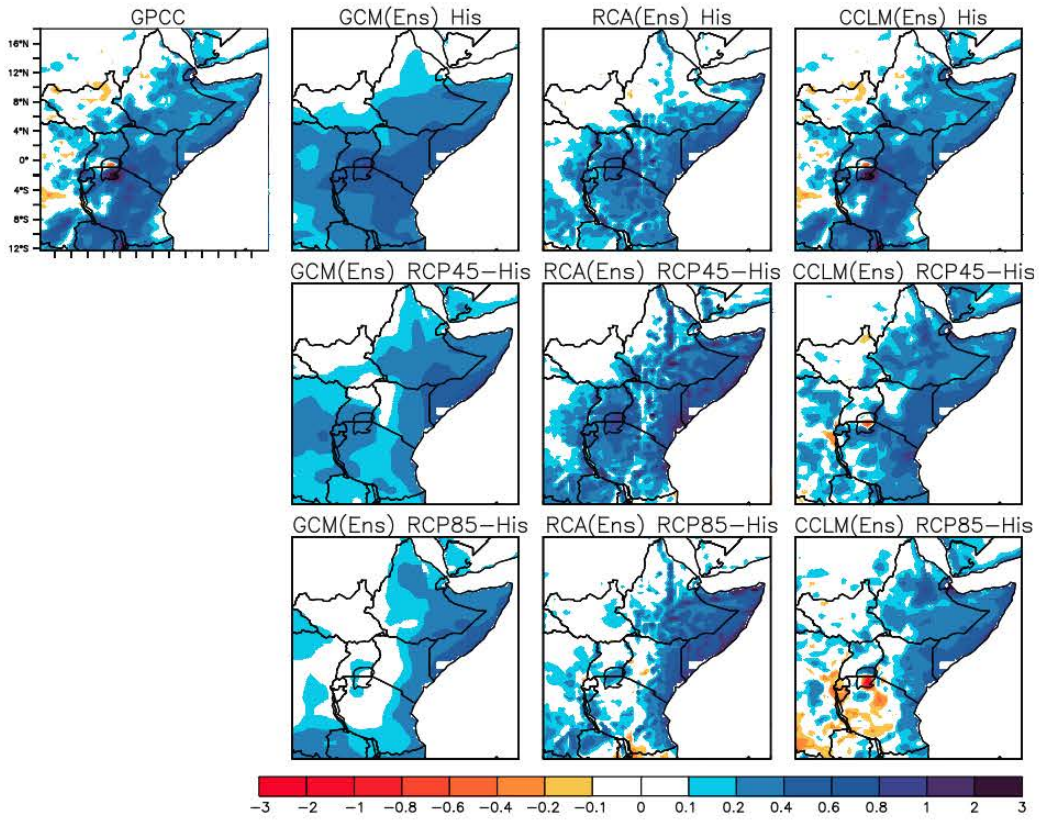

Figure 6: OND teleconnections computed using linear regression against Niño3.4 index. The first row indicates the historical teleconnection patterns from observation, global ensemble mean, and corresponding downscaled regional ensemble means. The second and third rows show the future teleconnection patterns in the RCP4.5 and RCP8.5, scenarios. Units are mm/day/deg ^{o}C.

the OND rainfall telconnection against Niño3.4 and DMI for the historical and future periods, respectively, in which Niño3.4 is the measure strength or phase of ENSO and DMI is the measure of the strength or phase of IOD. Both the positive phases of ENSO and IOD are associated with above normal rainfall over the region. Conversely, the negative phases of ENSO and IOD are associated with below normal rainfall. It is notable that IOD-rainfall teleconnection patterns are more robust than the ENSO-rainfall teleconnection patterns, which is in agreement with previous studies (e.g., Black, 2005; Behera et al., 2005; Bahaga et al., 2015). It can be seen that both the global and regional simulations robustly reproduce the positive relationship between the ENSO and IOD, and OND rainfall in the present climate. In future, the positive association between ENSO/IOD and OND rainfall over the equatorial part of the Eastern Africa is preserved. However, the positive association over the southern part of Eastern Africa is reversed to be negative association. This feature is particularly noticeable in the regional ensemble means in the RCP8.5 scenario.

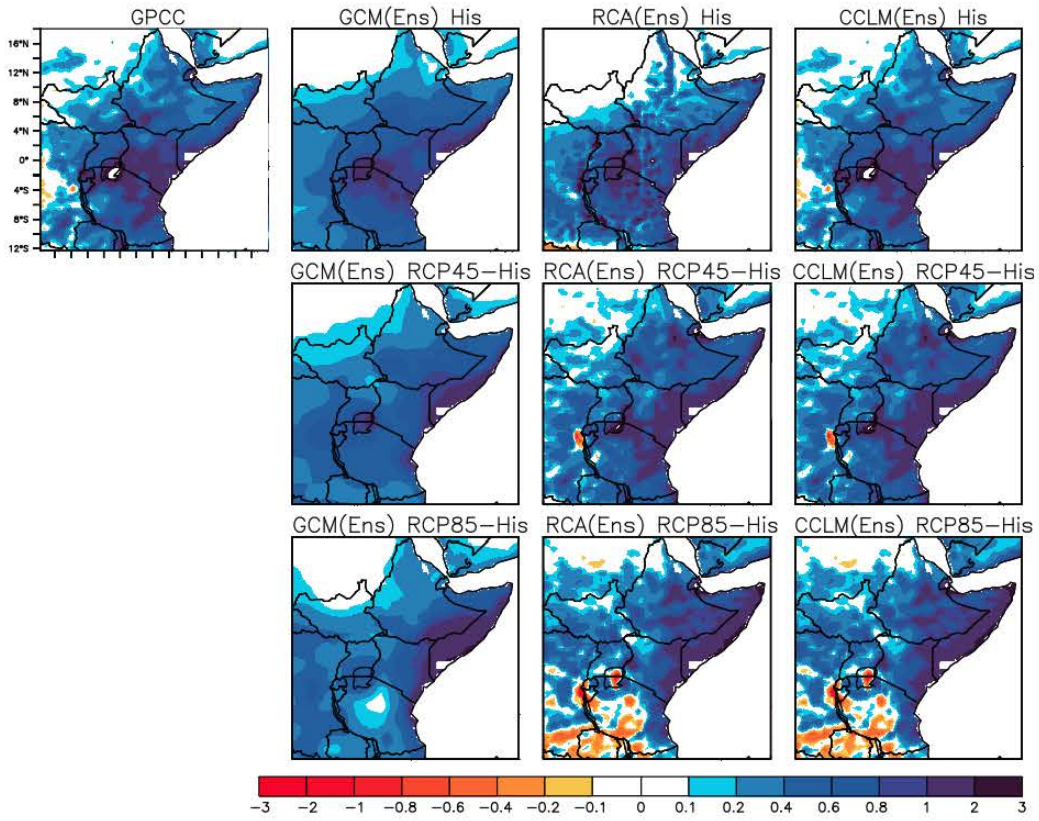

Figure 7: OND teleconnections computed using linear regression against DMI index. The first row indicates the historical teleconnection patterns from observation, global ensemble mean, and corresponding downscaled regional ensemble means. The second and third rows show the future teleconnection patterns in the RCP4.5 and RCP8.5, scenarios. Units are mm/day/deg ^{o}C.

Circulation patterns associated with ENSO and IOD

To understand the circulation mechanisms associated with the dry and wet years, composite maps of different parameters for positive and negative ENSO/IOD events are analyzed. Different studies have shown rainfall over Eastern Africa is strongly associated with low-level and upper level winds. In particular, the low level winds are very important for low-level moisture advection (Lyon et al., 2014). Also the surface pressure directly relates to the mass of air in a vertical column above the surface and gives a measure of the total atmospheric mass distribution. For this reason, we have analyzed the 850hPa wind and the air pressure at sea level (SLP).

Fig 8 shows the composite of JJAS sea level pressure and low-level wind (850hPa) anomalies during El Niño (top panel) and La Niña (bottom panel) events from the Era-Interim reanalysis, regional and global simulations for historical (first rows) and future periods (second and third rows). The El Niño and La Niña composites of multimodel ensemble mean are created from the composites of Individual models (i.e. the single model composite is firstly calculated). During El Niño years, strong positive SLP anomalies are observed over the domain, extending from the Arabian Peninsula towards the Greater Horn of Africa. The presence of this positive anomaly

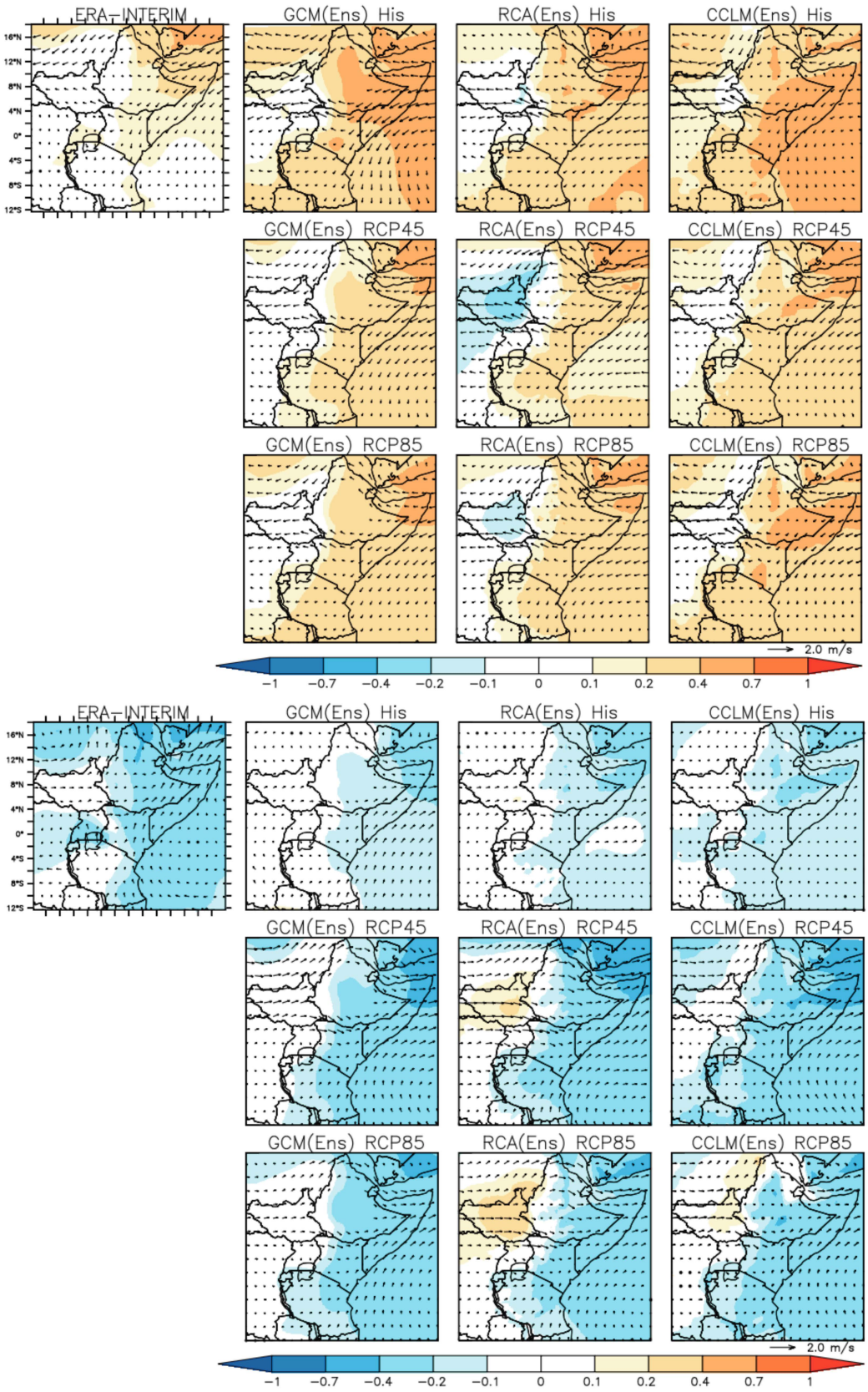

Figure 8: JJAS El Niño (top) and La Niña (bottom) composite map of SLP (shaded in hPa) and 850hPa wind (vectors in m/s) for historical and future periods.

suggests the existence of anticyclonic activity (descending air) that leads to a reduction of rainfall over the region. It is also indicative of a clear a reduction of westerly and southwesterly winds from the south Atlantic high, and the Somali Low Level Jets (SLLJ) from the Mascarene high. These are the main sources of moisture over the northern part of the domain during JJAS. The reduction of these winds is demonstrated by the presence of easterly wind anomaly vectors over western part of Eastern Africa and northeasterly wind anomaly vectors off the coast of East Africa. Conversely, the composite for La Niña events show opposite patterns (i.e negative SLP anomalies over the Arabian Peninsula extended down to the region), which reflects the deepening of the monsoon trough over the Arabian Peninsula. The deeper monsoon trough over the Arabian area is strongly associated with greater rainfall over the eastern Africa during JJAS (Diro et al., 2011; Endris et al., 2015). During La Niña an increase low-level Somali jets (LLSJ) anomalies is clear. There is also a marked increase in the strength of westerly wind anomalies from Gulf of Guinea and southwesterly wind anomalies from Congo rainforest basin, resulting more moisture advected to the region. There is a fairly good agreement between the reanalysis, and the regional and global ensemble means in reproducing the anomalous circulations patterns associated with El Niño and La Niña events in the historical period. The anomalous circulation patterns in the future are similar to the historical patterns (Fig. 8 second and third rows). However, it appears that there is an intensification of the low-level Somali jets (LLSJ) and westerly wind anomalies associated with La Niña years in future, compared to the historical pattern. In regional simulations, positive SLP anomalies are noted over western part of the domain (Sudan and South Sudan), which are not present in the GCM simulation.

Composite anomalies of SLP and 850hPa wind associated with El Niño and La Niña during OND are shown in Fig. 9. Results of this study show that during El Niño positive surface pressure anomalies are observed over the western part of the region, and negative surface pressure anomalies are observed over the southwestern part of the Indian Ocean (Fig. 9, Era-Interim). The two 850hpa wind anomalies, easterly from the equatorial Indian Ocean and westerly from the Congo rainforest basin, converge at the eastern horn of Africa. The low-level convergence leads to ascending motion and favors rainfall. The La Niña composites, on the other hand, show results that are opposite to the El Niño counterparts, in which negative SLP anomalies observed over most part of the domain. Also, during El Niño, the easterly winds over the equatorial Indian Ocean becomes weaker (even switched to westerlies) and reduces the rainfall over the region. In the examination of the anomalous SLP and wind vectors associated with El Niño and La Niña events over the region of study, results indicate that the models captures well the anomalous patterns in the region. In future, models show a reduction in SLP anomalies particularly over the southern part of the domain, and the reduction is stronger for RCP8.5. These features will be discussed in the next section.

Composite anomalies of SLP and 850hPa wind associated with pIOD and nIOD in present and future periods are presented in Fig. 10. As it is widely known, during pIOD, the western Indian Ocean becomes unusually warm and the eastern equatorial Indian Ocean unusually cold.

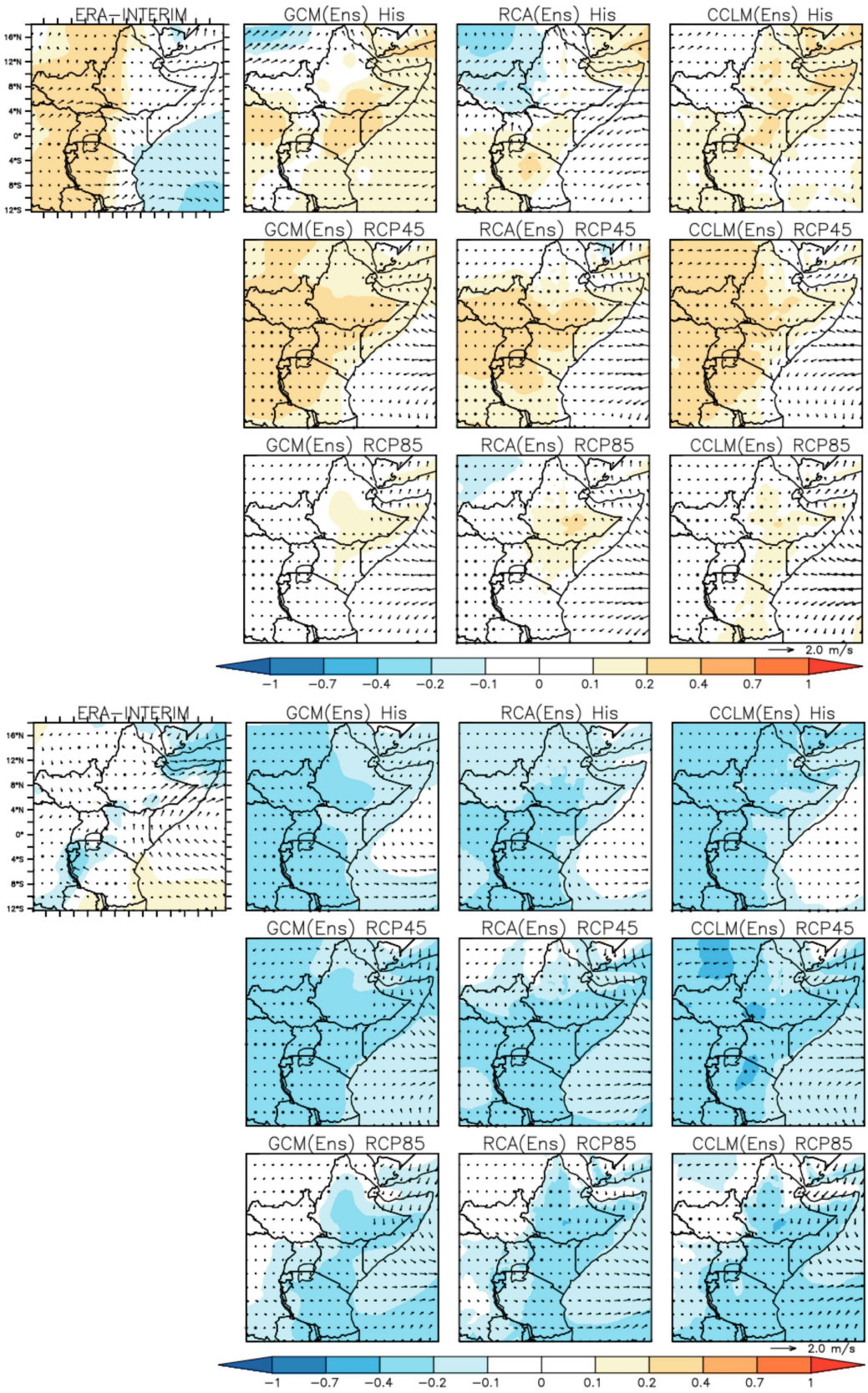

Figure 9: OND El Niño (top) and La Niña (bottom) composite map of SLP (shaded in hPa) and 850hPa wind (vectors in m/s) for historical and future periods.

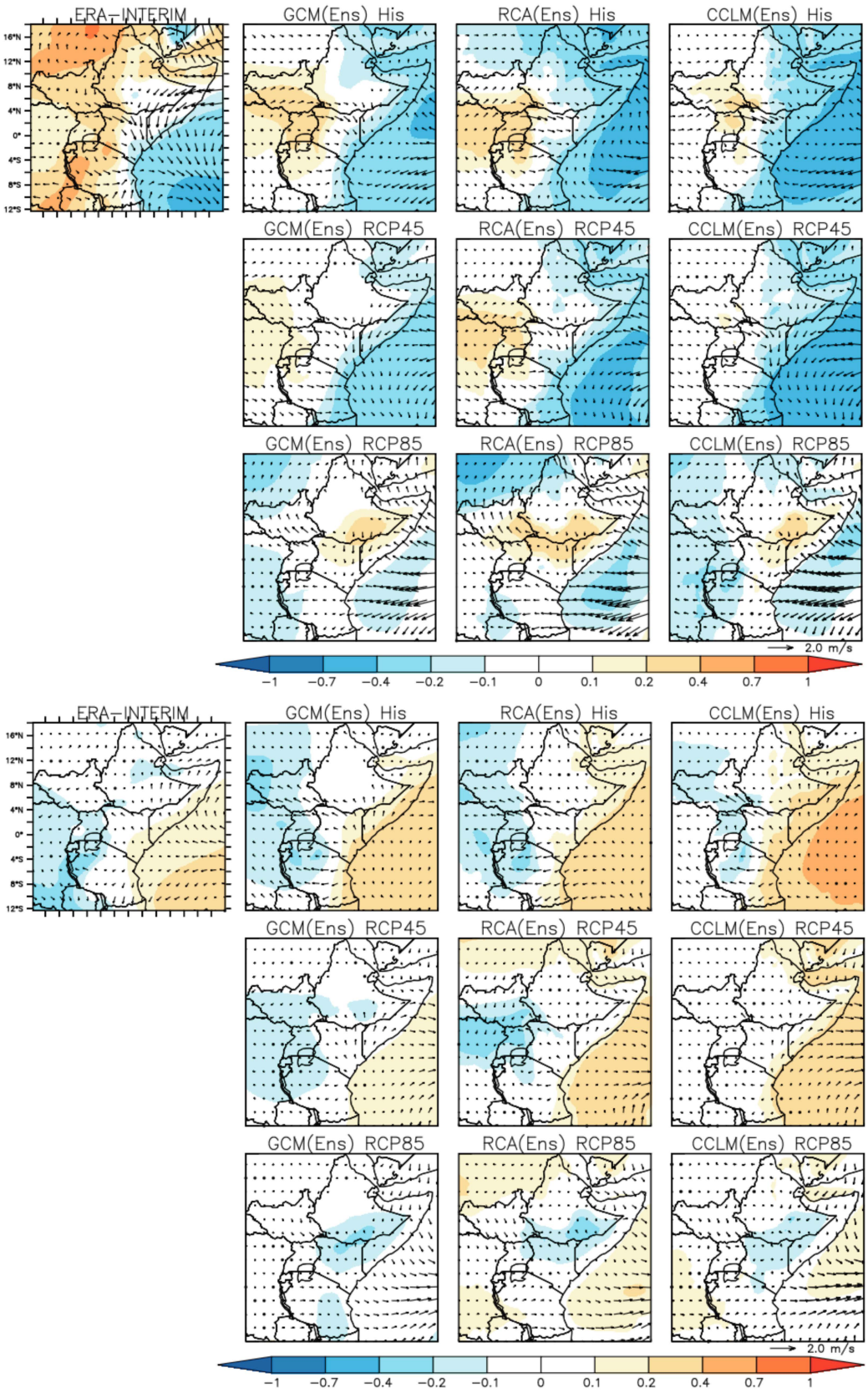

Figure 10: OND pIOD (top) and nIOD (bottom) composite map of SLP (shaded in hPa) and 850hPa wind (vectors in m/s) for historical and future periods.

A reduction in SLP as a result of warm SST anomaly over the western half of the Indian Ocean and converging wind anomalies over East Africa (i.e convergence of westerly airflow over central Africa and easterly onshore anomalies from the equatorial Indian Ocean) lead to moisture convergence and increased convective activity over the region. Conversely, during nIOD years, an anomalous anticyclonic circulation occurs over the western part of the Indian Ocean with westerly wind anomalies. The anomalous anticyclonic combined with the westerlies reduce the convective over the region. In present climate, it can be clearly seen that all simulations reproduce the anomalous easterlies over the equatorial Indian Ocean that extends to Eastern horn of Africa during pIOD. The models also reproduce the negative SLP anomalies over the western part of the Indian Ocean and the positive SLP anomalies over the western part of the domain during pIOD, although the simulated positive SLP anomalies over western part of the domain are weaker than Era-Interim reanalysis. The anomalous circulation patterns associated with nIOD events are also captured relatively well by the regional and global ensemble means in comparison to the Era-Interim reanalysis.

In future projections, even though the general anomalous circulation patterns are similar to those of the current decades, important changes are identified. One of the prominent changes is a reduction of the SLP anomalies over the western part of the domain for both warm and cold phases of IOD (Fig. 10). This reduction is more noticeable in RCP8.5 scenario. In RCP8.5, the (current) positive SLP anomaly associated with warm phase of IOD over the western part the domain is switched to negative anomaly. As a result, the easterly flow to extend far beyond the East coast to central Africa (Fig. 10, top panel, 3rd row). These changes will be further discussed in section 3.4.2. During cold phase of IOD for RCP8.5 (Fig. 10, bottom panel, 3rd row), the positive SLP anomaly is absent in the GCM ensemble.

3.4 Future changes in teleconnection patterns associated with ENSO and IOD

Changes in rainfall patterns associated with ENSO and IOD

In this section we explore the change in teleconnection patterns. Teleconnection changes are computed based on the difference in teleconnection patterns between the future (2070-2099) and historical (1976-2005) period (i.e. taking their absolute values). By looking at the difference in teleconnection patterns, we can deduce the strength of the teleconnection. Figure 11 shows the difference of the JJAS rainfall teleconnection patterns obtained from regression analysis between the future and historical experiments associated with ENSO. It can be seen that a positive anomalies are dominating over the northern part of the domain. It means that the strength of the teleconnection between ENSO and JJAS rainfall is expected to get stronger in the future (in both RCP4.5 and RCP8.5 scenarios) compared to the present. We further investigate the future changes in teleconnection patterns using the composite analysis to confirm the results and to reveal some important information that was not shown by the regression analysis (Figure not

shown). Like the regression analysis, the composite analysis shows an enhancement of ENSO and summer rainfall relationship in future compared to the present period, however, this enhancement is associated with La Niña events only. The magnitude of rainfall anomalies associated with El Niño years is likely to be reduced in the future. This supports the idea of a non-linear, rather than symmetrical, association between ENSO and Eastern Africa rainfall.

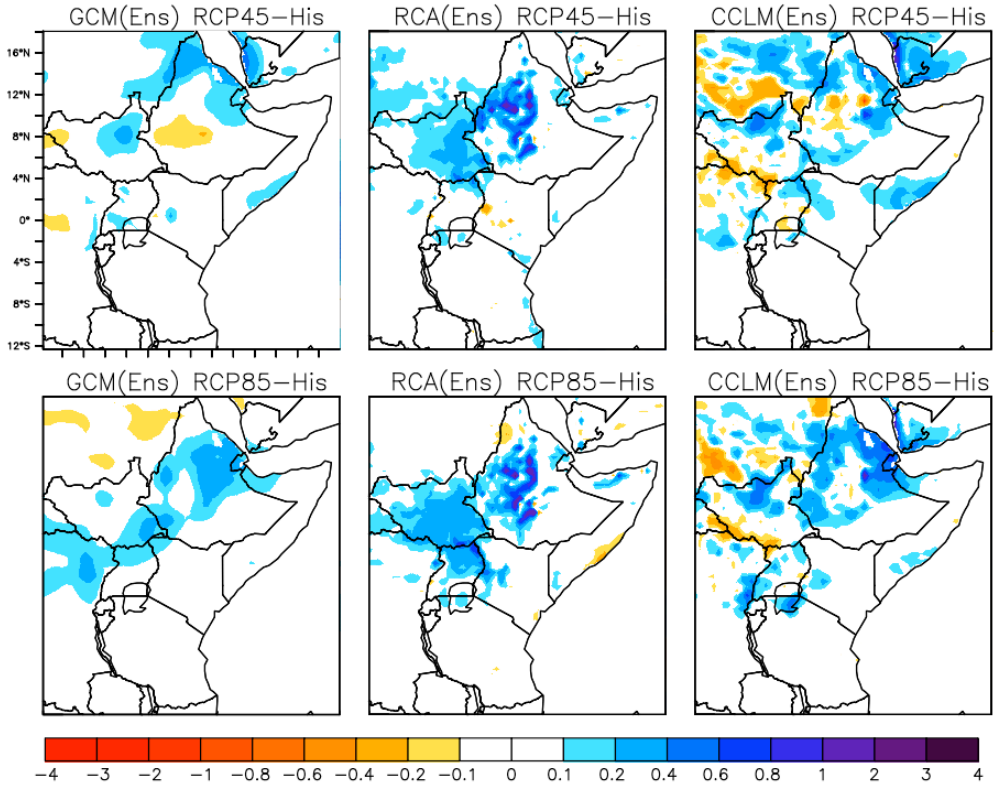

Figure 11: Differences in JJAS teleconnection patterns resulted from regression coefficients against Niño3.4 index between future and historical period for the regional and global simulations in the RCP4.5 and RCP8.5 scenarios. Units are mm/day ^{o}C.

Figure 12 shows the difference in OND rainfall teleconnection patterns between the future and historical experiments associated with ENSO. Results indicate that there is a dipole change signal, i.e. a positive change over the eastern horn of Africa (Somalia, South-eastern part of Ethiopia and eastern part of Kenya), and negative change over the southern parts of eastern Africa (over most part Tanzania, Kenya and Uganda). This implies that the link between ENSO and rainfall over eastern horn of Africa gets stronger in the future compared to the present climate. Conversely, the link will get weaker over the southern part of the region. There are however slight differences in the magnitude teleconnection patterns between the GCM ensemble and RCM ensembles. Positive change over the eastern horn of Africa is not visible in the GCM ensemble, there are some spots of positive values but they dont coincide in RCP4.5 and RCP8.5. In RCA4 ensemble negative signal is weak for RCP4.5 but getting stronger and emerging in RCP8.5.

Both CGCM and RCMs ensembles means show a dipole change signal, i.e. a positive change

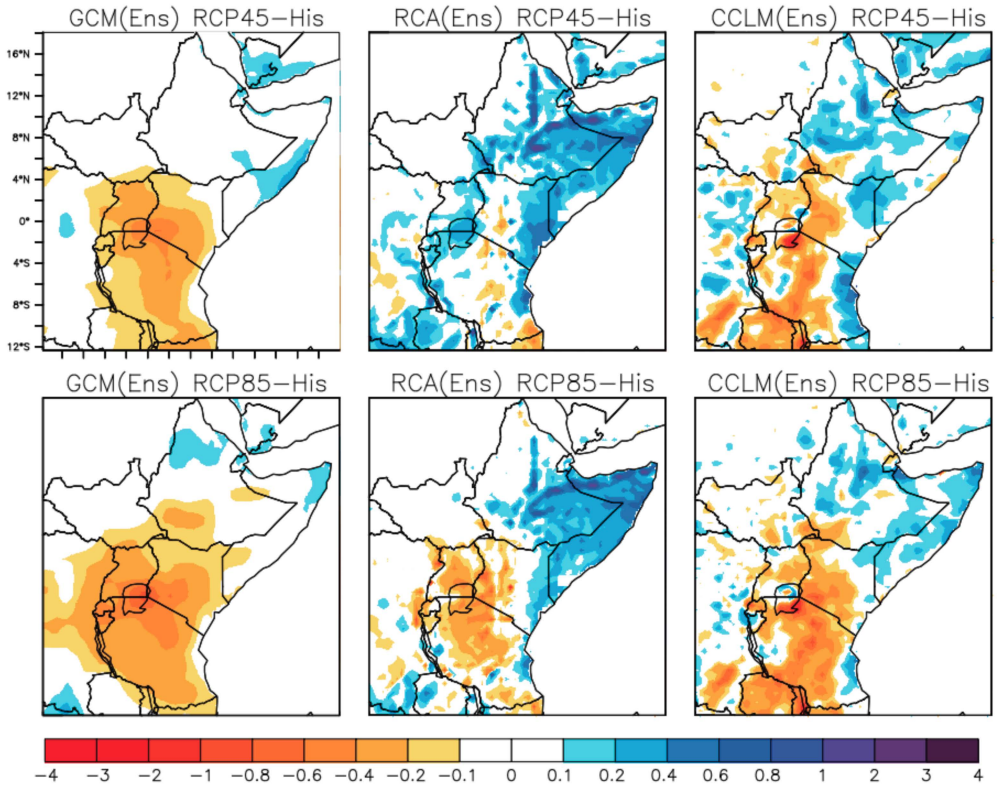

Figure 12: Differences in OND teleconnection patterns resulted from regression coefficients against Niño3.4 index between future and historical period for the regional and global simulations in the RCP4.5 and RCP8.5 scenarios. Units are mm/day ^{o}C.

over the eastern horn of Africa (Somalia, South-eastern part of Ethiopia and eastern part of Kenya), and negative change over the southern parts of eastern Africa (over most part Tanzania, Kenya and Uganda).

The differences in OND rainfall teleconnection patterns between the future and historical experiments associated with IOD are presented in Fig. 13. The changes in teleconnection patterns are similar to those of the ENSO patterns, despite the changes associated with IOD are stronger compared to ENSO. Enhanced in IOD signal is identified over the East horn of Africa, while a reduced signal is observed over the South Eastern part of the region.

We further performed a composite analysis associated with ENSO and IOD to verify the results obtained from regression analysis. The results obtained from composite analysis are consistent with results of the regression map. The strengthening (weakening) in relationship between ENSO/IOD and OND rainfall over east horn of (south Eastern) Africa are still persisted in composite results. It is expected these features might be linked to changes to the mean state, or to a shift in the balance competing feedback processes. A thorough investigation of feedback processes was not possible here; however, mean state metrics are presented in Fig. 3 indicate an El Niño-like (positive IOD-like) warming pattern over the tropical Pacific (Indian) Ocean. Thus the enhanced in teleconnection over the East horn of Africa might be partly linked with enhanced warming in the western part of the Indian Ocean, which also has a link with warming

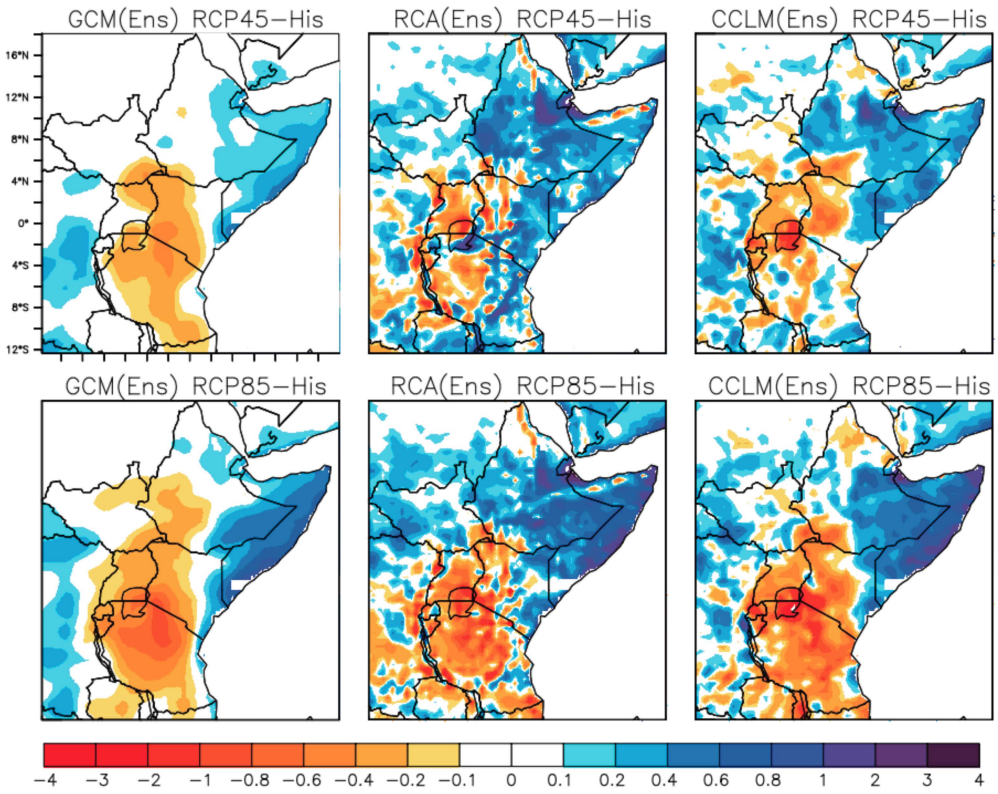

Figure 13: Differences in OND teleconnection patterns resulted from regression coefficients against DMI index between future and historical period for the regional and global simulations in the RCP4.5 and RCP8.5 scenarios. Units are mm/day ^{o}C.

in the eastern part of the Pacific Ocean.

Changes in circulation patterns associated with ENSO and IOD

The difference in circulation anomalies associated with ENSO and IOD are presented in this section. As with rainfall, the difference in SLP anomalies associated with ENSO and IOD between the future and historical period are computed by taking their absolute values. Composite results associated with wet events (i.e. La Niña composites for JJAS, and El Niño and pIOD composites for OND) are only shown here. Fig. 14 shows the difference in SLP and 850hPa wind anomalies associated with La Niña between the future and the historical period. Consistent with the rainfall increase, there is an intensification of the low-level Somali jets (LLSJ) and westerly wind anomalies associated with La Niña years in future compared to the historical pattern. This is the likely driver of the increased rainfall anomalies associated with La Niña events in future compared to the historical period (see Fig. 11). It is also evident that the deeper the monsoon trough over the Arabian Peninsula is associated with greater rainfall over the northern part of the region during JJAS.

Fig. 15 shows the difference in SLP and 850hPa wind anomalies associated with El Niño (top panel) and pIOD (bottom panel) between the future and the historical period. During El

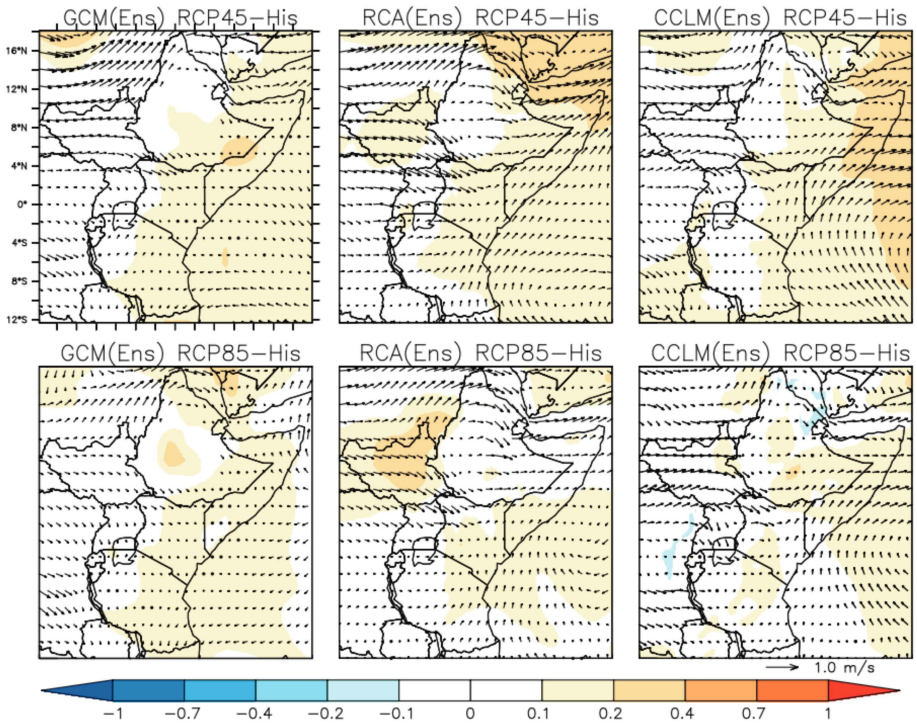

Figure 14: Differences in JJAS SLP anomalies (shade in hPa) and 850 wind anomalies (vectors in m/s) between future and current La Niña years.

Niño (Fig. 15 top panel), two anomalous airstreams, southeasterly and northeasterly anomaly components, are noted over the Indian Ocean. We expect the dipole change in rainfall teleconnection pattern might be partially linked with these two anomalous wind patterns. During pIOD (Fig. 15 lower panel), the differences in anomalous circulation patterns are not consistent between the RCP4.5 and RCP8.5 scenarios. In RCP4.5, the easterlies from the equatorial Indian Ocean become northeasterlies over the coast of Somalia, and later turned to northwesterly over the southern part of the Indian Ocean. In contrast, in RCP8.5 the easterlies from equatorial Indian Ocean extend to the southern part of Eastern Africa. It appears there is a reduction in SLP anomaly over western part of the domain compared to present period. This might be linked with greater warming rate of the western part of the Indian Ocean. A thorough investigation of feedback processes is required to examine changes in circulation patterns.

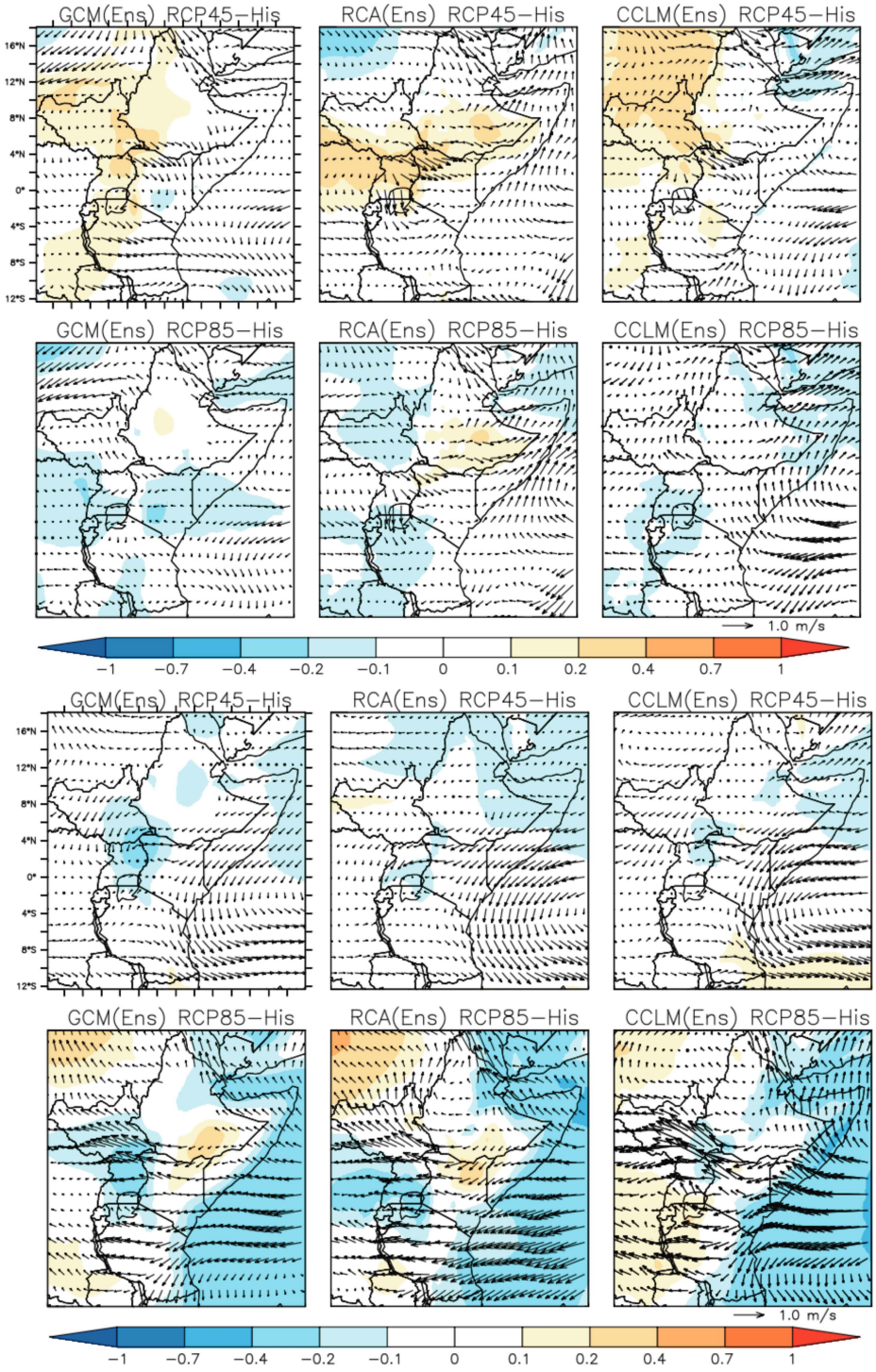

Figure 15: Differences in OND SLP (shade in hPa) and 850 wind (vectors in m/s) anomalies between future and current El Niño (top panel) and pIOD (bottom panel) years.

4 Summary and conclusions

In this study an ensemble of regional and global simulations have been analyzed to investigate whether the Eastern Africa rainfall characters associated with ENSO and IOD will change in the late twenty-first century. Our analysis focuses on two rainfall seasons JJAS and OND. Two

regional climate models (RCA and CCLM) and the corresponding CGCM simulations are used to investigate the changes in teleconnection patterns in projection of the future climate under two scenarios (RCP4.5 and RCP8.5).

For the present climate, both the regional and global ensemble means reproduce the observed dry and wet teleconnection patterns associated with ENSO and IOD. For the future climate, the spatial pattern of teleconnections between ENSO/IOD and rainfall still persist in regional and global simulations. However, important changes in the strength of the teleconnection have been identified. During JJAS, ENSO is important driver of rainfall variability, both regional and global ensemble simulations show higher rainfall during La Niña and lower rainfall during El Niño over the northern part of the region. During OND, the magnitude of the teleconnection pattern associated with both the ENSO and IOD is enhanced over Eastern of horn Africa (Somalia, Djibouti, and eastern part of Ethiopia and Kenya) and reduced over the southern part of Eastern Africa (most part of Tanzania, Uganda, and western Kenya). The OND rainfall teleconnections are stronger and also more consistent between the models and scenarios as compared to the JJAS teleconnections.

The change in teleconnections could be attributed to changes in the amplitude and frequency of the ENSO/IOD events themselves or changes to the mean state and mid-latitude atmospheric circulation as a response to increase of greenhouse gases. Analyses of the change in characteristics of ENSO and IOD events (frequency and intensity) based on driving CGCMs do not show consistent patterns. Some models show increase while others show a decrease or no change. Only in RCP8.5, all the models agree that the frequency of El Niño events will increase, but degree of change varies model to model. Changes in mean SSTs for the future over the tropical Pacific and Indian Ocean show an El Niño-like (positive IOD-like) warming pattern over the tropical Pacific (Indian) Ocean. This is consistent with earlier studies Müller and Roeckner (2008), Zheng et al. (2013) and Cai et al. (2013). We suggest high rainfall events over the eastern horn of Africa attributable to ENSO and IOD phases are probably linked to a warmer western region of the Indian Ocean in future compared to the present.

Assessment of the projected seasonal mean rainfall over the domain varies widely depending on the sub-region and season. During JJAS season, rainfall changes are not very significant in both RCP4.5 and RCP8.5 scenarios. However, during OND there is a significant agreement in the models that there will be an increase of mean rainfall in equatorial part of the Eastern Africa.

Generally, the results from this study provided important information about the future changes in rainfall associated with ENSO and IOD over Eastern Africa, which have not been addressed before. The study particularly has an important implication for water and agricultural managers and policies in the region. Consideration of changes in both the mean and variability of rainfall associated with ENSO and IOD is necessary to tackle the anticipated droughts and floods associated anthropogenic climate change. The study also provides additional insight/implication for seasonal forecasting in future, as there is still a strong reliance on empirical

relationships. However, the physical mechanisms responsible for the change in teleconnection patterns in future are not well known. A further experimental analysis (thorough investigation of feedback processes) is required to help and contribute towards in understanding of these physical processes.

5 References

Bahaga, T., Mengistu Tsidu, G., Kucharski, F., and Diro, G. (2015). Potential predictability of the sea-surface temperature forced equatorial east african short rains interannual variability in the 20th century. *Quarterly Journal of the Royal Meteorological Society*, 141(686):16–26.

Behera, S. K., Luo, J.-J., Masson, S., Delecluse, P., Gualdi, S., Navarra, A., and Yamagata, T. (2005). Paramount impact of the indian ocean dipole on the east african short rains: A cgcm study. *Journal of Climate*, 18(21):4514–4530.

Black, E. (2005). The relationship between indian ocean sea–surface temperature and east african rainfall. *Philosophical Transactions of the Royal Society of London A: Mathematical, Physical and Engineering Sciences*, 363(1826):43–47.

Cai, W., Borlace, S., Lengaigne, M., Van Rensch, P., Collins, M., Vecchi, G., Timmermann, A., Santoso, A., McPhaden, M. J., Wu, L., et al. (2014a). Increasing frequency of extreme el niño events due to greenhouse warming. *Nature climate change*, 4(2):111–116.

Cai, W., Santoso, A., Wang, G., Weller, E., Wu, L., Ashok, K., Masumoto, Y., and Yamagata, T. (2014b). Increased frequency of extreme indian ocean dipole events due to greenhouse warming. *Nature*, 510(7504):254–258.

Cai, W., Zheng, X.-T., Weller, E., Collins, M., Cowan, T., Lengaigne, M., Yu, W., and Yamagata, T. (2013). Projected response of the indian ocean dipole to greenhouse warming. *Nature Geoscience*, 6(12):999–1007.

Collins, M., An, S.-I., Cai, W., Ganachaud, A., Guilyardi, E., Jin, F.-F., Jochum, M., Lengaigne, M., Power, S., Timmermann, A., et al. (2010). The impact of global warming on the tropical pacific ocean and el niño. *Nature Geoscience*, 3(6):391–397.

Diro, G., Grimes, D. I. F., and Black, E. (2011). Teleconnections between ethiopian summer rainfall and sea surface temperature: part iobservation and modelling. *Climate Dynamics*, 37(1-2):103–119.

Dosio, A. and Panitz, H.-J. (2015). Climate change projections for cordex-africa with cosmo-clm regional climate model and differences with the driving global climate models. *Climate Dynamics*, 46(5-6):1599–1625.

Endris, H. S., Lennard, C., Hewitson, B., Dosio, A., Nikulin, G., and Panitz, H.-J. (2015). Teleconnection responses in multi-gcm driven cordex rcms over eastern africa. *Climate Dynamics*, 46(9-10):2821–2846.

Endris, H. S., Omondi, P., Jain, S., Lennard, C., Hewitson, B., Chang'a, L., Awange, J., Dosio, A., Ketiem, P., Nikulin, G., et al. (2013). Assessment of the performance of cordex regional climate models in simulating east african rainfall. *Journal of Climate*, 26(21):8453–8475.

Hastenrath, S. (2007). Circulation mechanisms of climate anomalies in east africa and the equatorial indian ocean. *Dynamics of Atmospheres and Oceans*, 43(1):25–35.

IPCC (2013). The physical science basis. contribution of working group i to the fifth assessment report of the intergovernmental panel on climate change. *K., Tignor, M., Allen, SK, Boschung, J., Nauels, A., Xia, Y., Bex, V., Midgley, PM, Eds*, page 1535.

IPCC, I. (2007). *Climate change 2007-the physical science basis: Working group I contribution to the fourth assessment report of the IPCC*, volume 4. Cambridge University Press.

Kug, J.-S., An, S.-I., Ham, Y.-G., and Kang, I.-S. (2010). Changes in el niño and la niña teleconnections over north pacific–america in the global warming simulations. *Theoretical and applied climatology*, 100(3-4):275–282.

Langenbrunner, B. and Neelin, J. D. (2013). Analyzing enso teleconnections in cmip models as a measure of model fidelity in simulating precipitation. *Journal of Climate*, 26(13):4431–4446.

Lau, N.-C., Leetmaa, A., and Nath, M. J. (2008). Interactions between the responses of north american climate to el niño-la niña and to the secular warming trend in the indian-western pacific oceans. *Journal of Climate*, 21(3):476–494.

Lyon, B., Barnston, A. G., and DeWitt, D. G. (2014). Tropical pacific forcing of a 1998–1999 climate shift: observational analysis and climate model results for the boreal spring season. *Climate Dynamics*, 43(3-4):893–909.

Meehl, G. A. and Teng, H. (2007). Multi-model changes in el niño teleconnections over north america in a future warmer climate. *Climate Dynamics*, 29(7-8):779–790.

Meehl, G. A., Teng, H., and Branstator, G. (2006). Future changes of el niño in two global coupled climate models. *Climate Dynamics*, 26(6):549–566.

Meinshausen, M., Smith, S. J., Calvin, K., Daniel, J. S., Kainuma, M., Lamarque, J., Matsumoto, K., Montzka, S., Raper, S., Riahi, K., et al. (2011). The rcp greenhouse gas concentrations and their extensions from 1765 to 2300. *Climatic change*, 109(1-2):213–241.

Merryfield, W. J. (2006). Changes to enso under co2 doubling in a multimodel ensemble. *Journal of Climate*, 19(16):4009–4027.

Moss, R. H., Edmonds, J. A., Hibbard, K. A., Manning, M. R., Rose, S. K., Van Vuuren, D. P., Carter, T. R., Emori, S., Kainuma, M., Kram, T., et al. (2010). The next generation of scenarios for climate change research and assessment. *Nature*, 463(7282):747–756.

Müller, W. and Roeckner, E. (2008). Enso teleconnections in projections of future climate in echam5/mpi-om. *Climate dynamics*, 31(5):533–549.

5

Summary and concluding remarks

5.1 Summary of the results

In this study, the ability of coupled general circulation models (CGCMs) and regional climate models (RCMs) to reproduce the teleconnection between tropical SST and rainfall over Eastern Africa is examined.

The first step evaluated the ability of RCMs to reproduce the characteristics of Eastern Africa rainfall when driven by perfect boundary conditions (reanalysis data) over the period 1990 - 2008. The analysis considered 10 RCM (ARPEGE, CCLM, CRCM, HIRHAM, PRECIS, RACMO, RCA, RegCM3, REMO and WRF) simulations forced by the European Centre for Medium-Range Weather Forecasts (ECMWF) ERA-Interim re-analysis as perfect boundary conditions. These simulations were evaluated for their ability to capture and characterize rainfall patterns as well as their ability to reproduce the response to large-scale global signals over Eastern Africa in comparison with different gridded observational datasets. The results show that the 10 RCMs are able to capture the climatological seasonal mean rainfall distribution over the region, and annual cycle of rainfall in different sub-regions with reasonable accuracy. The annual rainfall cycle is better reproduced over uni-modal rainfall regimes (northern and southern part of the region) than the bi-model rainfall regime. Some models fail to capture the correct peak of the bimodal rainfall (OND peak in particular) over equatorial sector of the region. Over the domain as a whole most RCMs showed excessive rainfall (wet bias). Results from the time series

and composite analysis show that most of the models capture the regional rainfall anomalies associated with ENSO and IOD in agreement with the observation. Moreover, some regional climate models have out-performed the ERA-Interim rainfall in comparison to the reference data (GPCC). It has been noted that the multi-model ensemble mean generally outperforms the skill of individual models, likely because of the cancellation of opposite signed biases across the models, and indicating the usefulness of multi-model assessments for past and future climate of the region.

The second step in this study assessed the ability of CGCMs and RCMs forced by the CGCMs at the boundaries to reproduce rainfall climate statistics over the region for the historical period (1982 - 2005) as well as investigate the propagation of teleconnection signals across the boundary of the RCMs into the downscaled domain. In this analysis, two RCMs (RCA driven by 8 CGCMs, and CCLM driven by 4 of the common CGCMs) and their driving CGCMs were investigated for their capability to reproduce the observed relationships between large-scale oceanic modes and regional seasonal rainfall. The reanalysis-driven simulations from the two RCMs are also analyzed to estimate error produced by the RCMs and those transmitted from driving CGCMs. The ERA-Interim driven downscaled results show better agreement with observed spatial teleconnection patterns than the CGCM driven downscaled results. Analysis of the CGCMs and corresponding downscaled results showed that in some cases both had similar teleconnection patterns, but in other cases the teleconnection patterns of RCM simulations differ from the corresponding CGCM simulations. For example, the NorESM1-M model shows positive correlation with eastern equatorial Pacific (which is opposite to the observed signal), while the downscaled result RCA (NorESM1-M) reproduced well the observed patterns. Conversely, CNRM-CM5 captured the teleconnection with eastern equatorial Pacific Ocean, while the RCMs degraded the signal, especially RCA model. CanESM2 and MIROC5 show negative correlations with central Indian Ocean, with RCA (CanESM2) and RCA (MIROC5) producing similar correlation patterns, which is not seen in the observation. It has been demonstrated that similarities in SST-rainfall teleconnection patterns between the RCM simulations and respective driving CGCM simulations are noted over the equatorial and southern part of the region during OND season, where the rainfall is primarily controlled by large-scale (synoptic-scale) features, with the RCMs maintaining the overall regional patterns from the forcing models. Differences in RCM simulations from corresponding driving simulations are noted mainly over northern part of the domain during JJAS, which is most likely related to mesoscale processes that are not resolved by CGCMs. Some models (both CGCMs and the RCMs) simulated the sign and strength of correlations of rainfall with SSTs. Overall, HadGEM2-ES, MPI-ESM-LR, GFDL-ESM2M CGCMs and the multi-model ensemble mean captured the pattern correlation better than any other models, while CanESM2 and MIROC5 performed poorly.

Analysis of the ability of individual models to simulate the amplitude of rainfall teleconnections have shown that that the CGCMs underestimate the amplitude of the teleconnection, while the RCMs overestimate it in most of the sub-regions against the different indices. The

high amplitude of teleconnection in the RCM simulations might be primarily a better capture of precipitation, enhanced by a better-resolved topography. On the other hand, the low amplitude of teleconnection in CGCMs may be associated with a poorly resolved topography and other small-scale features due to coarse resolution. Composite analyses of large-scale fields (SLP and wind field) indicate that the models performance in reproducing the anomalies in SLP and low- level winds are consistent with their performance at representing the rainfall anomalies. The ERA-Interim driven downscalings produce a more realistic representation in the magnitude of circulation anomalies. This suggest that it is not only the parameterizations in the RCMs that are the cause of the errors in the downscaled CGCM rainfall fields, but that the driving circulation states were not captured as the CGCM-derived boundary conditions were imperfect.

The third step investigated the CGCM and RCM-downscaled CGCM projections for future periods under two Representative Concentration Pathways (RCPs). The climate projections used CMIP5 simulations for boundary conditions. The two RCMs (RCA and CCLM) and the corresponding CGCM simulations are used to investigate the projected changes in teleconnection patterns in the future climate. The period 1976 - 2005 is considered as the reference for the present climate, and projected analysis is performed for the far-future climate (2070 - 2099). The analysis focus on two emission scenarios known as RCP4.5 and RCP8.5 which represent a mid and a high-level emission scenario. Investigation of the future changes in ENSO/IOD frequency and intensity from the CGCMs reveals a spread amongst the models, with some models indicating an increase of ENSO/IOD frequency and intensity, but others indicating a decrease or even no/small change. However, there is a general agreement in CGCMs with an El Nino-like (positive IOD- like) warming pattern over the tropical Pacific (Indian) ocean. Both CGCMs and downscaled results indicate an increase of OND mean rainfall over the Eastern horn of Africa under both RCPs, which might be linked with a faster warming rate in the western parts of the Indian ocean that is critical region for East African rainfall. During ENSO and IOD years, two important changes were found in the teleconnection signals of the future: 1) over eastern part of the domain (Eastern horn of Africa), the ENSO/IOD related rainfall anomaly is stronger compared to the present, and 2) over the southern part of the region the ENSO/IOD signal is weakened. This signal is consistent in all global and regional model simulations.

5.2 Concluding remarks

In this section, the conclusions of the research described in the thesis are presented. The aim and objectives of the research, outlined in the first chapter, are reviewed and the findings obtained for each of the objectives are stated. The overall aim of this study is to examine the ability of climate models (regional and global) to reproduce the telconnection forcing of tropical SST on rainfall over eastern Africa and investigate whether or not the present teleconnection patterns persist in the future under increase greenhouse gas scenarios. Particular emphasis has been given in examining the propagation of a large-scale teleconnection pattern, such as the ENSO

and IOD, from a reanalysis or GCMs to RCMs. To this end a number of objectives were set that evaluated the ability of regional models to reproduce rainfall over the region and their ability to transmit teleconnection signals across the boundary.

Objectives:

1. **To evaluate the ability of the RCMs to simulate the observed spatial and temporal characteristics of rainfall**

   An initial evaluation of the ability of regional models to reproduce regional rainfall characteristics of eastern Africa showed that many RCMs simulated better rainfall climatology that of the driving reanalyses, demonstrating that the downscaling can add value to the driving data by resolving small-scale processes, as found by Di Luca et al. (2012) and Nikulin et al. (2012). Moreover, the analysis revealed that the multi-model ensemble mean outperformed the results from individual regional models as well as driving reanalysis, largely as a consequence of cancellation errors between the models. While the multi-model ensemble mean provides better representation of the average climate, it does still indicate that single model downscalings do not adequately sample the uncertainty space. Thus, it is prudent to use downscaled data from as many sources as possible, for example the CORDEX programme, when assessing downscaled rainfall products.

2. **To evaluate the ability of the RCMs reproduce the regional teleconnection responses to the propagated signal via the boundary forcing**

   Examination of the ability of RCMs to simulate SST-rainfall teleconnection patterns shows RCMs have the capability to reproduce the observed regional teleconnection patterns (regional responses). The study has demonstrated that the largest source of uncertainty in the regional climate model simulations is the choice of boundary condition dataset. The ERA-Interim driven RCM simulations have better agreement with observation than the CGCM-driven RCMs in reproducing regional teleconnection patterns (regional responses). When RCMs are driven by CGCMs at the boundaries, the teleconnections between large-scale climate modes and regions rainfall patterns depend on the selection of the driving CGCM. This implies the use of a single GCM for downscaling and using downscaled product for assessment of climate change projections is not adequate. Moreover, while many of the differences in regional teleconnection patterns are related to the driving fields, disagreements in regional responses are also existed due to differences in RCMs physics and parameterizations. Therefore, a prudent approach for reducing uncertainties in future regional scale climate change projection is using as many GCM-RCM combinations as possible.

3. **To assess how well models (global and regional) can simulate the atmospheric circulation patterns/anomalies associated with the teleconnections in the historical period**

Sea level pressure (SLP) and low-level (850 hPa) wind anomalies associated with the warm and cold phases of ENSO and IOD simulated by global and regional are examined for the present and future period.

The results show that the models performance in reproducing the large-scale anomalies in SLP and low-level winds are consistent with their performance at representing the rainfall anomalies. The ERA-Interim driven simulations produce a more realistic representation in the magnitude of circulations fields. Consistent with the rainfall anomalies, CanESM2 and MIROC5 and their corresponding downscaled results fail to represent anomalous circulation patterns associated with ENSO and IOD in most of the examined regions and seasons. This reflects that its not only the parameterizations in the RCMs that are the cause of the errors in the downscaled rainfall fields, the driving circulation states were not captured, as CGCM-derived boundary conditions were incorrect.

4. **To investigate the whether the historical teleconnections persist in future under a global warming scenario**

   In projections of the future, the spatial pattern of teleconnections between ENSO/IOD and rainfall still persist. However, important changes in the strength of the teleconnection have been identified as represented by the models. During JJAS, ENSO is important driver of rainfall variability, both regional and global ensemble simulations show higher rainfall during La Niña and lower rainfall during El Niño over the northern part of the region. This implies increase in intense rainfall events over the region during future La Niña events. In OND, the magnitude of the teleconnection pattern associated with both the ENSO and IOD is enhanced over Eastern of horn Africa (Somalia, Djibouti, and eastern part of Ethiopia and Kenya) and reduced over the southern part of Eastern Africa (most part of Tanzania, Uganda, and western Kenya). The OND rainfall teleconnections are stronger and also more consistent between the models and scenarios as compared to the JJAS teleconnections. This suggests heavy rains and flooding events will increase across the Eastern horn of Africa during positive ENSO and IOD phases. On the one hand, these findings have an important implication for water and agricultural managers and policies in the region to tackle the anticipated droughts and floods associated anthropogenic climate change. On the other hand, the results provide insight/implication for seasonal forecasting in future, as there is still a strong reliance on empirical relationships.

The work here demonstrates that models, both CGCMs and RCMs, are useful tools for examining the teleconnective control of rainfall over Eastern Africa. As teleconnection patterns connected to large-scale circulation, they are mainly described in the GCMs, and the RCMs are generally "slave" to the CGCM boundary conditions. The results show that Era-Interim driven RCMs adequately reproduce the sign and strength of observed teleconnections with large scale climate modes. The largest source of uncertainty in the regional simulations in reproducing in regional teleconnection patterns is the choice of the driving CGCM, suggesting the use of a single

CGCM for downscaling and examining teleconnection forcing of regional rainfall is insufficient. Additionally, as there are some differences in results due to regional model physics, it is vital that the largest possible ensemble of CGCM and RCM be examined in order to better characterize the attendant uncertainties and that single model studies be avoided.

5.3 Caveats and recommendations for future work

Identifying and acknowledging the study's limitations and making a proposal for further study is an essential part of a research work. In this regard, some limitations of this research study have been identified and recommendations for further research are made.

- The different gridded observational datasets used for model validation shows large differences, which highlight significant uncertainties and errors in observational datasets over the region. It is thus critical to improve the observational network and assess the uncertainty among gridded observational datasets so that the model can be validated well for the region. The availability of good quality of observational data will further help to better understand the observed climate variability and extremes and to improve confidence in projected changes.

- This study is used only part of the CORDEX RCMs due to availability of the simulations at the time of the analysis. Thus, to establish the robustness and solidity of the results further work may assess the rest of CORDEX RCMs to reproduce the historical teleconnection patterns and investigate future projected changes.

- Our analysis focused on two rainfall seasons - JJAS and OND. The long rainfall season that occurs in MAM was not considered in the analysis since the MAM rainfall variability has a weak association with tropical SST anomalies at inter-annual time scale. Although the response of MAM to SSTs at inter-annual time scale is known to be weak, the season has recently experienced a series of devastating droughts and a decline in rainfall totals for the last 2-3 decades. In this context, recent studies using the CMIP5 GCM simulations have shown that the majority of CMIP5 projections projected/predicted an increase in MAM rainfall for the coming decades (e.g., Rowell et al., 2015), which is contrary to the recent downward trend. This contrast has been named the East African climate paradox. Therefore, there is a need for evaluating the CORDEX models to capture the recent decline of the long rains, and assess whether or not the RCMs agree with CMIP5 GCMs on contrasting past and future MAM rainfall trends.

- This study provided important information about the future changes in rainfall associated with ENSO and IOD over Eastern Africa. However, the physical mechanisms responsible for the change in teleconnection patterns are not fully investigated. Thus, a further experimental analysis (including thorough investigation of feedback processes) is required to

help and contribute towards in understanding of the key physical processes that drive the change in teleconnections.

- Finally this study has indicated that the largest source of uncertainty in the regional climate model simulations in the context of teleconnective forcing of rainfall over East Africa is the choice of a GCM. Therefore, the use of a single GCM for downscaling and using downscaled product for assessment of climate change projections is insufficient. Results from multi-RCM nested in more than one GCM, like CORDEX experiments, are required for dealing with the uncertainty and providing estimates of likely ranges of future climate changes.